FACULDADE DE ENGENHARIA DA UNIVERSIDADE DO PORTO

RF Transmitter and Receiver for OFDM

Bruno Miguel Silva Neiva

Mestrado Integrado em Engenharia Eletrotécnica e de Computadores

Supervisor: Cândido Duarte

Second Supervisor: Rui Gomes

July 27, 2018

Resumo

RoMoVi é um robô cooperativo e autônomo que está a ser desenvolvido para as vinhas de encosta do rio Douro, com o objetivo de monitorar e executar operações logísticas. No entanto, devido ao declive dos vales e da vegetação densa, uma cobertura precisa com as tecnologias atuais torna-se uma tarefa difícil. A cobertura insuficiente de satélites nega qualquer possibilidade de confiar em um sitema de GPS e a maioria das soluções comerciais não oferece cobertura suficiente.

Durante a transição da televisão analógica para a televisão digital várias bandas de frequência na região de sub-GHz ficaram sem comunicação. Perto destas bandas de frequência existem também algumas bandas ISM disponíveis. Estas bandas de frequência, onde as restrições de comunicação são baixas, podem ser usadas para estabelecer comunicação entre o RoMoVi e uma estação base, que usa como ponto de referência para navegar pelas vinhas.

Este documento apresenta um sistema de comunicação analogica sem fios, que devido à sua comunicação de banda larga, permite estabelecer comunicação em todos os Tv white spaces disponíveis na região sub-GHz. Como comunicação de banda de base, esta solução será suportada por uma modulação OFDM. Este sistema de comunicação permitirá explorar o espectro livre na região sub-GHz e combiná-lo com uma modulação OFDM que permite eficiência espectral enquanto reduz o "multipath propagation".

Abstract

RoMoVi is a cooperative and autonomous robot that is being deployed in the vineyards of Douro river, with the objective of monitoring and executing logistics operations. However, due to the characteristics of the slope valley and dense vegetation, accurate coverage trough GPS with current technologies becomes a difficult task. Insufficient satellite coverage denies any possibility of relying on GPS, and most commercial solutions do not provide sufficient coverage.

The transition from analogue television to digital television left several frequency bands in sub-GHz region without communication. Close to these frequency bands there are also some ISM bands available. These frequency bands, where communication constraints are lower, can be used to establish communication between RoMoVi and a base station, which it uses as a reference point for navigating the vineyards.

This document presents a RF Front-end wireless communication system, which due to its wideband communication allows establish communication in all the freed Tv white spaces available in the sub-GHz region. As baseband communication, this solution it will be supported by an OFDM modulation. Which will allow to explore the freed spectrum in the sub-GHz region and combine it with an OFDM modulation, allowing spectral efficiency while mitigating multipath propagation.

Acknowledgements

I thank first of all to my parents for all the support and patience shown throughout this dissertation.

I want to thank the advisors, professor Candido Duarte and PhD student Rui Gomes, for the support and time available during the development of this dissertation.

Finally, I thank all my friends for being present and for supporting me.

Bruno Neiva

"Try not to become a man of success, but rather try to become a man of value"

Albert Einstein

Contents

List of Figures

List of Tables

Abbreviations

QAM	Quadrature Amplitude Modulatio
OFDM	Orthogonal Frequency Division Multiplexing
RFID	Radio Frequency Identification
GNSS	Global Navigation Satellite System
GPS	Global Positioning System
RoMoVi	Robot Modular e Coperativo para Vinhas de Encosta
RF	Radio Frequency
ICI	Inter-Channel Interference
ISI	Intersymbol Interference
FDM	Frequency Division Multiplexing
PSK	Phase Frequency Keying
DFT	Discrete Fourier Transform
IDFT	Inverse Discrete Fourier Transform
SNR	Signal-to-Noise ratio
LNA	Low Noise Amplifier
NF	Noise Figure
PA	Power Amplifier
S-parameters	Scattering parameters
ENR	Excess Noise Ratio
DUT	Device Under Test
SPI	Serial Peripheral Interface
PAPR	Peak-to-Average Power Ratio
EVM	Error Vector Magnitude

Chapter 1

Introduction

1.1 Context

Autonomous robots were created in the middle 20th century. The first ones had as main application the industrial sector, where they replaced the traditional workers in the production lines performing the heavy and repetitive tasks. But soon, it was realized that they could be applied in other areas like space exploration, agriculture, military, safe and rescue.

With increasing computational capacity and lower hardware acquisition costs, they are becoming increasingly independent and able to perform complex and meticulous tasks. However, some physical limitations continue to prevent greater autonomy in the real world due to the different scenarios in which they need to operate. One of the biggest challenges is to operate in harsh scenarios, where efficient and effective wireless communication is required, allowing them to be in permanent communication with a base station and other robots. This is particularly important in areas such as agriculture, where it takes several robots to cover vast areas.

The convergence of multiple technologies such as wireless communication, real-time analytics, machine learning, commodity sensors, and embedded systems, where machines and devices exchange information in real time creating intelligent networks, it becomes clear the need to transmit large amounts of data in real time. However, with the proliferation of small gadgets that communicate wirelessly and much of the radio spectrum attributed to television, telephone and military communications, it is a challenge to communicate over on the overcrowded RF spectrum.

To mitigate this problem, signal processing techniques developed during the 1980s and 1990s have been implemented, such as orthogonal frequency division multiplexing (OFDM), which allows high data rates combined with a significant reduction in the bandwidth. In some fields these solutions are already implemented, such as telecommunications and television companies, through integrated circuits. However, these highly customized solutions do not allow the application in other fields.

1.2 Motivation

Nowadays global navigation satellite system (GNSS) is the predominant systems for navigation in outdoor scenarios. However, to determine the correct position it is necessary coverage from three global positioning system (GPS) satellites (four or more for a greater precision). Occasionally in the agriculture and forest patrol, the soil has a high slopes creating shadowing, making it difficult meet this requirement.

This dissertation appears integrated in project RoMoVi, a cooperative and autonomous robot deployed along the slopes of the Douro River that aims to help in the harvesting and monitoring the vineyards. This robot uses GPS as navigation system in the Douro River vineyards. However, due to the great slope of the soil, it is not achieved a full coverage of GPS satellites, remaining for several periods without navigation system. Thus, to solve this navigation problem has been developed an algorithm of terrestrial navigation, in which through constant communication with a base station allows to determine the exact location of the robot across the vineyards.

During the transition from analogue to digital television, several frequency bands, called "Tv white spaces", between 470 MHz and 790 MHz, became available. These channels where there is no communication can be used to establish communication between the robot and the base station. Communicating in this frequency bands is particularly beneficial because it allows the communication to have a longer range, in the order of 10 km, and due to its wavelength, the communication becomes less susceptible to attenuation.

In order to make communication possible, it is necessary to develop a radio frequency communication system capable of supporting an OFDM based navigation system, allowing the RoMoVi to continue operating when GPS is not available. With this communication system it will be possible exchange large amounts of data between a base station and the RoMoVi, allowing not only to assist in navigation, but to monitor in real time the vineyards.

1.3 Goals

The purpose of this dissertation is to design and develop a RF transmitter and receiver to establish wireless communication in sub-1 GHz, covering the Tv white spaces. The baseband communication system has been developed using an OFDM technique, thus, the RF communication must be able to receive and transmit data in quadrature and in-phase to baseband communication.

The development of this system must be through discrete components available in the electronics market, so one of the main goals is to build a low-cost solution, since finishied the RoMoVi project in 2020, will be proposed to be commercialized.

Chapter 2

State of the Art

This chapter will present the fundamental concepts necessary to develop this dissertation. An overview of the key steps in the development of an OFDM system and its evolution over the years will be studied. The various side effects and possible solutions to be considered during the design and validation of an RF communication will also be studied.

2.1 Orthogonal frequency division multiplexing (OFDM)

The OFDM arises as evolution of Frequency Division Modulation (FDM) and in the years that followed, significant improvements were achieved in order to mitigate inter-channel interference (ICI) and intersymbol interference (ISI). This modulation explores the orthogonality between sub-carriers, since 1966 Robert W. Chang demonstrated [1] that instead of transmitting in a single-carrier as in FDM, the carrier was divided in N equal sub-carriers separated by Δf, allowing the transmission of symbols simultaneously.

The data transmission in each sub-carrier with QAM and PSK modulations lead to lower baseband frequencies in each sub-carrier as higher the number of sub-carriers. This allows to extend the duration of each symbol by N, which led to elimination of the multi-path propagation delay $\tau_{max} \ll Ts = 1/\Delta f$.

Since QAM symbols can be represented in the frequency domain by $sinc(fT)$, with zeros crossings in multiples of $1/Ts$, where Ts is the duration of each symbol it allows OFDM achieve orthogonality between sub-carriers, where each signal heavily overlapping its neighbours spaced by multiples of $\Delta f = 1/Ts$ as shown in figure 2.1. Mitigating the problem of ICI with superposition, allow bandwidth savings by 50% compared to FDM.

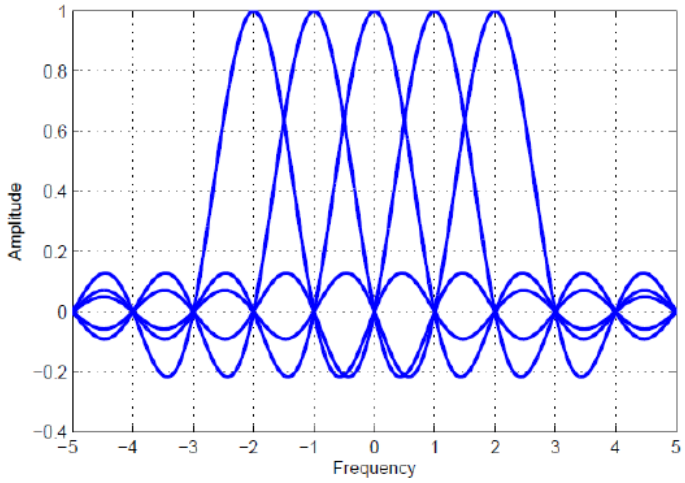

Figure 2.1: Signal Spectrum [2]

To transmit all the sub-carriers, N oscillators are required, which makes this technique expensive, therefore in 1971 Weinstein and Ebert [13] introduced discrete Fourier transform (DFT) to perform baseband modulation and demodulation by passing the signal from the time domain to the frequency domain. This suppresses the oscillator banks and coherent demodulators, thus reducing the implementation complexity, allowing OFDM to become a low cost modulation.

In order to suppress even more ISI problem, in 1980 Peled and Ruiz[10] solved the problem of orthogonality between consecutive symbols by introducing the cyclic prefix. Instead of adding null guards to the beginning of each symbol OFDM as Weinstein and Ebert had proposed a few years before, they added part of the end of each symbol to the beginning, allowing to maintain the orthogonality between symbols.

2.1.1 OFDM Transmission

As mentioned above, the idea behind OFDM technique is to divide the total bandwidth B, into N narrowband sub-channels at equidistant frequencies Δf. Where each sub-channel is modulated with a QAM symbol and spaced by multiples of Δf. Since the QAM symbols are represented by frequency domain sinc-functions, it allows the sub-channels to partially overlap with the others and ensure orthogonality within the symbol duration $Ts = 1/\Delta f$. The k-th unmodulated subcarrier of the OFDM signal is described by the following complex exponential function with a carrier frequency $k\Delta f, K = 0, ..., N-1$.

$$\tilde{g}_k(t) = \begin{cases} e^{j2\pi k\Delta f t} & \forall t \in [0, Ts] \\ 0 & \forall t \notin [0, Ts] \end{cases} \tag{2.1}$$

For OFDM systems, the symbol duration Ts must be much larger than the maximum multipath delay $\tau(max)$. Therefore, the number of subcarriers is chosen in a way that the symbol duration Ts is sufficiently large compared to the maximum multi-path delay τ_{max} of the radio channel.

To limit ICI to a tolerable level, the subcarrier spacing Δf must be such that the maximum frequency of Doopler or f_{Dmax} satisfies the condition.

$$4\tau_{max} \leq Ts \leq 0.03\frac{1}{f_{Dmax}} \tag{2.2}$$

In order to avoid ISI between two adjacent OFDM symbols, the duration Ts of each subacrrier signal $\tilde{g}_k(t)$ is extended by a cyclic prefix with length Tg, which led a total OFDM symbol duration $T = Ts + Tg$.

$$g_k(t) = \begin{cases} e^{j2\pi k\Delta ft} & \forall t \in [-Tg, Ts] \\ 0 & \forall t \notin [-Tg, Ts] \end{cases} \tag{2.3}$$

The cyclic prefix or guard interval is removed at the receiver, becoming an overhead for transmission, but the zero ICI generally compensates the reduction of efficiency.

On the transmitter side, each subcarrier is modulated independently and individually by the modulated symbol $S_{n,k}$, where n refers to the symbol number OFDM signal and k refers to the number of the subcarrier in the OFDM symbol. Thus, OFDM symbol of period T is described by (2.4) where it is formed by the superposition of the N subcarriers with the same period T.

$$S_n(t) = \sum_{k=0}^{N-1} S_{n,k} g_k(t - nT) \tag{2.4}$$

The transmitted signal generated by the n sequential OFDM symbols is described by (2.5).

$$S_n(t) = \sum_{n=0}^{\infty} \sum_{k=0}^{N-1} S_{n,k} e^{j2\pi k\Delta ft(n-nT)} \text{rect}\left(\frac{2(t-nT) + T_G - T_S}{2T}\right) \tag{2.5}$$

The expression (2.5) demonstrates that a rectangular pulse shaping is applied to each OFDM symbol and to each subcarrier. Therefore, the k subcarriers will be represented by sinc-functions and the signal spectrum can be represented by (2.6).

$$G_k(f) = T \cdot \text{sinc}[\pi T(f - k\Delta f)] \tag{2.6}$$

On the receiver side, the modulated symbols $S_{n,k}$ can be recovered using a correlation technique, assuming the radio channel to be ideal;

$$\frac{1}{T_s}\int_0^{Ts} g_k(t) g_l^*(t) \mathrm{d}t = \begin{cases} 1 & k = l \\ 0 & k \neq l \end{cases} \tag{2.7}$$

$$S_{n,k} = \frac{1}{T_s}\int_0^{Ts} s_n(t) g_k^*(t) \mathrm{d}t = \frac{1}{T_s}\int_0^{Ts} s_n(t) e^{-j2\pi k\Delta ft} \mathrm{d}t \tag{2.8}$$

Where $g_k^*(t)$ is the conjugate complex of the subcarrier signal $g_k(t)$.

The correlation process, can be found with more detail in (2.9)

$$Corr = \frac{1}{T_s}\int_0^{Ts} s_n(t)g_k^*(t)\mathrm{d}t = \frac{1}{T_s}\int_0^{Ts}\sum_{m=0}^{N-1} S_{n,m}g_m(t)g_k^*(t)\mathrm{d}t = \sum_{m=0}^{N-1} S_{n,m}\frac{1}{T_s}\int_0^{Ts} g_m(t)g_k^*(t)\mathrm{d}t = \sum_{m=0}^{N-1} S_{n,m}\delta_{m,k} = S_{n,k} \tag{2.9}$$

In practical applications with a high number of subcarriers, the OFDM transmit signal $s_n(t)$ is generated as a time-discrete signal in the digital baseband and then, the transmit signal is sampled with the sampling interval $\Delta t = 1/B = 1/N\Delta f$. Thus, the k-th sampled equivalent baseband OFDM signal can be calculated as follows:

$$\begin{aligned} S(t) &= \sum_{k=0}^{N-1} S_{n,k}e^{j2\pi k\Delta f t} \\ S(i\Delta t) &= \sum_{k=0}^{N-1} S_{n,k}e^{j2\pi k\Delta f i\Delta} \\ Sn,i &= \sum_{k=0}^{N-1} S_{n,k}e^{j2\pi ik/N} = IDFT\{S_{n,k}\} \end{aligned} \tag{2.10}$$

The expression (2.10) describes the inverse discrete Fourier transform (IDFT) applied to the complex valued modulation symbols $S_{n,k}$ of all subcarrier signals inside a single OFDM symbol.

The receiver just performs a discrete Fourier transform to recover the data symbols from the signal.

2.2 RF Communication

2.2.1 Effects of Nonlinearity

The nonlinearity of a system can be expressed as a Taylor series in terms of the input signal voltage:

$$v_0 = a_0 + a_1 v_i + a_2 v_i^2 + a_3 v_i^3 + \cdots . \tag{2.11}$$

where the Taylor coefficients are defined as

$$a_0 = v_0 \qquad (DC\ output) \tag{2.12}$$

$$a_1 = \frac{dv_0}{dv_i}|_{vi=0} \qquad (linear\ output) \tag{2.13}$$

$$a_2 = \frac{d^2 v_0}{dv_i^2}|_{vi=0} \quad (squared\ output) \tag{2.14}$$

and higher order terms[8]. Therefore, different expressions can be obtained from the nonlinear system depending on the dominance terms in the expansion. If a_1 is the only nonzero coefficient is achieved the linearity and system will work as linear attenuator($a_1 < 1$) or as amplifier($a_1 > 1$). If a_2 is the only nonzero coefficient the system will work as a mixer and other frequency conversion functions. However, in many cases a series expansion containing many nonzero terms will occur.

2.2.2 Gain Compression

When a single sinusoid is applied to the input of a nonlinear system, such as an amplifier:

$$v_i = V_o \cos w_0 t \tag{2.15}$$

Then, through (2.22) the output voltage will appear as

$$\begin{aligned} v_0 &= a_0 + a_1 V_o \cos w_0 t + a_2 V_o^2 \cos^2 w_0 t + a_3 V_o^3 \cos^3 w_0 t + \cdots \\ &= (a_0 + \frac{1}{2} a_2 V_0) + (a_1 V_0 + \frac{3}{4} a_3 V_0^3) \cos w_0 t \\ &+ \frac{1}{2} a_2 V_0^2 \cos 2 w_0 t + \frac{1}{4} a_3 V_0^3 \cos 3 w_0 t + \cdots \end{aligned} \tag{2.16}$$

From the above expansion, an voltage gain expression at frequency w_0 can be obtained:

$$G_v = \frac{v_0^{(w_0)}}{v_i^{(w_0)}} = \frac{a_1 V_0 + \frac{3}{4} a_3 V_0^3}{V_0} = a_1 + \frac{3}{4} a_3 V_0^2. \tag{2.17}$$

retaining only terms through the third order.

The expression (2.17) shows that the voltage gain is defined by a_1 coefficient, that represents the linear response, added with $3a_3 V_0^2/4$ coefficient that is proportional to the square of the input voltage amplitude. Since in many power amplifiers a_3 is negative, due power supply voltage used to bias the device, the gain voltage tends to decrease as a function of V_0^2. In RF circuits this effect is called gain compression or saturation and can be quantified by the "1-dB compression point", defined as the input signal level that causes the voltage gain drop by 1 dB.

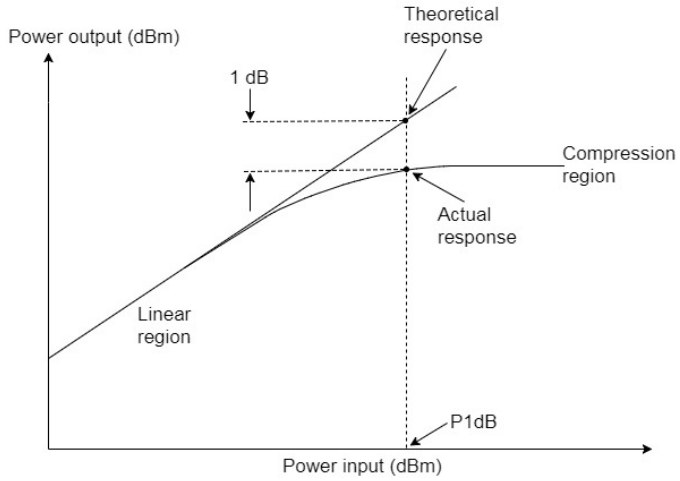

Figure 2.2: 1-dB compression point [5]

The figure 2.2 plots the input power versus output power, which represents the voltage gain. The straight line with a slope of unity defines the linear region, then the output power begins to decrease, resulting in reduced gain. The flat gain becomes nonlinear and produces signal distortion, harmonics, and potentially intermodulation products.

To quantify the linear operating region, it is defined the 1 dB compression point as the power level for which the output power has decreased by 1 dB from the ideal characteristic.

2.2.3 Intermodulation Distortion

Intermodulation distortion is a nonlinear effect of two or more signals mixing within a device to produce undesirable higher-order products. If the signals are close together in terms of frequency, some of the sum and difference frequencies called intermodulation products will fall within the band of interest.

When a two-tone input voltage with two closely frequencies , w1 and w2:

$$v_i = V_1 \cos w_1 t + V_2 \cos w_2 t \tag{2.18}$$

From expression (2.11) the output is:

$$v_0 = a_0 + a_1(V_1 \cos w_1 t + V_2 \cos w_2 t) + a_2(V_1 \cos w_1 t + V_2 \cos w_2 t)^2 \tag{2.19}$$

$$+ a_3(V_1 \cos w_1 t + V_2 \cos w_2 t)^3 + \cdots \tag{2.20}$$

Expanding the left side and discarding dc terms and harmonics, the following intermodulation

products are obtained:

$$
\begin{aligned}
w = w_1, w_2 &: (a_1 v_1 + \frac{3}{4} a_3 v_1^3 + \frac{3}{2} a_3 v_1 v_2^3) \cos w_1 t + (a_1 v_2 + \frac{3}{4} a_3 v_2^3 + \frac{3}{2} a_3 v_2 v_1^2) \cos w_2 t \\
&= w_1 \pm w_2 : a_2 v_1 v_2 \cos(w_1 + w_2)t + a_2 v_1 v_2 \cos(w_1 - w_2)t \\
&= 2w_1 \pm w_2 : \frac{3}{4} a_3 v_1^2 v_2 \cos(2w_1 + w_2)t + \frac{3}{4} a_2 v_1^2 \cos(2w_1 - w_2)t \\
&= 2w_2 \pm w_1 : \frac{3}{4} a_3 v_2^2 v_1 \cos(2w_2 + w_1)t + \frac{3}{4} a_3 v_2^2 v_1 \cos(2w_2 - w_1)t
\end{aligned}
\tag{2.21}
$$

Figure 2.3 plots the fundamental components and the intermodulation products. Of particular interest are the intermodualtion products at $2w_1 - w_2$ and $2w_2 - w_1$.

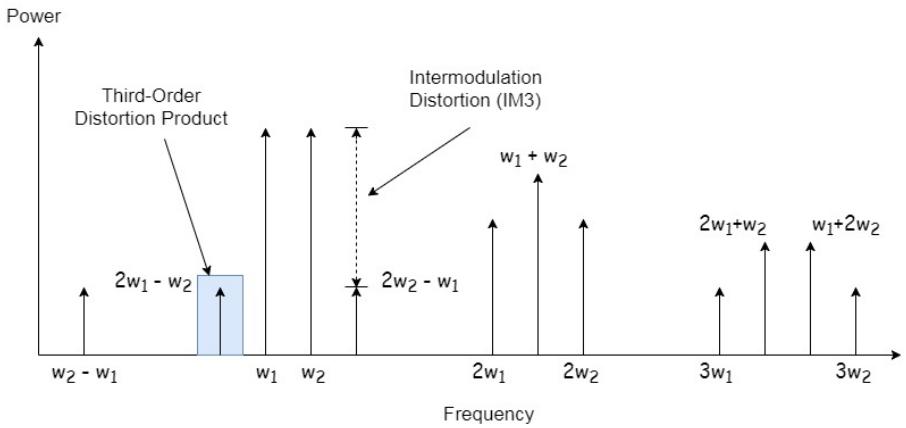

Figure 2.3: Output spectrum of second and third-order intermodulation products, assuming $w_1 < w_2$.[7]

Since the first and second order products are spaced enough from fundamental components, it can be easily filter out. However, if the difference between w_1 and w_2 is small, the components at $2w_1 - w_2$ and $2w_2 - w_1$ appear in the vicinity of w_1 and w_2. These cannot be filter out, so they ultimately become interfering signals to the main signals, causing distortion of the output signal. This effect is called third-order intermodulation distortion.

2.2.4 Thrid Order-Intercept point

To characterize the third-order intermodulation, has been used the third-order intercept point (IP_3) to characterize signal corruption due to third order products that appear in the vicinity of the fundamental tones. This parameter is measured by a two-tone test through expression (2.18), in which $V_1 = V_2 = V_{in}$,where the higher-order nonlinear terms with the same order will increase with the same power level.

Expression (2.21) shows that as the input voltage V_{in} increases, the fundamentals products increase in proportion to V_{in}, whereas the third-order products increase in proportion V_{in}^3. Since power is proportional to the square of voltage, the output power of third-order products should

increases as the cube of input power. Thus, output power for the first- and third-order products versus input power can be plotted on logarithmic scale, as shown in Figure 2.4.

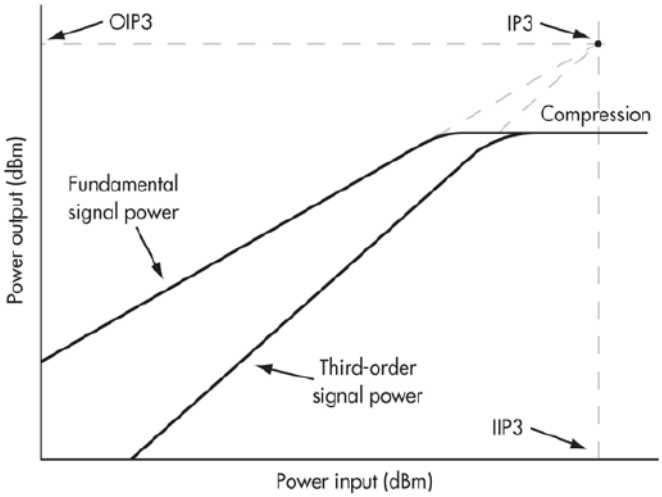

Figure 2.4: Third-order interception. [5]

The third order intercept point is defined to be at the intersection of two lines. The horizontal coordinate of this point is called the input $IP_3(IIP_3)$, and the vertical coordinate is called the output $IP_3(OIP_3)$ [9]. Both the first- and third- order responses will exhibit compression at high input powers, so the extension of their idealised responses are represented with dotted lines.

From the expansion of Taylor coefficients of expression 2.21, it can be expressed the output power of IP_3. Defining P_{w1} as the output power of the desired signal at frequency w_1 and assuming $V_1 = V_2 = V_{in}$. Then from expression 2.21:

$$P_{w1} = \frac{1}{2} a_1^2 V_{in}^2 \tag{2.22}$$

If we define P_{2w_1-w2} as the output power of third-order product, at frequency $2w_1 - w2$. Thus, from expression 2.21:

$$P_{2w_1-w2} = \frac{1}{2}(\frac{3}{4} a_3 V_{in}^3)^2 = \frac{9}{32} a_3^2 V_{in}^6 \tag{2.23}$$

By definition, these two powers are equal at the third- order interception point. Setting the input voltage at the interception point as V_{IP}, then equating expression 2.22 and 2.23:

$$\frac{1}{2} a_1^2 V_{IP}^2 = \frac{9}{32} a_3^2 V_{IP}^6 \tag{2.24}$$

Solving for V_{IP}:

$$V_{IP} = \sqrt{\frac{4a_1^2}{3a_3^2}} \tag{2.25}$$

Therefore, IP_3 is equal to P_{w1} at the interception point, so from expression 2.22 and 2.24:

$$P_3 = P_{w_1}\Big|_{V_{in}=V_{IP}} = \frac{1}{2}a_1^2 V_{IP}^2 = \frac{2a_1^3}{3a_3} \tag{2.26}$$

2.2.5 Dynamic Range

Dynamic range can be defined as the operating range for which a component or system has desirable characteristics. In power amplifiers, this means that power range is limited at the low end by the noise and at high end by the compression point. Resulting in a linear zone where it is desirable power amplifiers to operate, called dynamic range(DR_l). For low-noise amplifiers and mixers, the low end is limited by the noise and at high end is limited by intermodulation distortion. This defines the operating range for which spurious responses are minimal, and is called the spurious-free dynamic range(DR_f).

Superios-free dynamic range is defined for maximum output signal power at which the power of third-order intermodulation product is equal to the noise level. If P_{w1} represents the output power of desired signal at frequency $w1$, and P_{w2-1} represents the output power of third-order intermodulation, thus the spurious-free dynamic range is expressed as:

$$DR_f = \frac{P_{w_1}}{P_{2_{w_1}-w_2}}, \tag{2.27}$$

where P_{w2-1} is equal to the noise level[8].

From expressions (2.22) and (2.26), P_{w2-1} can be written as function of IP_3 and P_{w1}:

$$P_{2_{w_1}-w_2} = \frac{9}{32}a_3^2 V_{in}^6 = \frac{\frac{1}{8}a_1^6 V_{in}^6}{\frac{4a_1^6}{9a_3^2}} = \frac{(P_{w1})^3}{(P_3)^2} \tag{2.28}$$

Expression (2.28) shows that the third-order intermodulation power increases with the cube of the input signal power. Thus, equating expressions 2.27 and 2.28 gives the spurious free dynamic range in terms of IP_3 and N_0:

$$DR_f = \frac{P_{w_1}}{P_{2_{w_1}-w_2}}\Big|_{P_{2_{w1}-w_2}=N_0} = \left(\frac{IP_3}{N_0}\right)^{2/3} \tag{2.29}$$

Although the above expressions have been derived from the third-order intermodulation term, $2_{w1}-w_2$, the same result applies to the $2_{w2}-w_1$ term.

2.2.6 S-Parameters

S (scattering) parameters are used to characterize electrical networks using matched impedances. Traditional low-frequency parameters such as resistance, capacitance, and gain can be frequency-dependent, and thus may not fully describe the performance of eletronic circuits at the desired frequency. [4]

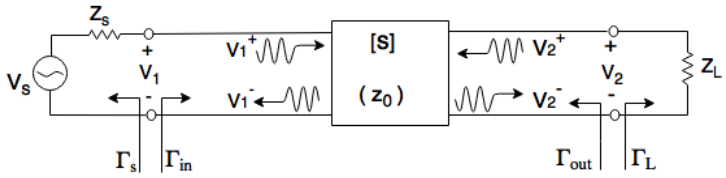

Figure 2.5: Two-port network with source and load impedances. [8]

Figure 2.5 shows a two-port network with scatering matrix[S], connected to source and load impedances Z_s and Z_L. In general case, mismatches exist at source and load, so these mismatches can be defined in terms of following reflection coefficients:

Γ_S = reflection coefficient looking toward generator
Γ_{in} = reflection coefficient looking from source to network
Γ_{out} = reflection coefficient looking from load to network
Γ_L = reflection coefficient looking towards load

In accordance with previous figure, the reflection coefficient looking toward the load is:

$$\Gamma_L = \frac{Z_L - Z_0}{Z_L + Z_0} \tag{2.30}$$

While the reflection coefficient looking toward the source is:

$$\Gamma_S = \frac{Z_S - Z_0}{Z_S + Z_0} \tag{2.31}$$

where Z_0 is the characteristic impedance reference for the S parameters of two port network.

Since the input impedance of two port network will be mismatched with a reflection coefficient given by Γ_{in}. Which can be determined from the definition of S-parameters and the fact that $V_2^+ = \Gamma_L V_2^-$, thus:

$$V_1^- = S_{11}V_1^+ + S_{12}V_2^+ = S_{11}V_1^+ + S_{12}\Gamma_L V_2^-, \tag{2.32}$$

$$V_2^- = S_{21}V_1^+ + S_{22}V_2^+ = S_{21}V_1^+ + S_{22}\Gamma_L V_2^-. \tag{2.33}$$

Suppressing V_2^- from expression (2.32) and computing V_1^-/V_1^+ gives:

$$\Gamma_{in} = \frac{V_1^-}{V_1^+} = S_{11} + \frac{S_{12}S_{21}\Gamma_L}{1 - S_{22}\Gamma_L} = \frac{Z_{in} - Z_0}{Z_{in} + Z_0} \tag{2.34}$$

Similarly, the reflection coefficient looking from load to network can be computed following the same approach:

$$\Gamma_{out} = \frac{V_2^-}{V_2^+} = S_{22} + \frac{S_{12}S_{21}\Gamma_S}{1 - S_{11}\Gamma_S}. \tag{2.35}$$

Solving for V_1 by voltage division,

$$V_1 = V_S \frac{Z_{in}}{Z_S + Z_{in}} = V_1^+ + V_1^- = V_1^+(1+\Gamma_{in}). \tag{2.36}$$

Thus, solving expression (2.34) for Z_{in} gives:

$$Z_{in} = Z_0 \frac{1+\Gamma_{in}}{1-\Gamma_{in}}, \tag{2.37}$$

and with these result, V_1^+ can be solved in terms of V_S,

$$V_1^+ = \frac{V_S}{2} \frac{1+\Gamma_S}{1-\Gamma_S\Gamma_{in}}. \tag{2.38}$$

Therefore, the average power delivered to the input network is:

$$P_{in} = \frac{1}{2Z_0}|V_1^+|^2(1-|\Gamma_{in}|^2) = \frac{|V_S|^2}{8Z_0} \frac{|1-\Gamma_S|^2}{|1-\Gamma_{in}\Gamma_S|^2}(1-|\Gamma_{in}|^2) \tag{2.39}$$

In the same way, the average power delivered to the output network is:

$$P_L = \frac{|V_2^-|^2}{2Z_0}(1-|\Gamma_L|^2) \tag{2.40}$$

Computing for V_2^- from expression (2.33), replacing in (2.40), and using expression (2.38) gives:

$$P_L = \frac{|V_1^+|^2}{2Z_0} \frac{|S_{21}|^2(1-|\Gamma_L|^2)}{|1-S_{22}\Gamma_L|^2} = \frac{|V_S|^2}{8Z_0} \frac{|S_{21}|^2(1-|\Gamma_L|^2)|1-\Gamma_S|^2}{|1-S_{22}\Gamma_L|^2|1-\Gamma_S\Gamma_{in}|^2} \tag{2.41}$$

The power gain can be given as:

$$G = \frac{P_L}{P_{in}} = \frac{|S_{21}|^2(1-|\Gamma_L|^2)}{(1-|\Gamma_{in}|^2)|1-S_{22}\Gamma L|^2} \tag{2.42}$$

When input and output network are perfected matched, then $\Gamma_L = 0$ and $\Gamma_S = 0$, where all the power delivered to the input network is transferred to the output network. Thus, power gain reduces to:

$$G = |S_{21}|^2. \tag{2.43}$$

2.2.7 Stability

The design of power amplifier circuit always requires a trade-off between performance and stability. The goal is to design an amplifier that is stable over the entire operating range, covering temperature, bias voltages, input power and load impedance, without sacrificing too much performance because of stability improvement.[12]

The stability analyses arises as a necessity to avoid oscillation of the amplifier, this can happen if at a given frequency the input or output port impedance of the amplifier circuit has a negative real part, what will imply $|\Gamma_{in}| > 1$ or $|\Gamma_{out}| > 1$.

Thus, it was defined two types of stability: unconditional stability and conditional stability.

Unconditional stability happens when $|\Gamma_{in}| < 1$ and $|\Gamma_{out}| < 1$ for all passive source and load impedances (i.e. $|\Gamma_S| < 1$ and $|\Gamma_L| < 1$).

Conditional stability means that $|\Gamma_{in}| < 1$ and $|\Gamma_{out}| < 1$ for a certain range of passive source and load impedances, also called potentially unstable.

2.2.7.1 Stability Test

Different tests are used to evaluate the stability of amplifier circuit. The stability circles allows compute the conditional stability and plot on the Smith chart the region where amplifier is stable. On the other hand, the Rollet factor and μ factor allows compute the unconditional stability.

The $K-\Delta$ test, known as Rollet factor, can be calculated by the following expression

$$K = \frac{1-|S_{11}|^2-|S_{22}|^2+|\Delta|^2}{2|S_{11}S_{22}|} > 1, \tag{2.44}$$

together with the auxiliary condition

$$|\Delta| = |S_{11}S_{22} - S_{12}S_{21}| < 1, \tag{2.45}$$

where both conditions must be satisfied. If both conditions are met, they are sufficient to ensure unconditionally stability, otherwise stability circles must be plotted to determine the stable region.

The μ factor is other method commonly used, where only one condition must be met to ensure unconditionally stability of the amplifier.

$$\mu = \frac{1-|S_{11}|^2}{|S_{22}-\Delta S_{11}^*| + |S_{12}S21|} > 1, \tag{2.46}$$

Since μ>1, unconditional stability will be guaranteed, where larger values will imply greater stability.

2.2.8 Noise Figure

Low noise amplifiers (LNAs) are one of the most critical elements used in modern wireless communication systems, where a small noise figure is a common requirement.[3] The noise figure (NF) allows to describe the noise performance and the sensitivity of receiving systems. An optimization of the NF leads to a gain degradation, so it is necessary to make some sort of compromise between the NF and the gain.

Several methods and formulas for analysing and compute the NF of the circuit have been proposed. In the book "Microwave And RF Design of Design Wireless Systems" it was derived the following expression that allows compute the NF of a two-port amplifier:

$$F = F_{mim} + \frac{4R_N}{Z_0}\frac{|\Gamma_S - \Gamma_{opt}|^2}{(1-|\Gamma_S|^2)|1+\Gamma_{opt}|^2}, \tag{2.47}$$

where:

R_N = equivalent noise resistance.

Γ_{opt} = optimal source reflection coefficient to obtain the minimum noise figure.

F_{min} = minimum noise figure, obtained when $\Gamma_{opt} = \Gamma_S$

2.2.9 Error Vector Magnitude (EVM)

EVM is defined by the vector subtraction of the reference signal from the corresponding measured signal at a specific point in a constellation. The reference signal, is a ideal signal with perfect modulation and has an infinitesimal Bit Error Rate in a noiseless environment. Magnitude error and phase error are defined as the magnitude and phase differences between the measured signal and the reference signal. See Figure 2.6

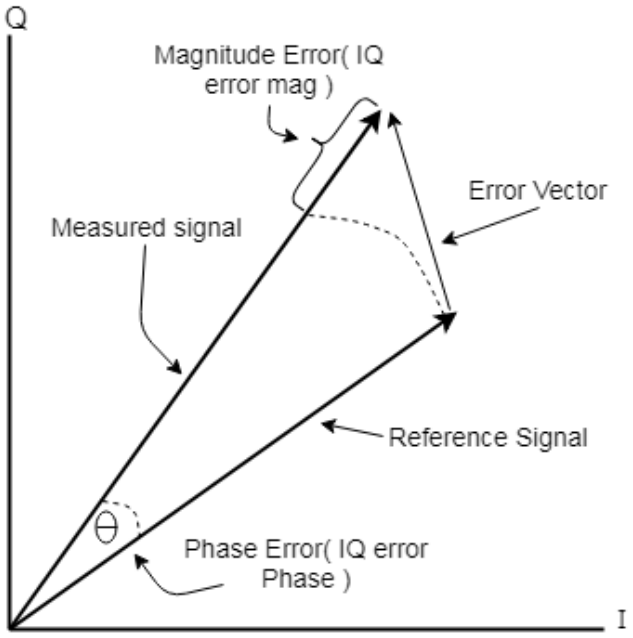

Figure 2.6: Signal Spectrum [6]

Different modulation systems have different amplitude levels. To calculate and compare the EVM measurements effectively some normalization is typically carried out. Normalization is derived in such a way that the mean square amplitude of all possible symbols in the constellation of any modulation scheme is one. Thus, EVM is defined as the root-mean-square (RMS) value of the difference between a collection of measured symbols and ideal symbols. These differences are calculated over a given large number of symbols, and are generally shown as a percent of the average power per symbols of the constellation.

EVM can be expressed mathematically as

$$EVM_{RMS} = \frac{\frac{1}{N}\sum_{n=1}^{N}|S_n - S_{n,0}|^2}{\frac{1}{N}\sum_{n=1}^{N}|S_{n,0}|^2}, \tag{2.48}$$

where S_n is the normalized nth symbol in the stream of measured symbols, $S_{0,n}$ is the ideal normalized constellation point of the nth symbol and N is the number of unique symbols in the constellation. The expression in (2.48) cannot be replaced by their unnormalized value since the normalization constant for the measured constellation and the ideal constellation are not the same. The normalization scaling factor for ideal symbols is given by

$$|A| = \sqrt{\frac{1}{\frac{P_v}{T}}} = \sqrt{\frac{T}{P_v}}, \tag{2.49}$$

where Pv is the total power of the measured constellation of T symbols. For *RMS* voltage levels of inphase and quadrature components, V_I and V_Q and for $T >> N$, it can be shown that P_v can be expressed as

$$P_v = \sum_{t=1}^{T} \left[(V_{I,t})^2 + (V_{Q,t})^2\right](W), \tag{2.50}$$

The normalization factor for ideal case can be directly measured from N unique ideal constellation points and is given by

$$|A_0| = \sqrt{\frac{N}{\sum_{t=1}^{T} \left[(V_{I0,n})^2 + (V_{Q0,n})^2\right]}}, \tag{2.51}$$

Hence (2.48) can be further extended using normalization factors in (2.49) and (2.51) as

$$EVM_{RMS} = \frac{\frac{1}{T}\sum_{t=1}^{T} |I_t - I_{0,t}|^2 + |Q_t - Q_{0,t}|^2}{\frac{1}{T}\sum_{t=1}^{T} |I_{0,t}|^2 + |Q_{0,t}|^2}, \tag{2.52}$$

where $I_t = (V_{It})|A|$ is the normalized in-phase voltage for measured symbols and $I_{0,t} = (V_{I0,t})|A_0|$ is the normalized in-phase voltage for ideal symbols in the constellation, $Q_t = (V_{Qt})|A|$ is the normalized quadrature voltage for measured symbols and $Q_{0,t} = (V_{Q0,t})|A_0|$ is the normalized quadrature voltage for ideal symbols in the constellation [11].

Note that the EVM increases as a function of input power level at the high end due to intermodulation distortion. At the lower power levels, the increase in EVM is attributed to a reduction in SNR.

Chapter 3

Development

In this chapter the various solutions chosen to develop the RF transmitter and the RF receiver will be presented. Some design concerns have been taken into account to make RF communication as wideband as possible.

3.1 Design overview

The RF communication proposed and developed in this dissertation comprise the integration of several discrete components available in the electronics market. All of these components have as main feature, to operate on a wide range of frequencies below 1 GHz.

Figure 3.1 shows an overview of the purposed solution and the elements that compose each stage of communication.

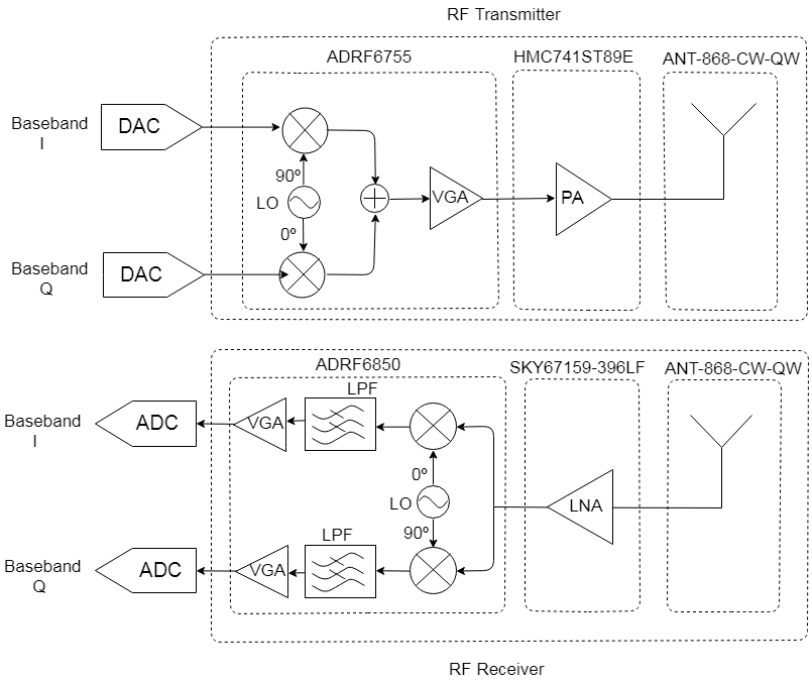

Figure 3.1: Block diagram RF

To develop up-conversion stage, it was used ADRF6755 from Analog Devices. This solution comprises a highly integrated quadrature modulator, frequency synthesizer, and programmable attenuator. Thus, it was possible to reduce the complexity and cost of development of such solution.

To the down-conversion stage, it was used a similar solution as used for the up-conversion stage. ADRF6850 from Analog Devices embrace a quadrature demodulator, frequency synthesizer, low pass filter, and variable gain amplifier.

As mentioned above, both solutions allow to fulfill all requirements and to build a low cost solution, which made them preferred over the remaining available in the electronics market.

The LNA was composed by the integrated circuit SKY67159-396LF from Skyworks. With a frequency range between 0.2 GHz and 3.8 GHz, it can cover all the desired frequency bands to establish communication bellow 1 GHz. With a power consumption of 148.5 mW and with an average noise figure of 1.2 dB, it makes this solution suitable to meet all the necessary requirements.

The power amplifier (PA) was developed with the integrated circuit HMC741ST89E from the Analog Devices. This solution has a frequency operation between 0.05 GHz and 3GHz, with an average power consumption of 480 mW .

To establish a wireless communication between the transmitter and the receiver it was used the antennas ANT-868-CW-QW-SMA from Linx Technologies. With a frequency range between 750 MHz and 950 MHz, only cover some of the desired frequency bands bellow 1 GHz.

3.2 Modulator

The quadrature modulator, ADRF6755, comprises an integrated fractional-N PLL and VCO with an operating frequency range from 100 MHz to 2400 MHz. Since the ADRF6755 is controlled by a bus interface, SPI, it allows to perform several tasks, just changing registers data. One of the most important settings is the ability to change the frequency of the local oscillator in less than 200μ seconds, just by updating a new instruction through SPI. This is one of the most important features of this solution, since communication between the RoMoVi and the base station will be done at non-reserved frequencies, other communications may occur at the same frequency.

Through SPI is possible to perform several tasks by programming and re-programming the data registers during normal operation without interrupt communication, if not required acquisition of a new transmission frequency.

With concerns to acquisition and resolution of PLL, ADRF6755 allows to configure a integer number of 12-bit and a fractional number with a 25-bit fixed modulus, allowing a frequency resolution of less than 1 Hz.

When everything is fully operational, the modulator has a power consumption of 1.9W, however, some functions are not required during a normal operation, such as differential outputs, that provide a replica of the internal local oscillator frequency. Since ADR6755 allows a power amplification of output RF signal between 0 and 47dB, it is possible to substantially reduce power consumption when such signal amplification is not required. RF output can be disabled when no data is transmitted, decreasing even more the power consumption. This is a better approach when

there is no communication for short intervals since disabling the entire device leads the PLL to lose lock.

Another interesting feature of ADRF6755 is the capability to drive baseband inputs with a maximum bandwidth of 600 MHz, although the OFDM baseband communication only requires a 6MHz bandwidth. To preserve a better signal integrity and maximum noise rejection, baseband inputs in-phase and quadrature are driven differential.

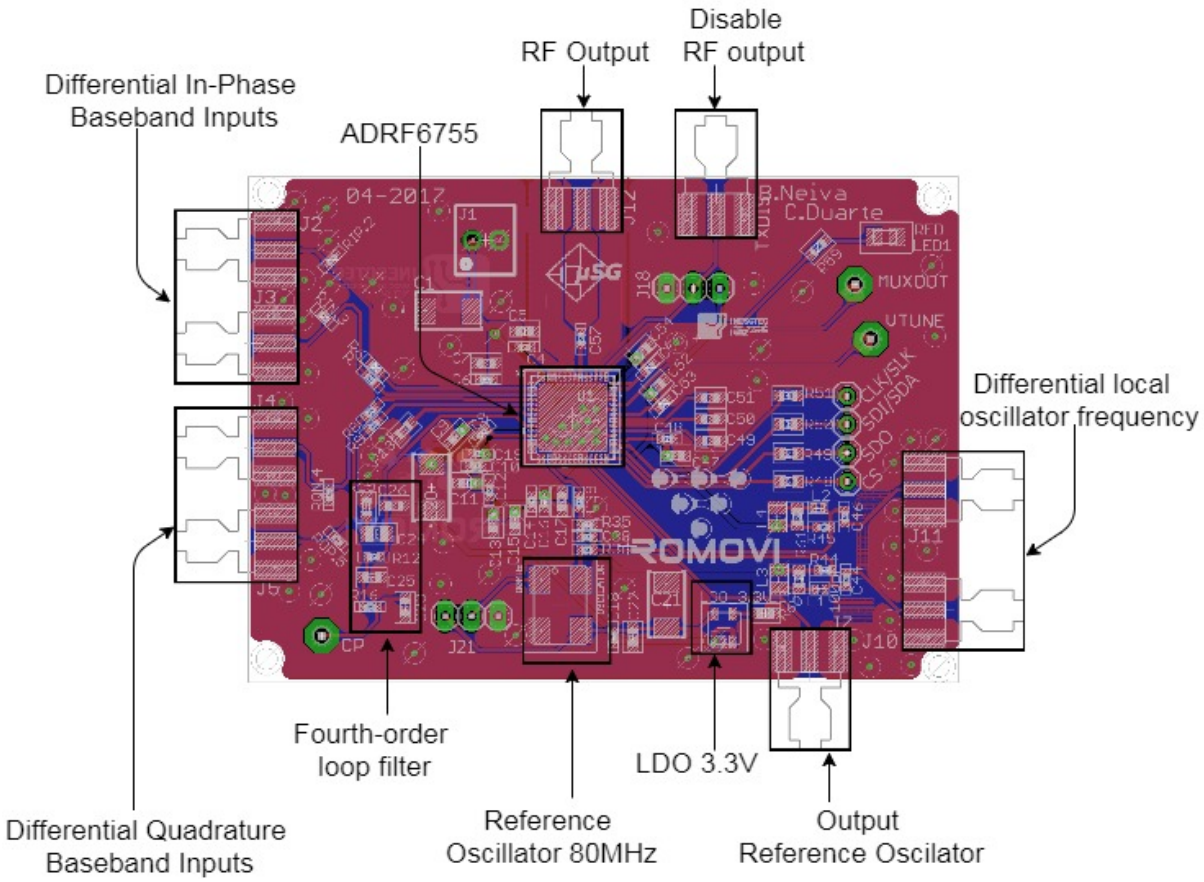

Figure 3.2: Layout modulador

From figure 3.2 can be seen the final PCB layout design to ADRF6850, where the main components of the modulator are highlighted. Although it is a very integrated solution, it required several external components, which increased the complexity of PCB design.

3.2.1 Design checking

3.2.1.1 Differential Baseband inputs

The ADRF6755 allows a maximum baseband bandwidth of 600MHz. However such bandwidth makes the impedance seen by the baseband inputs vary with the increase of the frequency. Thus, each baseband input was terminated with 50 ohm resistors, allowing the input impedance to remain flat across the baseband.

3.2.1.2 Reference oscillator

As a PLL clock reference, was used an SMD clock oscillator with a frequency of 80 MHz, with an average power consumption of 9.9mW. Some design concerns were taken, allowing to disable this reference through a digital port when it is not necessary.

3.2.1.3 Fourth-order loop filter

Analog Devices provides an ADIsimPLL software that assists in loop filter design, taking into account aspects such as loop bandwidth, output frequency and phase margin. After some designs in ADLsimPLL, it was realised that the loop filter has very closed to the one developed for the evaluation board and the constraints regarding how fast PLL acquire new lock are not critical.

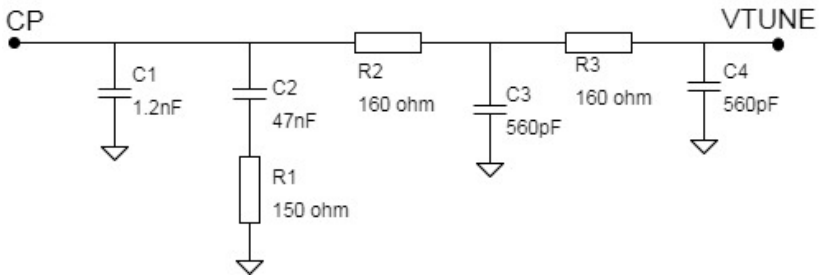

Figure 3.3: Fourth-order loop filter

The figure 3.3 shows the fourth-order loop filter, the same provided in the datasheet, as main features, a loop bandwidth with 100 kHz and a phase margin with 55°.

3.2.1.4 LDO 3.3V

To provide a 3.3V supply voltage to 80MHz reference oscillator was used a RT9193 LDO that allow drop 5V supply voltage to 3.3V.

3.2.1.5 Serial Peripheral Interface

ADRF6755 supports two different bus interfaces, SPI and I^2C. To control all data registers it was used an SPI interface, since allows to reduce the complexity due to each dedicated line. With this interface it is possible to program ADRF6755 at a maximum frequency of 20 MHz.

3.2.1.6 Local oscillator configuration

Local oscillator consists of a PLL and three VCOs, allowing to define a frequency range between 100 MHz and 2400 MHz. Through the expression (3.2), it is possible to compute the integer and fractional value to configure the local oscillator at desired frequency.

$$LO = f_{PFD} \times (INT + (FRAC/2^{25}))/2^{RFDIV}. \tag{3.1}$$

The VCOs can be configured through the divider, RFDIV, of Table 6 on the datasheet, it is possible to choose the correct value according to the local oscillator frequency.

The PLL consists of a fractional-N frequency synthesizer with a 25-bit fixed modulus, where through five registers it is possible to programme the fractional number, FRAC, and through two other registers programme the INT value with 12-bit.

3.2.2 Voltage Common Mode

SMIQ Vector Signal Generator from Rhodes & Schwartz will be used to test up-converter and down-converter stages. However, signal generator provides single-ended signals in-phase and quadrature. Thus, it was necessary to develop a PCB with two CX2041NLT Baluns, that could covert single-ended into differential signals.

Each in-phase and quadrature input signal of ADRF6755 must be dc-biased to approximately 500 mV. With baluns it is possible to provide a common voltage to each differential input of ADRF6755, since the signal generator is unable to add a offset dc voltage to the baseband signals.

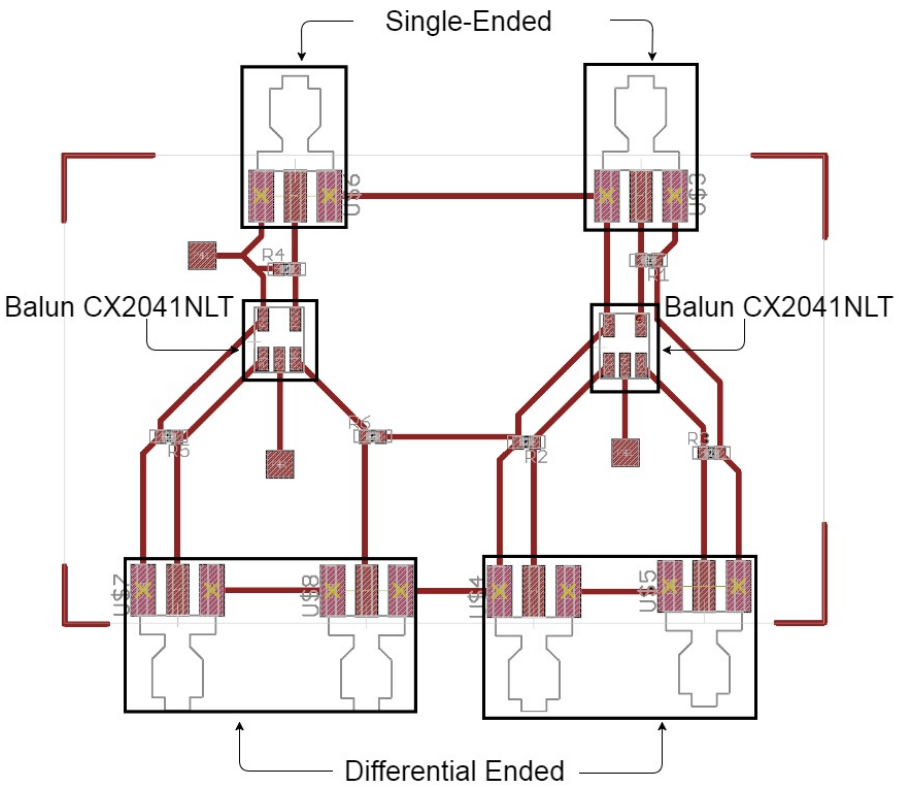

Figure 3.4: Layout voltage common mode

From figure 3.3 can be seen PCB layout that will do the interconnection between signal generator and up-converter stage, with the differential basebands driven with a dc voltage of 500 mV.

3.3 Demodulator

The quadrature demodulator ADRF6850 is a high integrated solution that allows a direct conversion to baseband signal. With a range between 0.1 GHz and 1 GHz, similar solution provided in up-converter stage, despite with some extra features that allow being a more complete solution and when configured in parallel with up converter, allows a synchronous communication.

From figure 3.5, it can be seen the final PCB layout and the main features that comprise the down-converter stage. As main feature, has the possibility of adding an internal or external dc voltage to the in-phase and quadrature differential baseband signals. Thus, it was decided that an internal reference dc voltage should be more appropriate to reduce the complexity of tests, however if it is necessary to set an external dc voltage, then resistor R20 must be removed

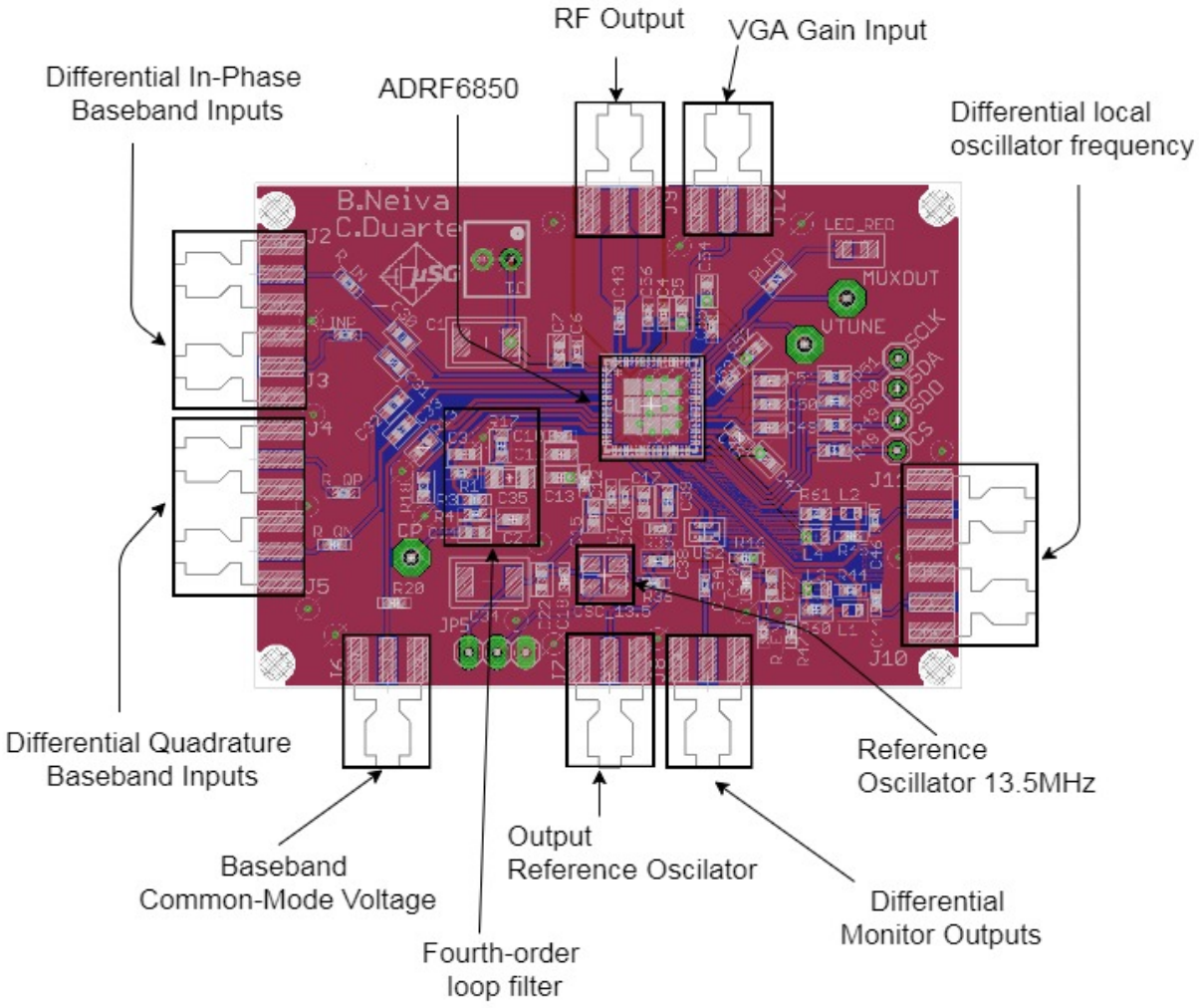

Figure 3.5: Layout demodulator

Through input VGAIN it is possible to drive a voltage between 0V and 1.5V, allowing an amplification of the in-phase and quadrature baseband outputs between 0dB and 60 dB.

To filter interferences, are provided four re-programmable filters with cutoff frequencies between 30 MHz and 50 MHz.

3.3.1 Design checking

3.3.1.1 Differential Baseband outputs

As mentioned in section 3.2.1.1, impedance seen by baseband signals changes across the bandwidth. Thus, each differential baseband signal was terminated with a series 50 ohm resistor, allowing the impedance seen for the output basebands to remain constant across the 250 MHz bandwidth.

3.3.1.2 Reference oscillator

ADRF6850 allows a input reference clock between 10 MHz and 165 MHz. As recommendation from manufactur was used a 13.5 MHz SMD Crystal oscillator with 3.3V voltage supply.

3.3.1.3 Fourth-order loop filter

ADIsimPLL software from Analog Devices was used to assist in loop filter design, however the datasheet provides the design of a loop filter with a 50 kHz loop bandwidth. Therefore, to avoid possible mistakes, it was decided to use the loop filter design provided in datasheet.

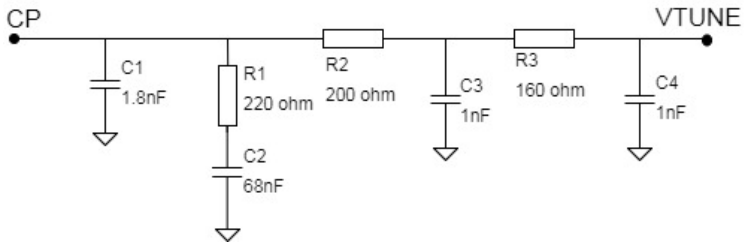

Figure 3.6: Fourth-order loop filter

From figure 3.6 it can be seen the components that compose the loop filter with a bandwidth of 50 kHz and a phase margin of 55°. Although a lower loop bandwidth increase the time to PLL acquire new lock. With this loop filter the PLL needs approximately 260μ seconds to acquire the lock.

3.3.1.4 Serial Peripheral Interface

ADRF6850 allows to control data registers through an SPI interface or an I^2C interface, but since it was used an SPI interface in the modulator, it becomes simpler to control data registers through the same interface. Therefore, in a future integration with baseband communication, both demodulator and modulator can be controlled through the same SPI interface.

3.3.1.5 Local oscillator configuration

The local oscillator, LO, is composed of a PLL and three VCOs, also as in ADRF6755, with a frequency range between 100 MHz and 1000 MHz. Through expression (3.2), it is possible to compute the integer and the fractional numbers to set the desired frequency of the local oscillator.

Through the divider, RFID, it is possible to choose the right VCO according with Table 6 provided in datasheet.

The fractional number, FRAC, with 25-bit fixed module is controlled by the first five registers and the integer number, INT, with 12-bit is controlled by registers 0x06 and 0x07, allows to configure the correct values. Thus, given the reference input frequency value, f_{PFD}, at input of PLL it is possible to set the desired local oscillator frequency.

3.4 Low Noise Amplifier

As mentioned in section 3.1, to design the low noise amplifier stage it was used the integrated circuit SKY67159-396LF, with the lowest power consumption of all RF communication.

To achieve the maximum efficiency in the desired frequency bands, it was necessary to develop a circuit with a matching network. Many possible architectures are suggested, however, a circuit with a matching network was provided on the manufacturer datasheet, allowing to cover all the frequencies of interest below 1 GHz. Figure 3.7 shows the components that compose this stage.

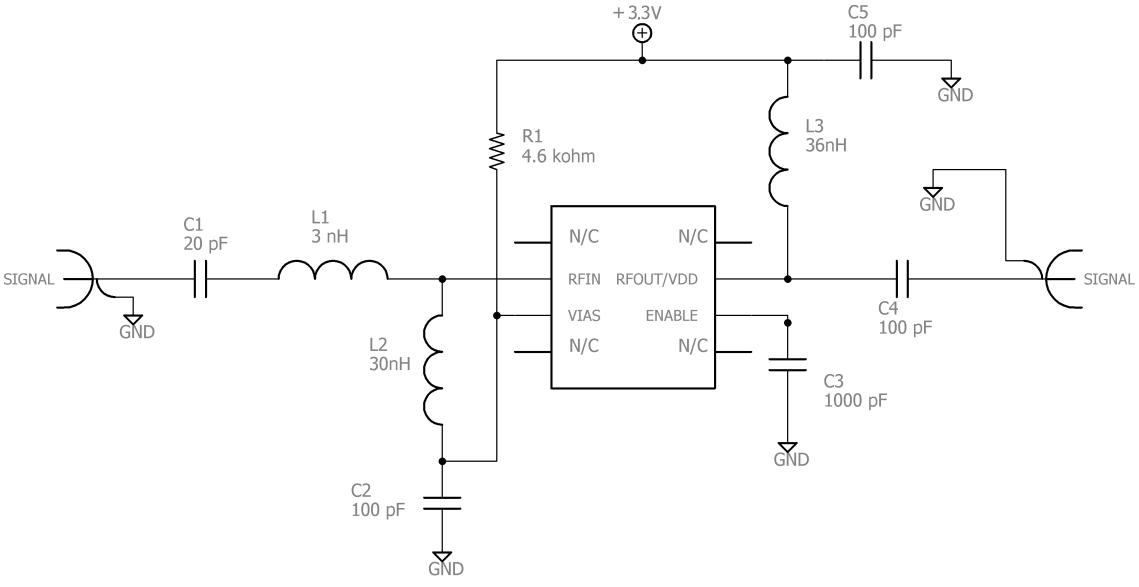

Figure 3.7: Schematic of low noise amplifier

Although the manufacturer provided the necessary circuit to operate at the desired frequencies, it was necessary to use the Agilent ADS from Keysight Technologies, a software strongly oriented to development of RF, microwave, and high speed digital applications, to take into account various

side effects during design and development, such as the different length and width of the signal lines.

Another interesting feature about Agilent ADS, is the possibility of using component libraries that contain their physical characteristics, so during a S-parameter simulation, it was possible to analyse the contribution of all elements.

With the desired performance during the schematic simulation, the PCB layout was designed, where a simulation was performed with all the components that compose the LNA. Through the ADS, it was possible to perform an electromagnetic simulation (EM simulation), where it was achieved a wide-band performance, covering all the frequencies of interest below 1 GHz (Figure 3.8).

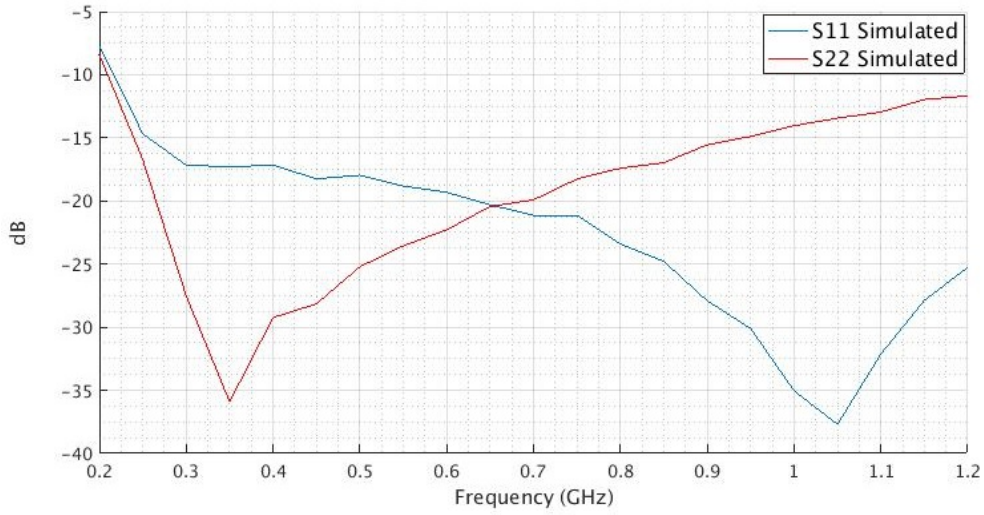

Figure 3.8: S11 and S22 of LNA

As shown in figure 3.8 the parameter S11 is bellow -16 dB between 0.3 GHz and 1.2 GHz, which means that less than 3% of the input signal is reflected to the source. A similar analysis can be done for the output signal, where S22 is below -14 dB between 0.3 GHz and 1 GHz, which means that 96% of the output signal is delivered to the load.

The design of an LNA stage always requires a trade-off between the lowest noise figure and the maximum gain, however, during the development it was realized that the manufacturer does not provide enough data to analyze the noise figure, so it was not possible to calculate the noise figure during the design. Since is being used the same circuit provided in the manufacturer datasheet, where it is described a noise figure lower than 1.3 dB across all the frequencies, it was decided to proceed with the development of the LNA stage. However, as will be seen in section 4.4.1, the laboratory tests showed a noise figure very close to that described in the manufacturer datasheet.

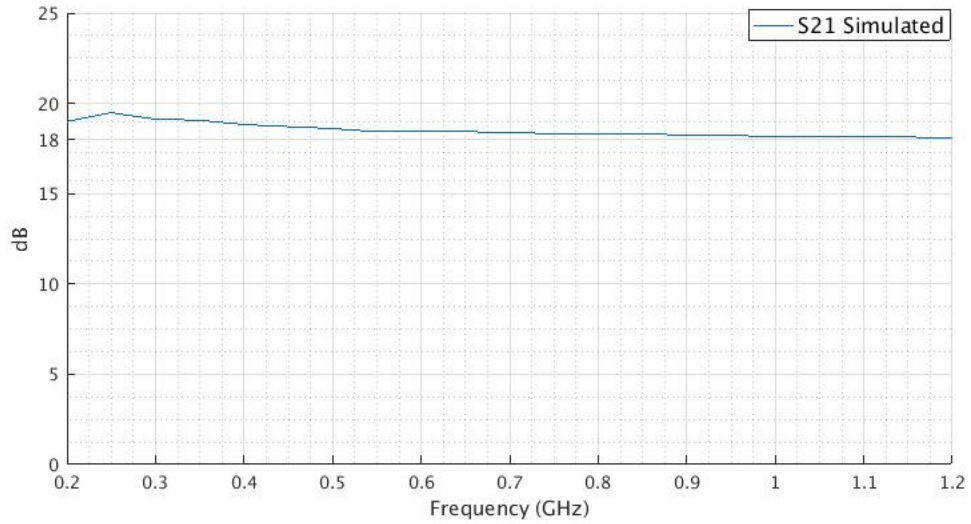

Figure 3.9: S21 of LNA

Figure 3.9 plots the S21 parameter, representing the gain, where an average gain of 19 dB was reached between 0.2 GHz and 1.2 GHz. After comparing with the gain plotted in the manufacturer datasheet, it can be concluded that, the different components and the different PCB substrate used did not decrease the LNA performance.

3.4.1 Stability

Design an amplifier always raises concerns about stability, that if it is not ensured, the amplifier can oscillate at a certain frequency, leading to instability.

As mentioned in section 2.2.7, several methods have been employed to test the stability, however one of the methods commonly used is the μ factor, which allows the expression (2.46) to ensure unconditional stability if μ>1.

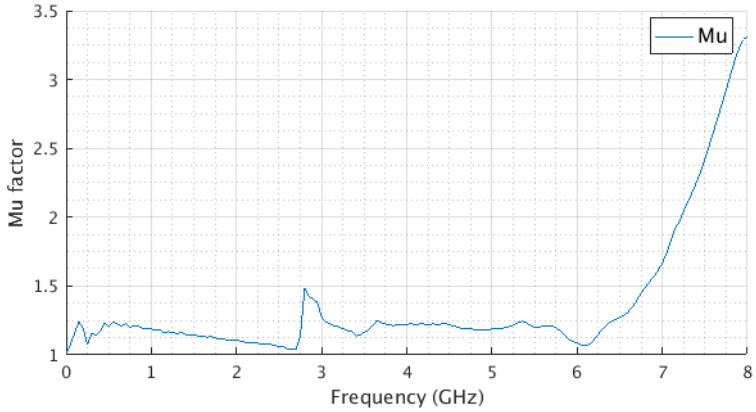

Figure 3.10: Stability factor of LNA

With the extracted S-parameters, μ can be easily computed through Matlab , however, ADS provides a function that directly compute the stability across all the frequencies. From figure 3.10

can be seen the μ factor, where is above 1 at all frequencies, then it can be concluded that the LNA is unconditionally stable, not raising stability concerns.

3.5 Power Amplifier

To design the PA, the same steps were followed as during the design of the LNA, however, some constraints were more relaxed, since it was not necessary to take into account the noise figure.

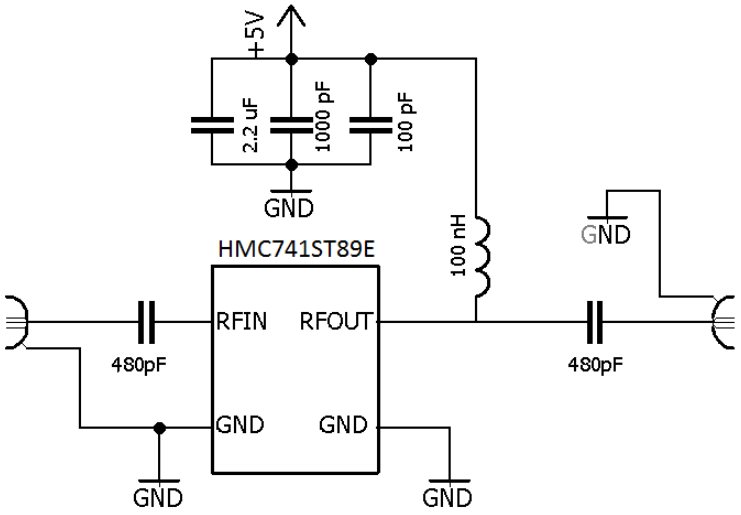

Figure 3.11: Schematic power amplifier

Figure 3.11 shows the schematic used to develop the PA, the same schematic suggested by the manufacturer. It is clear the absence of a matching network, because the IC that composes the PA is internally wideband matched, which made the development procedure much simpler.

Regarding the PA simulation, were followed the same steps as in the LNA simulation. In the schematic simulation, it was performed a simulation using the two-port measurement, where only was measured the S-parameters of the components, leaving out the side effects introduced by the PCB traces. This step was fundamental, because it allowed to guarantee the desired performance of the circuit suggested by the manufacturer.

During the layout simulation it was performed an accurate simulation as in the LNA simulation, through the EM simulation. This allowed not only measuring the effects of the traces, but also measuring the contribution of the vias that connect the top ground plane with the bottom ground plane.

The figure 3.12 shows the S11 and S22 parameters after performed the EM simulation. It becomes clear that the desired performance has been achieved since the PA can operate at all desired frequencies below 1 GHz with return losses below -10 dB.

With a more detailed analysis, it can be seen that the S11 is less than -11 dB between 0.2 GHz and 1GHz, which means that less 8% of the input signal is reflected back to the source. The S22,

remains below -15 dB in the same frequency bands, with more than 94% of the output power signal delivered to the load.

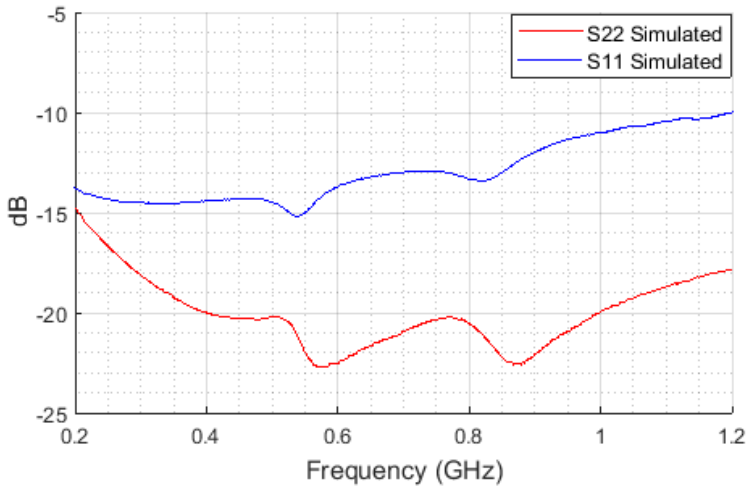

Figure 3.12: S11 and S22 PA

The gain, parameter S21 represented in figure 3.13, remains above 20 dB between 0.2 GHz and 1 GHz, with a maximum of 21 dB at 0.2 GHz.

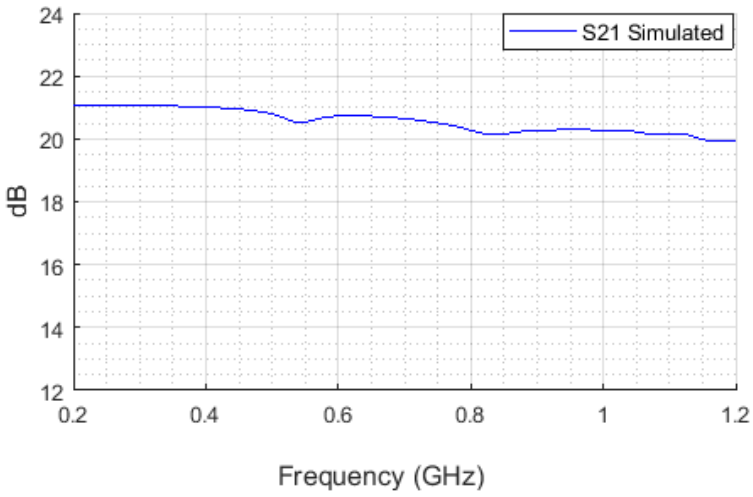

Figure 3.13: Stability factor PA

3.5.1 Stability

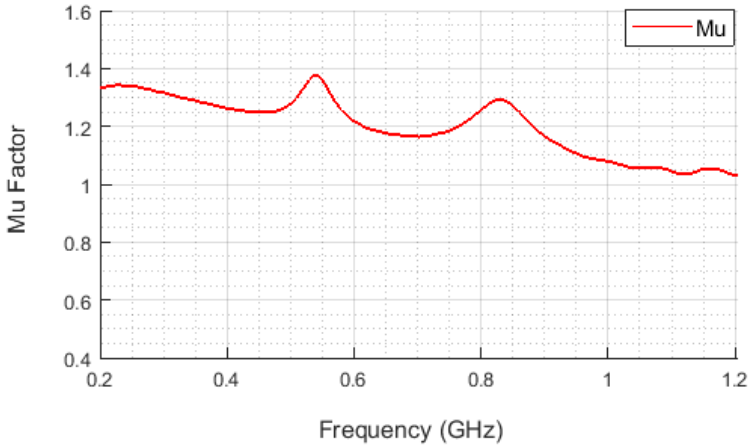

Figure 3.14: S21 PA

As done in the LNA stage, it was used the μ factor to calculate the stability factor of the PA . The figure 3.14 shows the μ factor between 0.2 GHz to 1.2 GHz, where it is above one at all frequencies.

Chapter 4

Testing & Debugging

This chapter guides through all measurements and results extracted from the solutions developed in previous chapter.

To control data registers of the demodulator and the modulator, it was used an Arduino Uno, with an SPI library that allows to define the bit rate and the ports to communicate. Thus, with Arduino acting as master, it was developed a C code that allowed programming and update data registers of the modulator and the demodulator during a normal operation.

4.1 Modulator

Figure 4.1 shows the PCB modulator with the required components to perform a normal operation. During the soldering stage, it was noticed that some errors were made during the design, so it was decided to just assemble the required components to ensure that the modulator was operating according as expected.

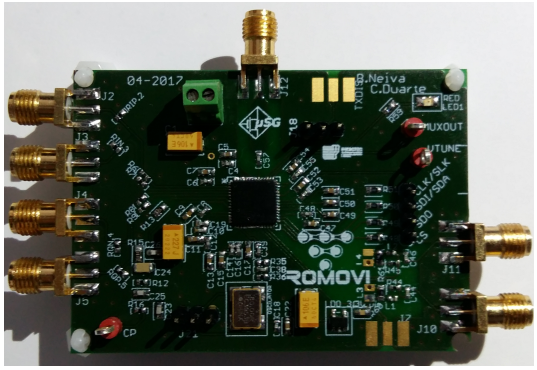

Figure 4.1: PCB modulador

As mentioned in a section 3.1.2, to provide a complete test of the modulator, it was used a signal generator SMIQ 03B from Rhodes & Schwartz. With a range frequency between 300 kHz and 3.3 GHz, it allows to define several digital modulations with a maximum $18M$ symbols per second. Thus, as main requirement from baseband communication, it is a 6 MHz bandwidth with a 16 QAM modulation.

To evaluate RF output signal it was used ZVL3 Vector Network Analyser from Rhodes & Schwartz, with a dynamic range between 9kHz and 3GHz and a maximum 27 dBm RF input signal, enabling a complete analysis of the radio frequency spectrum across the desired transmission frequency, which allowed to inspect the occupied bandwidth and the interferences present in the RF spectrum.

4.1.1 Local Oscillator

With everything fully biased, data registers were programmed in order to operate at 800 MHz frequency. Therefore, through the expression 3.2 provided in section 3.1.1.7, it was possible to setup PLL and VCO registers and analyse local oscillator at 800 MHz frequency.

Figure 4.2 provides a replica of the internal local oscillator with approximately 6 dB attenuation and a bandwidth of 1 kHz. The modulator allows three more levels of attenuation to LOMON differential outputs, since another purpose is bias other devices to operate at same frequency.

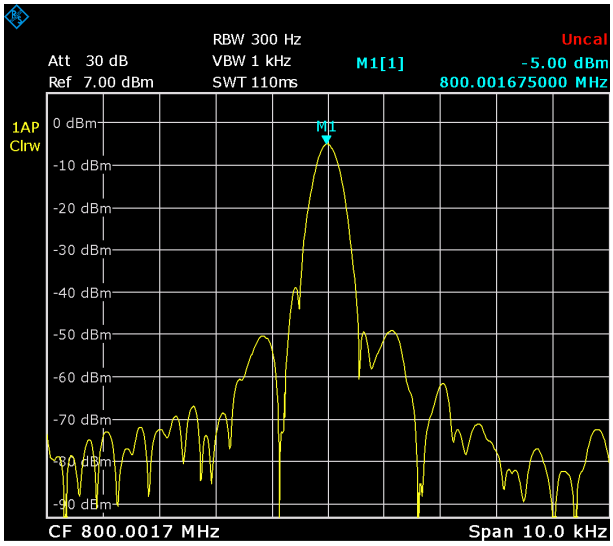

Figure 4.2: Local oscillator at 800MHz

Although the expression provided in the datasheet allows to compute the right values to setup the registers of the PLL and the VCO. It can be seen in figure 4.2 that the local oscillator has a deviation of 2.01 kHz above the desired frequency. Analysing the local oscillator at other frequencies, (see appendix A), it can be concluded this offset is not constant across the frequency band, arising the need to inspect the frequency of local oscillator.

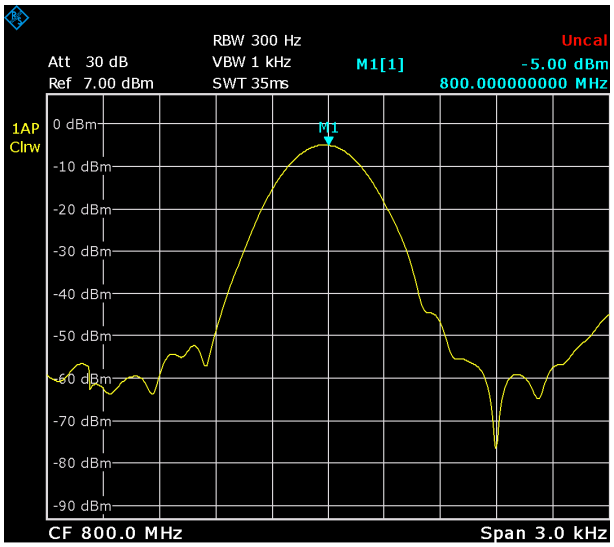

Figure 4.3: Local oscillator at 800 MHz with 0 Hz offset

Thus, through the 25-bit fractional number, it was possible to compensate this deviation, achieving a resolution with less than 1 Hz. Figure 4.3 shows local oscillator with 0 Hz offset at 800 MHz frequency, after inspecting the LOMON outputs.

4.1.2 Full Spectrum

Corrected the frequency offset of the local oscillator, the baseband inputs in-phase and quadrature were fed with a 16QAM signal with 6 M symbols. The full spectrum of RF signal can be seen in figure 4.4, with two different attenuation levels, where the carrier is centered at 800 MHz and the adjacent harmonics appear centered at 1.6 GHz and 2.4 GHz frequencies.

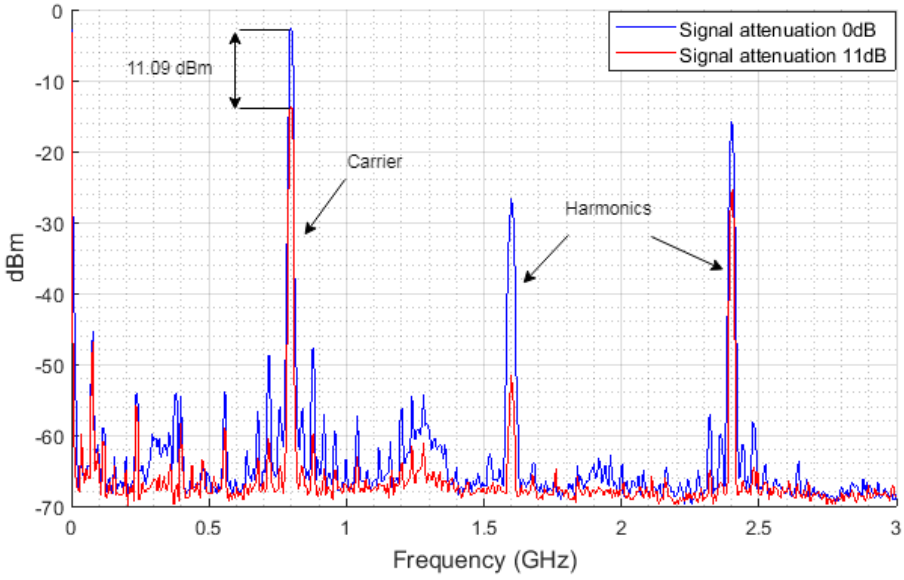

Figure 4.4: Full spectrum of RF output signal

Inspecting the RF signal with 11 dB attenuation, it can be concluded that brings a significant improvement to the RF spectrum, enhancing the second harmonic at 1.6 GHz with an attenuation of 24.8 dB.

Carrier signal is surrounded with interferences at well-defined frequencies, although not critical at this stage, when the signal is driven through the power amplifier, interferences will be amplified together with carrier, corrupting the desired signal at reception.

As mentioned in section 2.2.3, intermodulation distortion is a nonlinear effect of two or more signals mixing within a device that produce undesirable higher-order products, where the lower-order terms occur more close the fundamental and harmonics signals. Although it is impossible to know the order of intermodulation products, it is possible to claim that they are the main reason for such nonlinearities, since they occur at well defined frequencies in both sides of the fundamental and harmonics signals.

Above 1 GHz, these nonlinearities are irrelevant, since the communication system itself will filter out those side effects introduced by the modulator. However, the same cannot be stated for the intermodulation products that appear near the fundamental signal and above.

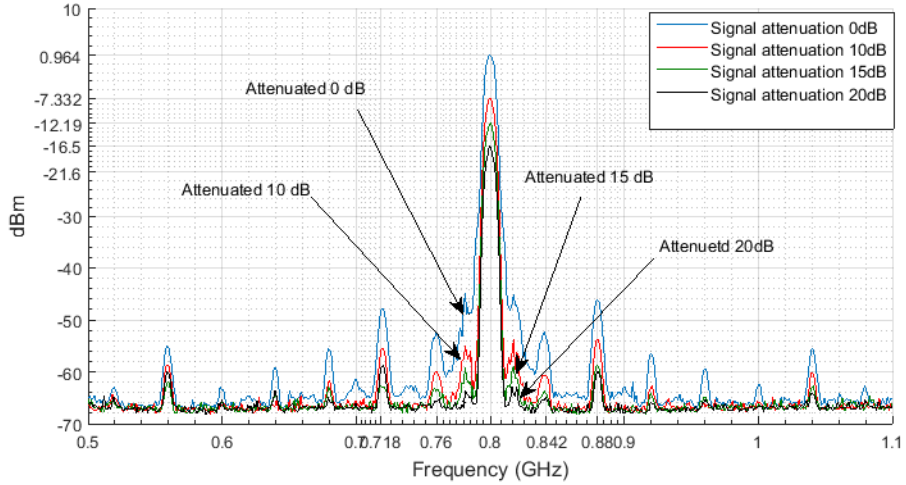

Figure 4.5: Carrier and intermodulation products

From figure 4.5 it can be seen with more detail the IM products with different attenuation levels that surround the carrier at 800 MHz. As mentioned earlier, due to non-linearities present in power amplifiers, these will produce intermodualtion products at the same frequencies as modulator produced. At the output of power amplifier in the RF Transmitter, the third order intermodulation products will be amplified with a ratio 6:2 in relation with the main signal.

Analysing the RF signal with different attenuation levels, it can be stated that an attenuation of 20 dB is capable to reduce the intermodulation products to the noise level near the fundamental signal. This means that modulator can amplify the fundamental signal in 27 dBm without the interference of intremodulation products.

Comparing the signal with a 10 dB attenuation with the signal without attenuation, it is possible to conclude that the signal with 0 dB attenuation already reached the P1dB.

At 600 MHz, the same side effects are present in the RF spectrum. Figure 4.6 shows the intermoduation products around the fundamental signal. It is clear that the only way to avoid the interference from intermodulation products is to limit the amplification of the fundamental signal to an upper limit.

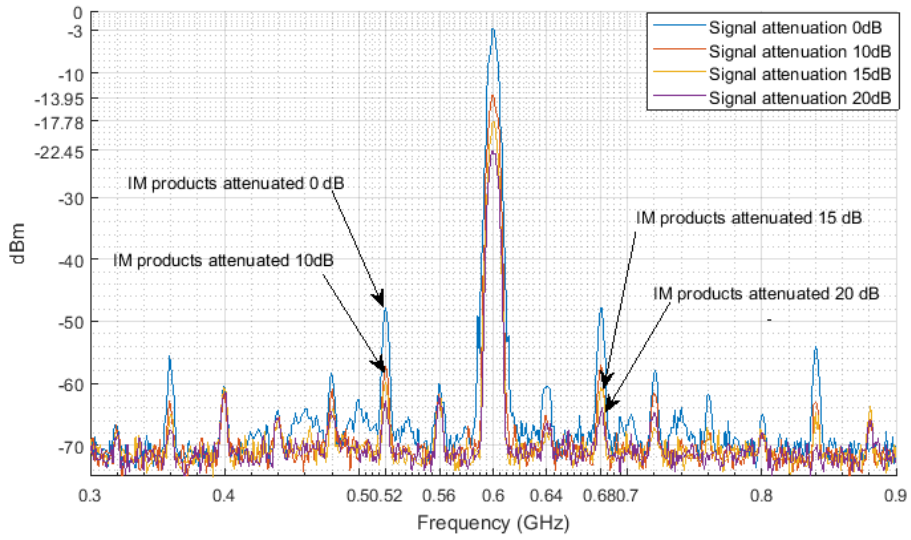

Figure 4.6: Carrier at 600 MHz with IM products

4.1.3 RF Output

The baseband communication is using the OFDM modulation scheme due to its ability to handle frequency selective channel fading and its resilience to timing errors. However, one of the main drawbacks of OFDM is that it has a high peak-to-average power ratio (PAPR). This high PAPR is due to the fact that, for a large number of sub-carriers, the OFDM signal approximates a random complex Gaussian process. Consequently, the amplitude of the signal has a Rayleigh distribution. For a large ("infinite") number of sub-carriers, N, the signal has a nonzero probability of being above any given threshold. For a finite N, each OFDM symbol has a maximum PAPR of N. When the OFDM signal is passed through a non-linear power amplifier , its peaks are clipped, which causes in-band and out-of-band distortion.[3]

From figure 4.7 it can be seen the RF output signal with a 6 MHz bandwidth, where it is affected by out-of-band distortion.

This side effect of the modulation scheme can not solved here, however through an attenuation in the fundamental signal can be prevented to be amplified by the intermodulation products in the next stages. The intermodualtions products also are present in the side bands of the fundamental signal, so through an 10 dB attenuation can be seen significant improvements in the spectrum. With an 10 dB attenuation, the modulator amplifies the fundamental signal with 37 dB, remaining 55 dB above the noise reference, 75dB.

With an attenuation between 15 dB and 20 dB, it can be achieved a better performance with regard to out-of-band distortion, bringing them to the same level of the noise reference. Although, it is obvious that will decrease the relation SNR.

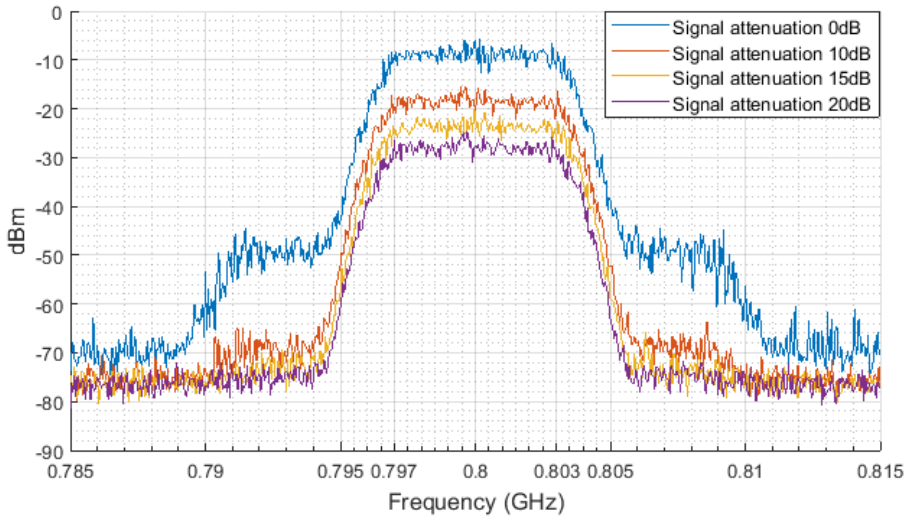

Figure 4.7: Carrier at 800 MHz

Figure 4.8 shows the RF output signal at 600 MHz with the same modulation scheme and the bandwidth used at 800 MHz. Comparing both, it is clear that the out-of-band distortion is not frequency dependent.

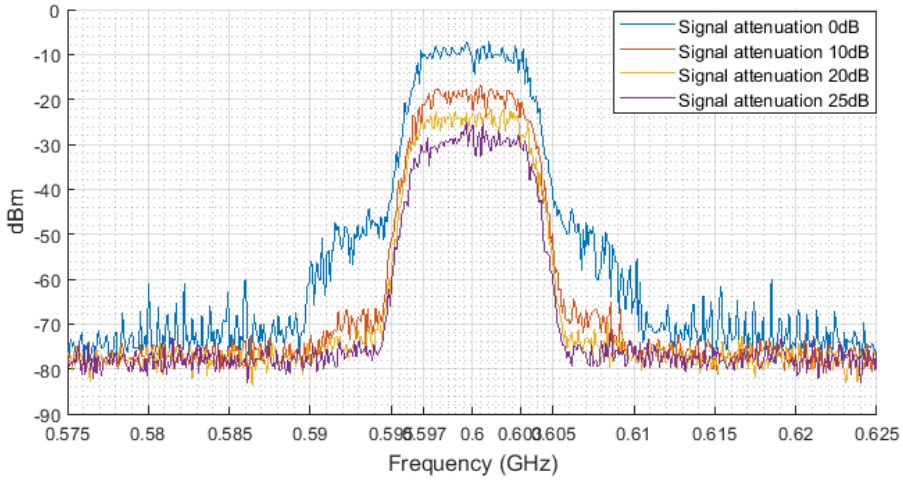

Figure 4.8: Carrier at 600 MHz

Although out-of-band distortions can be avoided at this point, due to the non-linearities present in the power amplifier, the fundamental signal will be affected at the output of the power amplifier.

A possible solution to address this problem could be through techniques such as iterative clipping and filtering for PAPR reduction. Several researchs have been conducted, proving that it is

possible to reduce out-of-band distortions without a degradation of signal-noise ratio, however, it will increase the complexity of baseband communication.

4.2 Demodulator

Assembled all components, the final board can be seen in figure 4.9. Although very similar to the modulator, this stage is more complete allowing to setup an external or internal voltage common mode.

To provide a full test of the Demodulator was used the signal generator SIMQ 03B, previously used to provide the baseband signals to modulator. Signal generator allows to set up in parallel an RF signal with several digital modulations in a frequency range between 300 kHz and 3.3 GHz and the baseband signals in-phase and quadrature that compose the RF signal, thus it was possible to check the correct operation of Demodulator by comparing the output baseband signals of the signal generator.

To evaluate both baseband signals was used the oscilloscope TDS 2022B of the Tektronixwith with a 200 MHz range frequency.

Figure 4.9: PCB demodulator

The demodulator was tested with an RF signal at a 800 MHz frequency and 6 M symbols per second. Three different modulations were used, in subsection 4.2.2 it can be seen the output basebands signals of the demodulator with a QPSK modulation. In the appendix B the remaining results can be seen with BPSK and 16QAM modulations.

4.2.1 Local Oscillator

After setup all the necessary registers through SPI to a 800 MHz frequency oscillation, it was possible to observe from figure 4.9 the internal replica of local oscillator, despite provided the correct values through SPI, it can be seen that local oscillator has a deviation of 5.08 kHz.

Analysing local oscillator frequency at several different frequencies was possible to conclude that local oscillator has a offset between 2.6 kHz and 5.4 kHz, despite this offset decrease with the frequency is not a linear function of frequency.

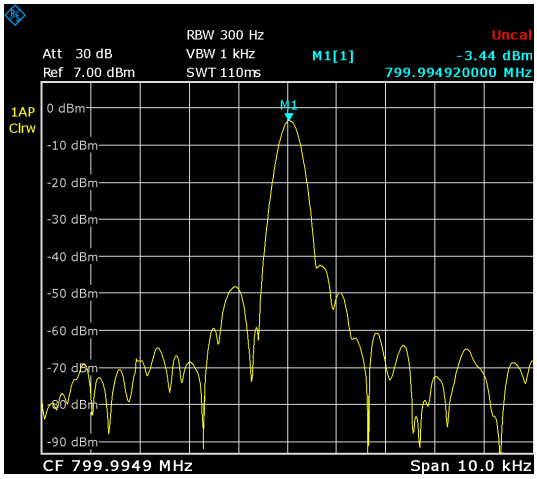

Figure 4.10: Local oscillator at 600 MHz with 5.08 kHz offset

After inspect the internal local oscillator through differentials outputs LOMON, the offset can be compensated through the 25-bit fractional number. From figure 4.11 it can be seen a new replica of internal local oscillator with an offset of 1.8 Hz.

Although offset is easy to compensate, it adds a considerable payload to the communication, since it is necessary to keep information about the offset at desired frequency, which leads to a great loss of flexibility. Another option could be, the microcontroller that manages communication inspect the frequency of the local oscillator, however this increases the complexity, since it is necessary to add a device that converts the analogue signal of the local oscillator to digital.

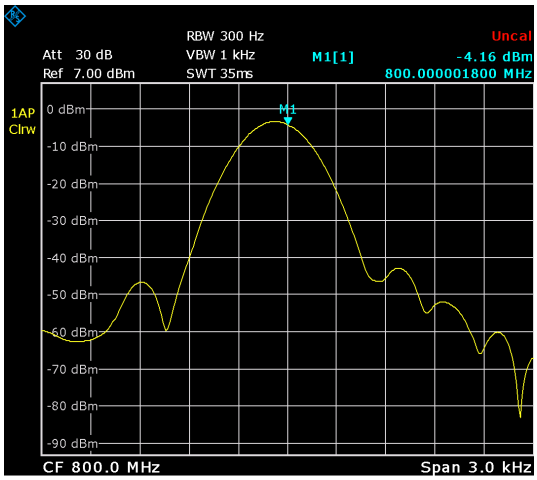

Figure 4.11: Local oscillator at 800 MHz with balanced offset by 25-bit fractional number

4.2.2 Baseband output

As mentioned above, to test the demodulator it was provided an RF signal at a frequency of 800 MHz, with a QPSK modulation and 6 M symbols per second. The basebands signals that compose the RF signal are generated arbitrarily by signal generator, thus the only way to ensure the correct operation of the demodulator was by comparing both signals.

From figure 4.12 it can be seen the in-phase baseband signal overlapped with the in-phase baseband signal of the signal generator, despite a small temporal offset it is clear that the baseband signal provided by demodulator is the desired signal.

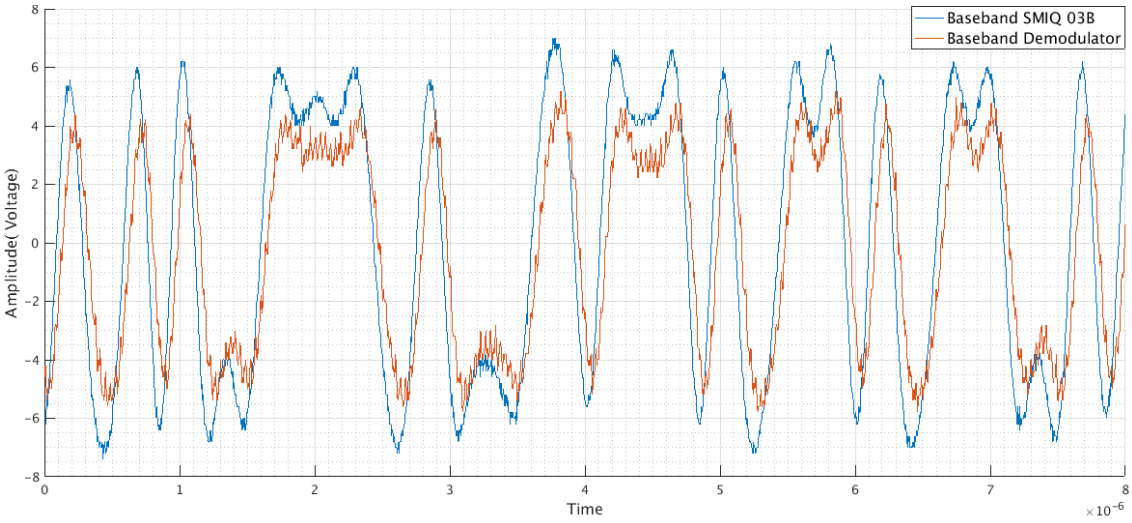

Figure 4.12: In-phase baseband signal with QPSK

Figure 4.13 shows the quadrature baseband signal of the signal generator overlapped with the quadrature baseband of the demodulator and comparing both signals becomes clear that it was achieved the desired signal. Due to the limitations of the laboratory equipment, it was only possible to test a baseband signal at each time, however comparing the temporal offset with in-phase baseband, it can be concluded that it is approximately the same.

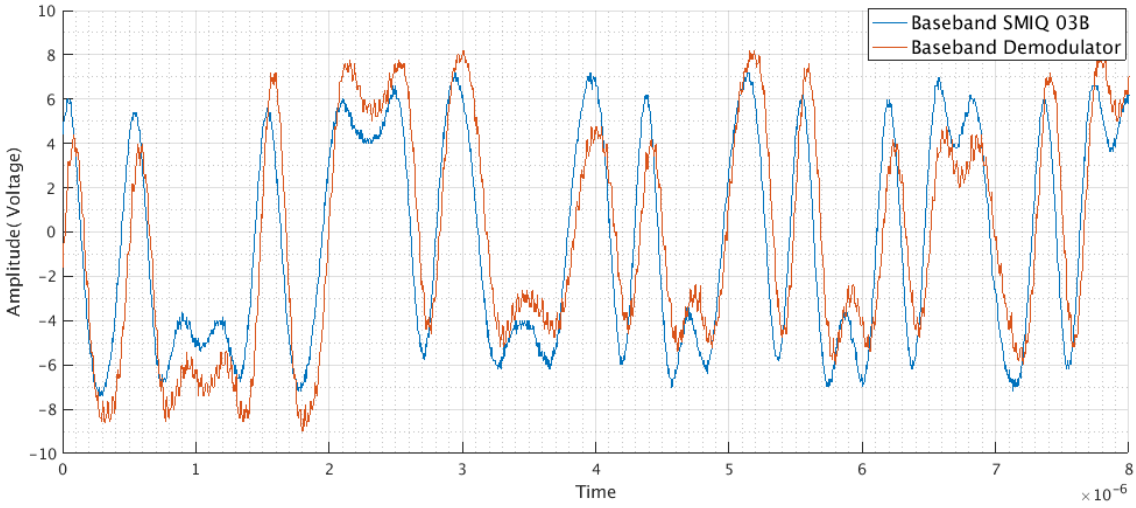

Figure 4.13: Quadrature baseband signal with QPSK

4.3 Loopback test

To perform a complete test of the modulator and the demodulator they were connected in loop, where the signal generator provides the baseband signals. The modulator converts the baseband signals into an RF signal at a frequency of 800 MHz and connected by a cable providing the signal to the RF input of the demodulator. The demodulator with a local oscillator at a 800 MHz frequency, converts the RF signal to a baseband signals in-phase and quadrature. Through a test probe it was possible inspect and compare the baseband signals of the signal generator and baseband signals of the demodulator.

Figure 4.14 shows the complete setup necessary to conduct the test, despite it was not mentioned in previous sections to program the ADRF6850 and the ADRF6755 registers through SPI, it was necessary to develop in a breadboard a voltage divider that allowed to covert the 5 V Arduino digital outputs to 2.5 V.

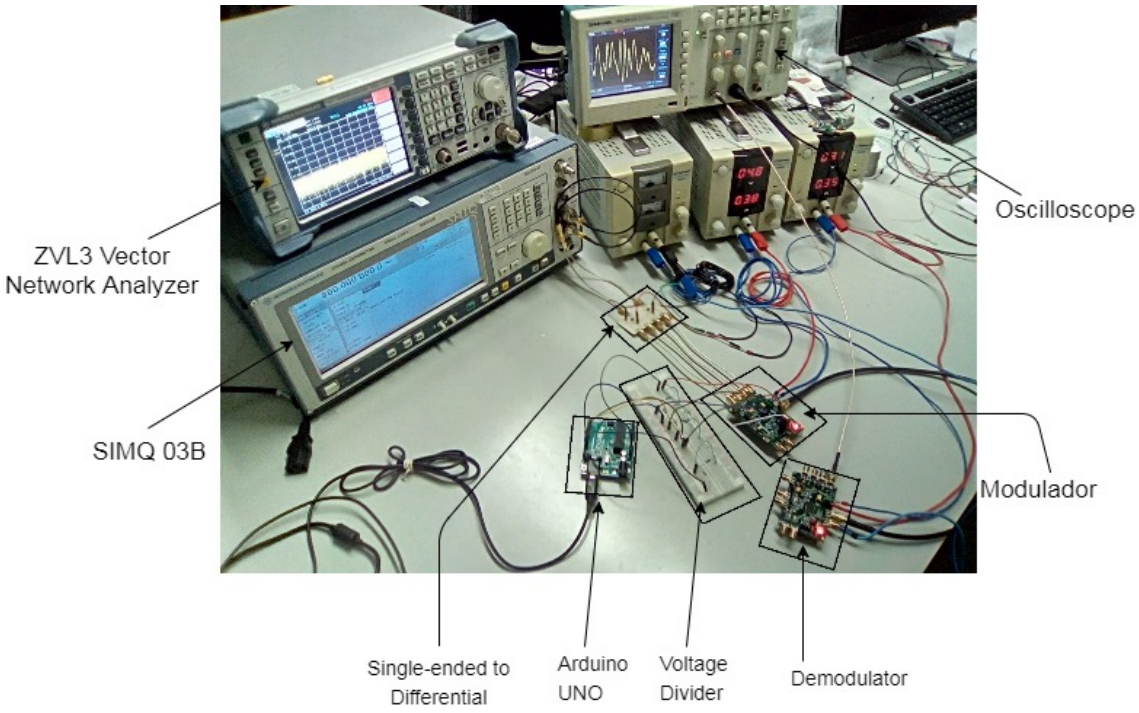

Figure 4.14: Loopback test at a 800 MHz frequency

Through the signal generator were conducted three test, although with different modulations, all were defined with 6 M symbols per second that allowed to reach a bandwidth of 6 MHz. Since the intention of the baseband communication is to use a 16 QAM modulation, in this section will be represented the results with this modulation, however the remaining results with a BPSK and QPSK modulation are present in the appendix C.

Signal generator does not allow to control the power level of the baseband signals, thus it was defined a 45 dB attenuation in the modulator and a 40 dB amplification in the demodulator, which allowed to compare the baseband signals of the demodulator and signal generator with the same power level.

To avoid interferences in the desired signal due to nonlinearities of the devices, it was setup a low pass filter with a cutoff frequency of 30 MHz, the lowest filter provided by demodulator.

From figure 4.15 it can be seen the in-phase baseband signal of the demodulator overlapped with the in-phase baseband signal of the signal generator. Since the output basebands signals of signal generator are connected through cables to the board that convert single-ended in differential signals, it was necessary through a probe test connected to the oscilloscope to extract the baseband signal from one of the exposed paths in the board.

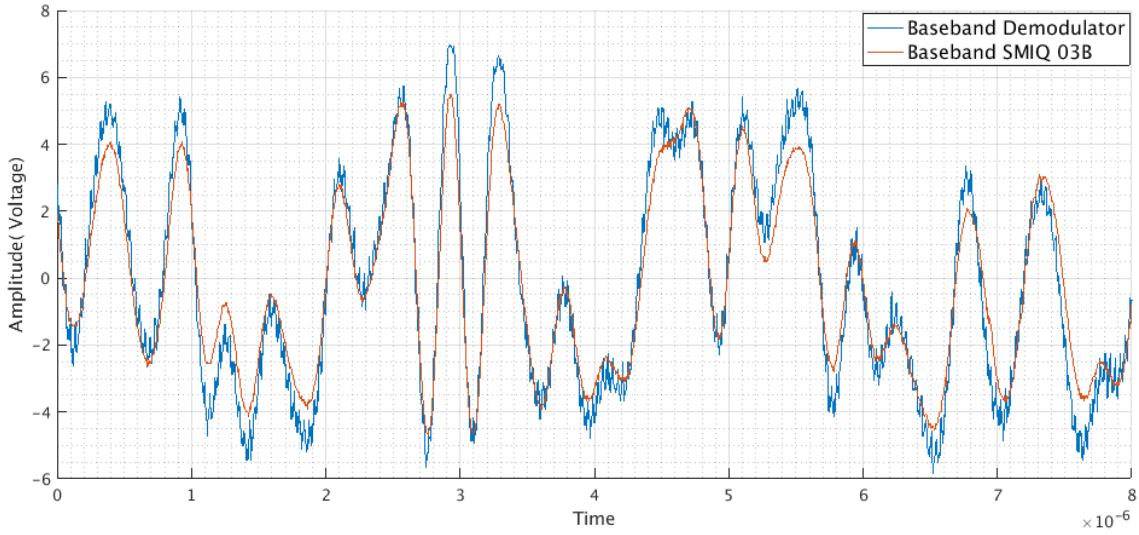

Figure 4.15: In-phase baseband signal with 16 QAM

Figure 4.16 shows both quadrature baseband signals of the signal generator and of the demodulator. Although both signals are what was expected, it can be seen that they are being affected by noise. One of the possible reasons for this effect is the 40 dB amplification imposed by the demodulator, which is amplifying the noise with main signal. However, comparing with the previous test, where demodulator was tested isolated with a 16 QAM modulation, were obtained better results despite the 24 dB amplification.

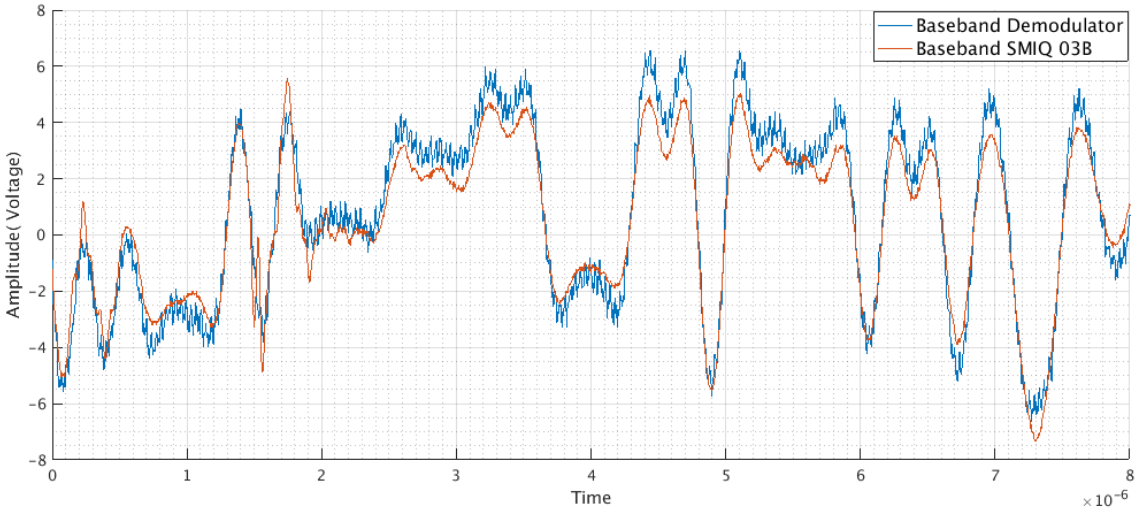

Figure 4.16: Quadrature baseband signal with 16 QAM

A probable reason for a degradation of baseband signals in-phase and quadrature may be due the noise introduced by modulator, which is being amplified by the demodulator. Therefore, should be achieved a relationship between the attenuation of the modulator and the amplification of the demodulator that reduces the noise introduced in the communication due to the nonlinearities.

However, this must be done with baseband communication, which defines an adequate noise level that enables communication with a certain noise.

4.4 Test LNA

To evaluate the correct behaviour of the LNA stage, it was performed a S-parameter test trough the ZVL3 Vector Network Analyser, where the outcome of this test overlaps with the expected results obtained in the section 3.4.

The figure 4.17 shows the parameter S11 simulated overlapping with the parameter S11 measured, it is clear the deviation between the two signals, during the design and simulation, the solder mask, which acts as a coating on the PCB, was not taken into account during the design. This side effect may be the main reason for such deviation in parameters S11 and S22.

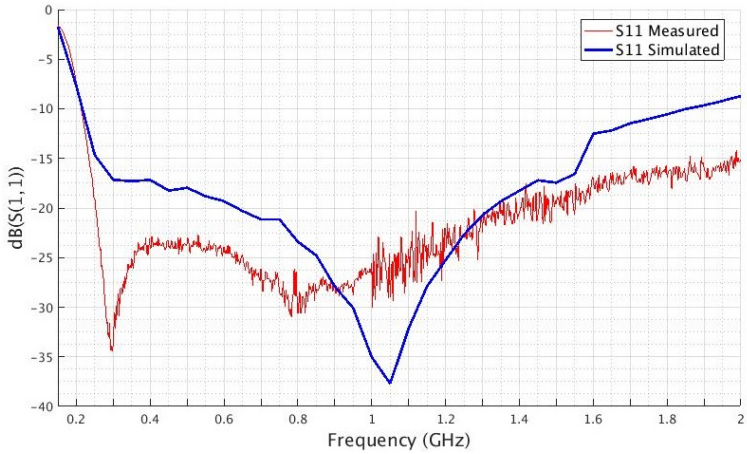

Figure 4.17: S11 LNA

The results bellow 0.3 GHz can not be considered since the minimum operating frequency is 0.3 GHz, however it is necessary to ensure that they are below 0 dB, in order to guarantee stability.

The analyse of parameter S11 allow conclude that the greatest deviation, appears exactly at the minimum operating frequency, but can be taken as a positive side effect, since it increased the efficiency by 15 dB.

On the other side, at 1.05 GHz, a negative deviation decreased the efficiency around 12.5 dB. Although this offset, the parameter S11 is less than -20 dB between 0.3 GHz and 1 GHz, which means more than 99% of the input signal is delivered to the source.

The figure 4.18 shows the parameter S22, where the maximum deviation occurs at 0.3 GHz, with a difference of 15 dBm. Despite this deviation, it was achieved an efficiency in the output signal above 90%, once the parameter S22 is less than -10 dBm between 0.3 GHz and 1 GHz.

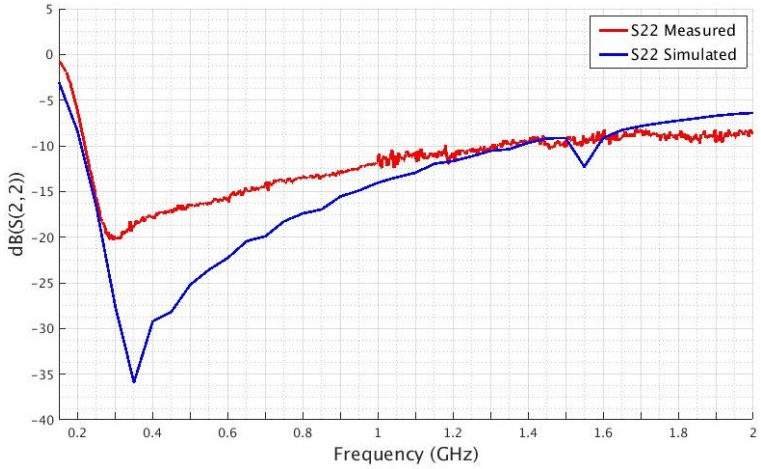

Figure 4.18: S22 LNA

The expression 2.43 establish a relation between the gain and the S-parameters, it is clear the deviation in the S11 and S22 will affect the expected gain.

The figure 4.19 shows the gain measured versus the simulated, where the expected gain decreased around 1 dB in all frequencies bands, although being more affect at frequencies above 1 GHz.

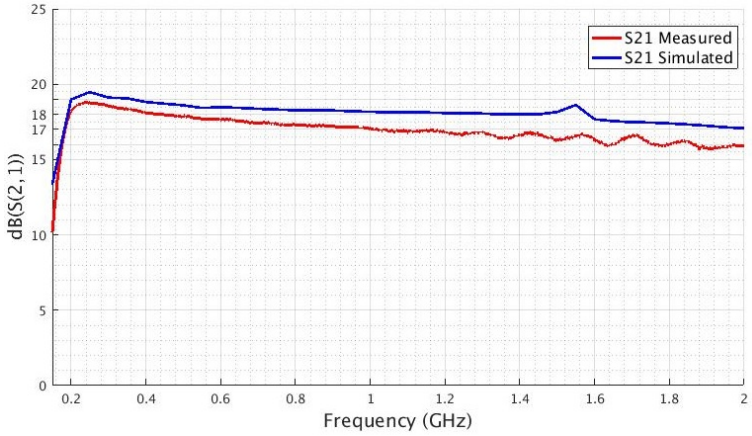

Figure 4.19: S21 LNA

4.4.1 Noise Figure

The noise figure is one of the most important features when developing a LNA, since it defines the achievable signal sensitivity on the receiver side.

As mention in a previous section, the manufacturer achieved a noise figure between 1 dB and 1.2 dB at frequencies between 0.7 GHz and 2.7 GHz. However, this value was never calculated during design due to absence of information in the LNA IC datasheet, as well as the rest of the components that are part of this stage. Therefore, it was extremely important to calculate the noise figure introduced by all components at frequencies below 1GHz.

To compute the noise figure it was used a N9030A PXA Signal Analyzer, from Keysight, with a frequency range between 3 Hz to 50 GHz and the 346A noise source, from Keysight, with a frequency range between 10 MHz and 18 GHz. In this test, it was necessary to use different equipments, since the ZVL3 Vector Network Analyser was not compliant with the noise source.

From figure 4.20 it can be seen the performed test, where on the right side is the schematic test and the left side is the equipment used to perform the noise figure test. Before perform the test, the system had to be calibrated to take into account all noise sources induced by all elements present in the measurement system.

As is obvious by the name, the noise source is a device that introduces noise in the Device Under Test (DUT), with predefined noise values, Excess Noise Ratio (ENR), and must be supplied to the signal generator before the calibration.

When the signal generator is loaded with ENR values, the noise source was connected to the signal analyser without the DUT, or in this case without the LNA stage. Thus, the signal generator was calibrated with noise induced by the noise source, as well as throughout the system itself, allowing a more accurate test.

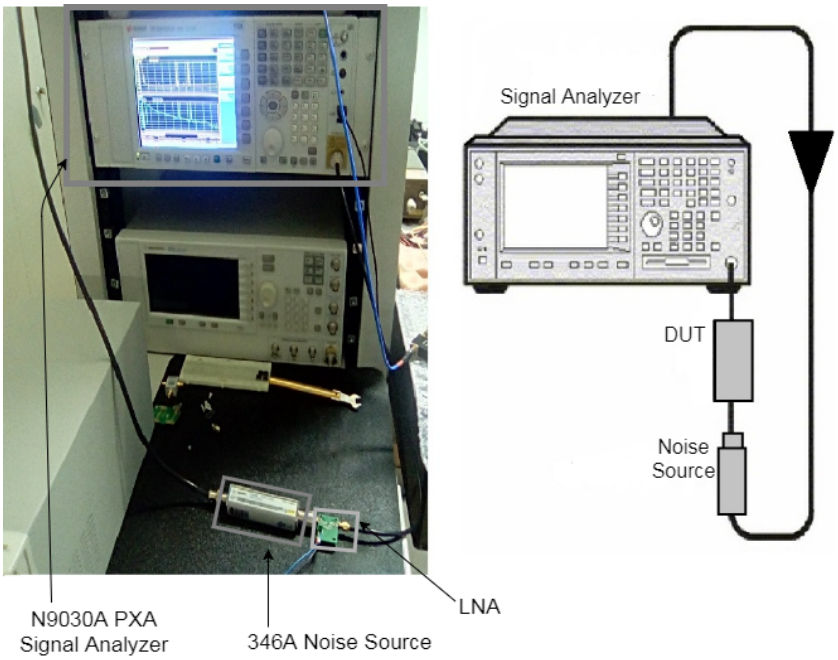

Figure 4.20: Noise figure test

With the whole calibrated system, the LNA is introduced, as shown in Figure 4.20, and the noise test is started. Since the signal generator incorporates the necessary software to calculate the noise figure through the Y-factor technique, it was not necessary to do extra calculations to obtain the noise figure.

Figure 4.21 represents the noise figure graph between 0.2 GHz and 1.2 GHz. The noise figure has a maximum of 2.5 dB at the minimum operating frequency, 0.2 GHz, and a minimum of 1.15 dB at 1 GHz. It not only allowed to conclude that the noise figure increased slightly compared to

the results obtained by the manufacturer, but to ensure that it remains at acceptable levels between 0.2 GHz and 0.7 GHz.

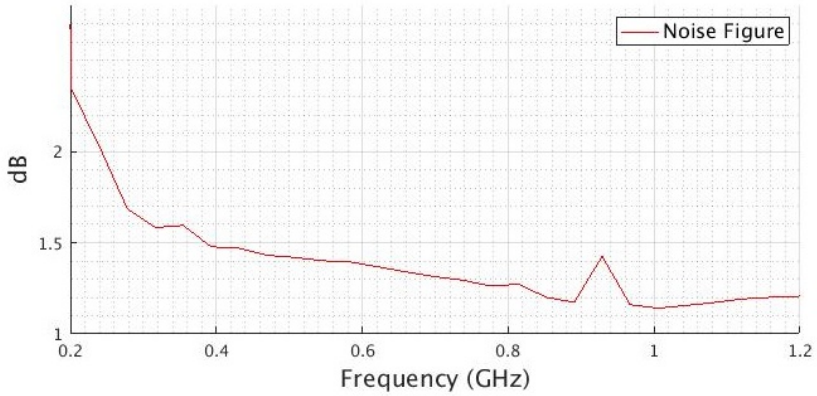

Figure 4.21: Noise figure LNA

Another important aspect to mention in this result is the peak between 0.8 GHz and 1 GHz, where it reaches the maximum around 1.4 dB at 0.93 GHz. It is difficult to explain this event, since the noise figure decreases steadily until reaching a minimum at 1GHz. However, the noise figure graph provided by the manufacturer, Appendix D, has the same peak around 0.9 GHz, although not as pronounced, being only a variation less than 0.1 dB.

Therefore, although the noise figure increased slight, when comparing with the 1 dB noise figure achieved by the manufacture, it can be concluded that the noise value increased by less than 0.5 dB if the frequency bands between 0.2 GHz and 0.4 GHz were excluded.

4.4.2 Third-Order Intermodulation Distortion (IM3)

Third order distortion products are typically introduced in an RF system by components such as mixers and amplifiers. A simple way to specify third order distortion products is with a two-tone intermodulation test. This test generates two tones of the same power level closely spaced in frequency.

The schematic test to measure the IM3 is shown in figure 4.22, where each signal generator produce a tone that is coupled by the power combiner to fed the DUT input. The output produced by the DUT will be measured and displayed in the signal analyser with the two-tone signal plus all intermodualtion products generated by the DUT. This outcome can be represented mathematically by the expression 2.19.

Figure 4.23 shows the setup test used to measure the intermodualtion products generated by the LNA. Where were used the N9030A PXA Signal Analyzer, the SMJ100A Vector Signal Generator from Rohde Schwarz and the Signal Generator e8257d from Agilent Technologies. The signals coming from the signal generators were coupled with an RF power combiner with -6 dB attenuation and fed the LNA input, where the LNA output signal was measured in the Signal Analyser.

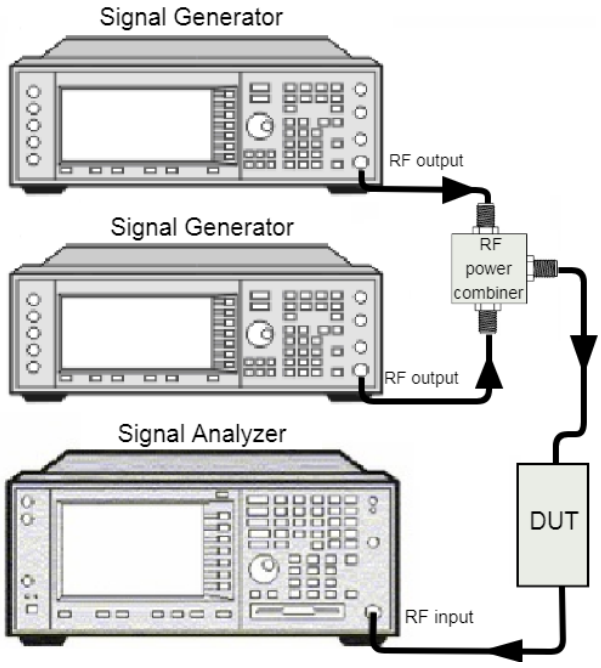

Figure 4.22: IM3 schematic test

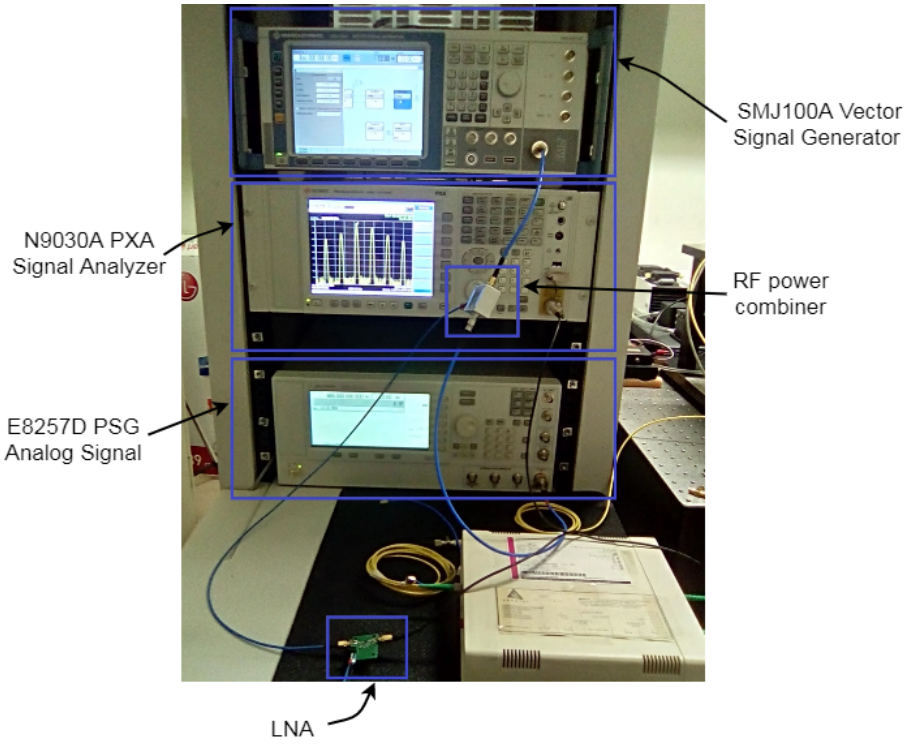

Figure 4.23: IM3 setup test

To perform this test it was generated the two-tones at 865 MHz and at 866 MHz, where the 1 MHz space between the two-tone allows expect the IM3 products occur at 864 MHz and at 866 MHz, as described by the expression 2.21 .

The cables, as well as the power combiner, introduce attenuation into the power signals, although they do not affect the relationship between the two-tones and the intermodulation products, it is important to achieve maximum accuracy during the test. Thus, before each IM3 test, it was measured the attenuation between the signal generators and the RF power combiner output by connecting the power combiner throughout a cable to the signal analyser.

Figure 4.24 shows the IM3 test results with several power levels, where was used a 5 dBm interval between -20 dBm and -5 dBm. Through this test, it was taken into account an attenuation around 6.4 dBm. So, when the two tones were generated with a power signal of 5 dBm, the LNA input was fed with a signal power level of -1.36 dBm.

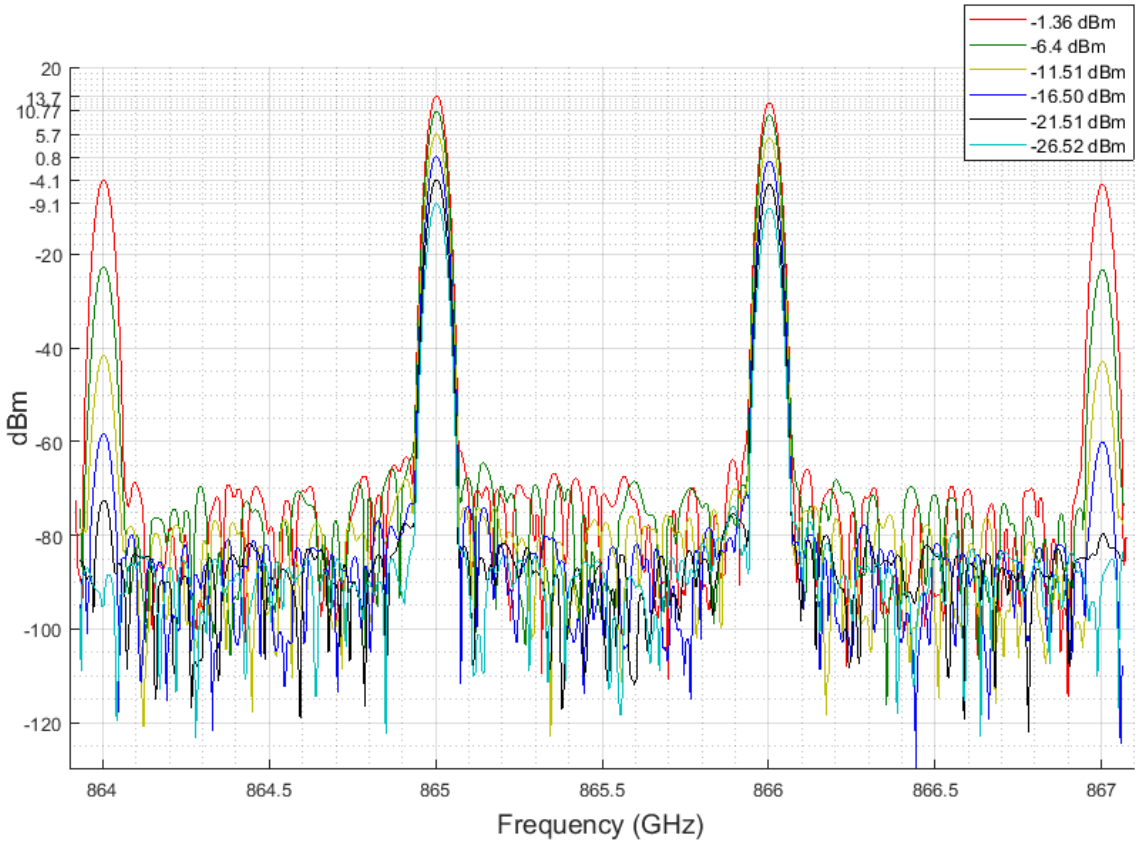

Figure 4.24: IM3 test

If we consider -70 dBm, the reference noise level, for all the power signals, the LNA is free of intermodulation products when the LNA input is fed with power signals less than -21.51 dBm. This means that the two lowest power signals, -26.52 dBm and -21.51 dBm, are free of IM3 products, despite the -21.51 dBm power signal has a small amplification at IM3 frequencies when it is analyzed separately. Thus, it was achieved an amplification of 17.4 dBm, in relation to the input signal, when the power signal is below -21.51 dBm.

When provided an input signal with a power level of -16.50 dBm, IM3 products appear 10 dBm above the reference noise level. The difference with the input power signal -21.51 dBm, -5 dBm

below, is 14.12 dBm, which means that IM3 products are being amplified at a rate three times more than the first-order products , two-tone signals, on a logarithmic scale.

With an increase of 5 dB in the input power signal to -11.51 dBm, the output signal increased by 5 dB, compared to the previous signal, however the IM3 products appear amplified at 16.7 dBm, when compared with the input power signal of -16.50 dBm. Looking at Figure 4.24, it is clear the 3:1 relationship between the amplification of the IM3 products and the two-tone signals.

At -1.36 dBm input signal, the output signals were amplified in 3 dBm compared with the -6.4 dBm input power signal, which means that it was reached the compression point, P1dB, despite IM3 continue to increase with a ratio of almost three times. The IM3 will stop increasing when reach the P1dB too, however, the signals of interest will be unrecognisable.

At this point, it makes sense introduce the third order intercept (TOI or IP3). This theoretical specification is the output power at which the distortion products will be equal in amplitude to the two-tone signal of interest.

Through the data extracted from the IM3 measurements, it was possible estimate the fundamental signal power line and the third-order signal power line, both represented in figure 4.25 by dotted lines. Therefore it was possible calculate the IP3, the 23.48 dBm output power signal when the LNA input is supplied with a 6.93 dBm power signal.

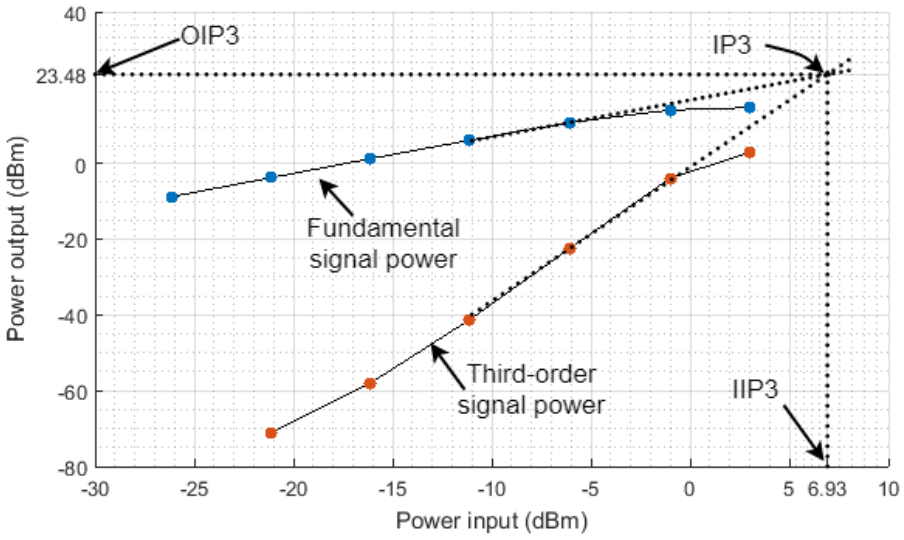

Figure 4.25: IP3

The solid lines that represent the fundamental signal power and the third-order signal power, were interpolated through the values extracted during the IM3 measurement. Looking at the highest input power signal provided, 2.6 dBm, it is clear that both signals are no longer in the linear region, which means that the IP3 never will be reached.

When the LNA input is supplied with a two-tone signal power of 2.6 dBm, the fundamental signal power is 5.88 dBm bellow the expected value of the linear region, while the power of the third order signal is 6,613 dBm below the value expected. If the input power continues to increase, eventually the LNA output power will be completely flat.

As mention in previous sections, it is intended to use a bandwidth of 6 MHz, so seems imperative to analyse the spectrum of frequencies that will be used by the communication.

When using an OFDM modulation that uses a multi-channel scheme, several intermodualtion products can occur inside the frequencies bands of interest.

From figure 4.26 it can be seen the 10 MHz spectrum of frequencies that surrounds fundamental frequencies, F1 and F2, between 860 MHz and 870 MHz. As described by expression 2.19, when the two-tone signal is amplified by the LNA, an infinite number of intermodulation products are generated, despite we are more interested in the IM3 since they are the intermodulation products that occur more closely to the signal of interest.

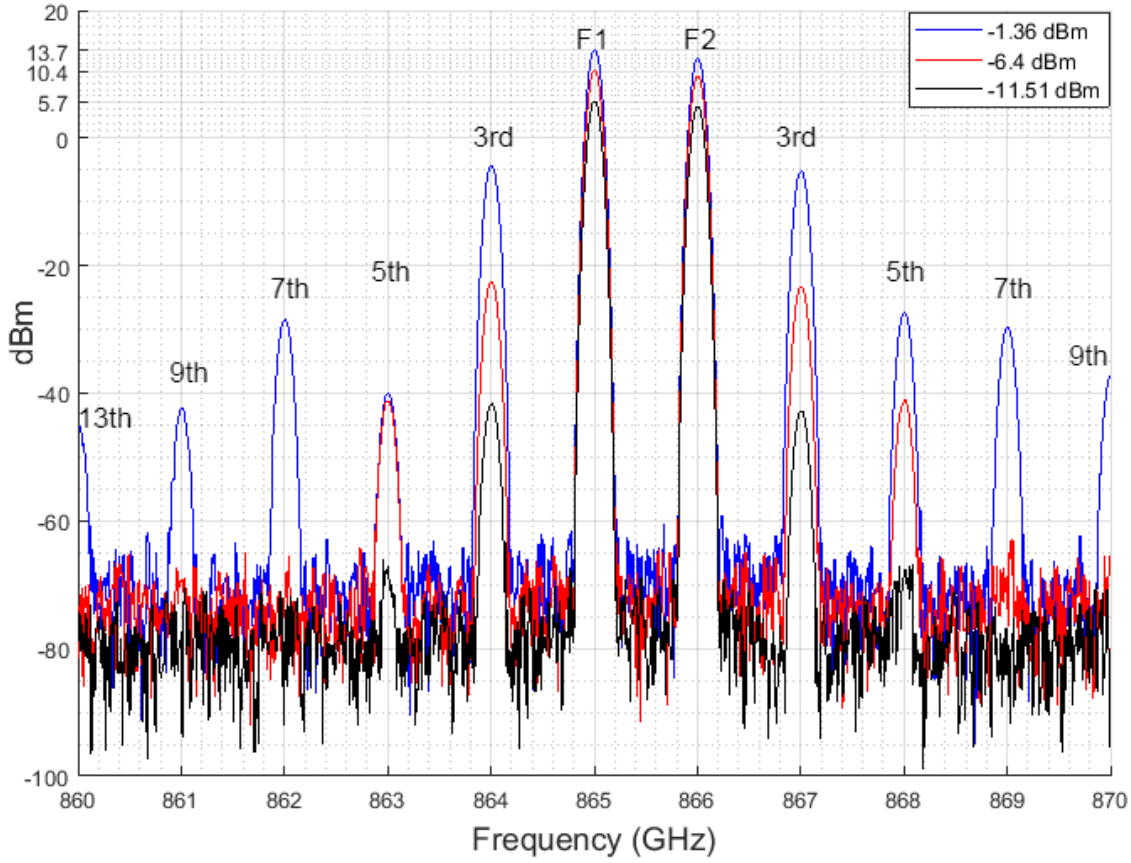

Figure 4.26: Noise Figure LNA

Of all intermodulation components produced during the amplification, we are only interested in those which can fall in the frequecies bands of interest. In table 4.1 were calculated the first six intermodulation products, where it can be easly understood that the even products occur fairly spaced from the fundamental frequencies.

Associating the table 4.1 with the figure 4.26 it is possible see the frequencies at which intermodulation products occur, as well the relation between the input power signal and the power of each intermodulation product was generated. Where lower order intermodulation products are generated at higher power levels

1st	F1	F2	865 MHz	866 MHz
2nd	F1+F2	F2-F1	1731 MHz	1 MHz
3rd	2F1-F2	2F2-F1	864 MHz	867 MHz
4th	2F1+2F2	2F2-2F1	3462 MHz	2 MHz
5th	3F1-2F2	3F2-2F1	863 MHz	868 MHz
6th	3F1+3F2	3F2-3F1	5193 MHz	3 MHz
Etc.				

Table 4.1: IM Products

The even intermodualation product that occur more close the fundamental signals, are the second order intermodualtion products, which in this test appear at 1731 MHz, F1+F2, and at 1 MHz, F2-F1, which mean that can be easily filtered out.

The same do not happen with the odd intermodualtion products that appear closely to the fundamental frequencies. If were used the frequencies bands beteween 862.5MHz and 868.5 MHz, where the two-tone are centered, the bandwidth signal will be affected by the IM3 products and the fifth order intermodualtion products.

It is clear that the desired signal will not be affected only by IM3, but also by the other odd products as well. So, to avoid the signal degradation during the LNA amplification, the input power signal may be limited to an upper limit of -21.51 dBm, thus it can be guaranteed that the IM3 products introduced by LNA are negligible.

LNA and PA do not allow power control, the only way to control the input power signal is through the 47 dB power control embedded into the modulator.

4.5 Test PA

To evaluate the PA performance, similar tests were performed to the previous section, although in some tests it was used different laboratory equipment.

As in the LNA test section, the first measurement was the two-port S-parameter, through the E8363B PNA Network Analyzer, with a frequency range between 10 MHz and 40 GHz.

Figure 4.27 shows the measured parameter S11 in contrast to the simulated parameter S11, the same as in section 3.5. Signals have a minimum deviation of 2.5 dB at 0.3 GHz and a maximum deviation of 15 dB at 1.2 GHz.

Small deviations between the simulated and the measured are always expected, since we are dealing with non-ideal elements, although this deviation, can be considered as a positive side effect, since it reduced the losses of the input signal in all frequency bands represented in figure 4.30.

With parameter S11 below -16 dB, it means that more than 97.49% of the input signal is delivered to the load.

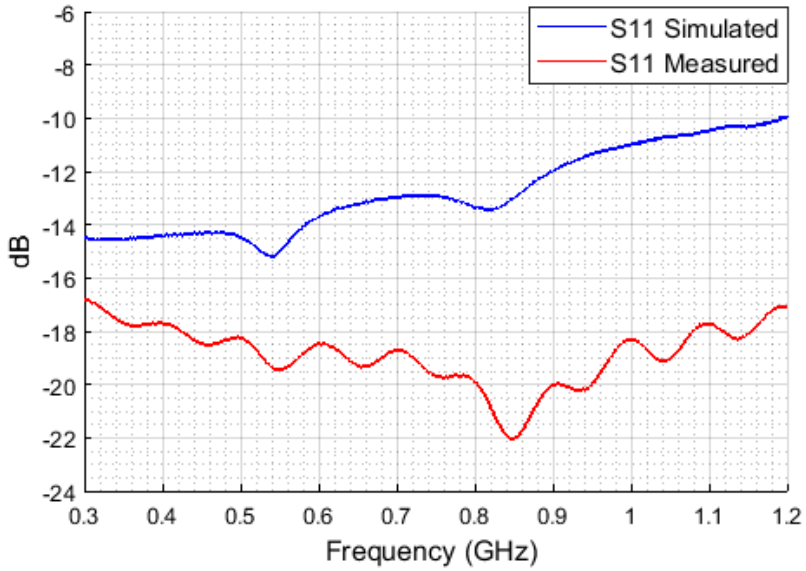

Figure 4.27: S11 PA

Regarding with the results of parameter S22, represented in figure 4.28, it can be seen that the parameter S22 measured is above in all frequency bands of what was simulated. Where the largest deviation appears between 0.56 and 0.58 GHz with 5 dB , and between 0.86 GHz and 0.88 GHz with a deviation of 4.6 dB.

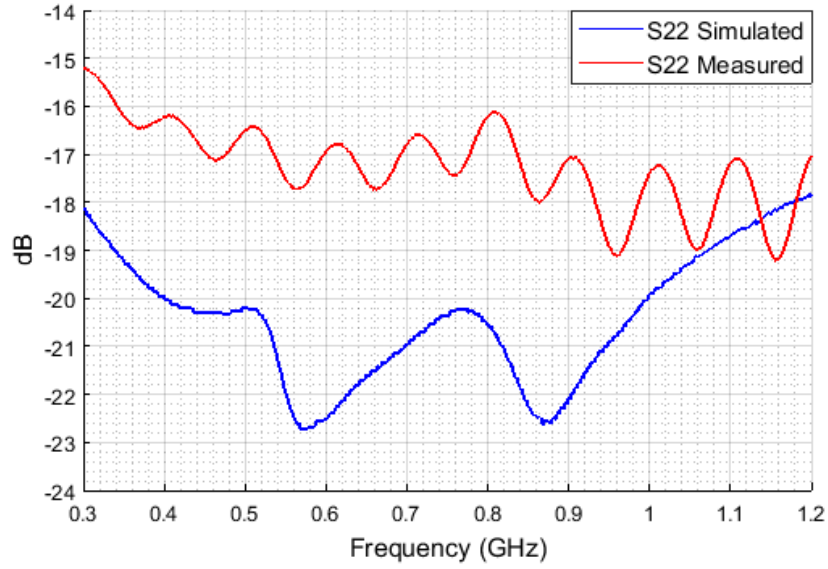

Figure 4.28: S22 PA

Despite this deviation, which causes a power loss of the output signal, the measured parameter S22 remains below -15 dB over the entire measured frequency spectrum, which ensures that more than 96% of the output signal is delivered to the output.

Figure 4.29 shows the simulated and measured parameter S21, which represents the PA gain. Despite the deviations found in S11 and S22 that could affect the gain, the measured parameter S21 is very close to the one simulated, with a maximum deviation of 1.2 dB and a minimum gain of 18.8dB at 1.2GHz.

At 0.3 GHz, the deviation between two signals is approximately zero and is reached a maximum gain, as expected, of 21dB.

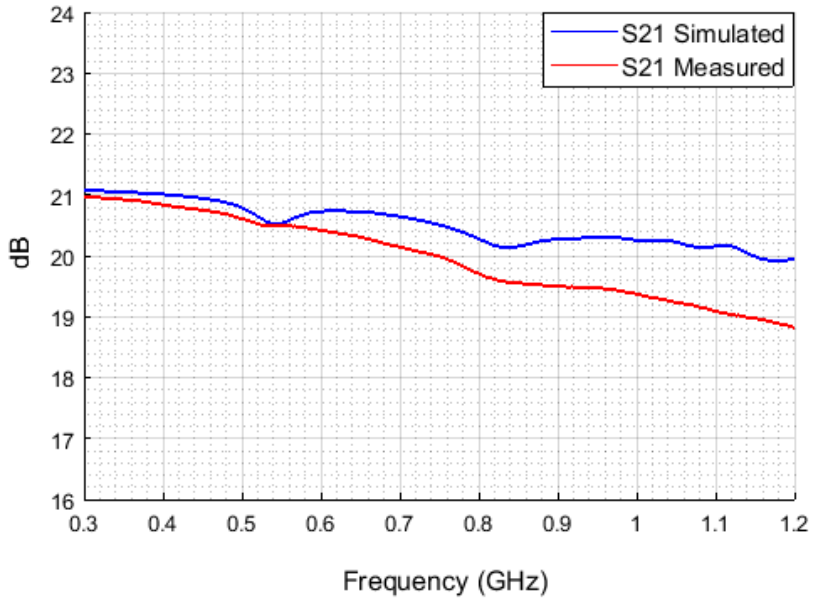

Figure 4.29: S21 PA

4.5.1 IM3

To perform the IM3 test, it was intended to use the same schematic test used during the IM3 LNA test, although during the tests a large difference in the power levels between the intermodulation products was found, when inspected in signal analyzer. The possible reason for this at the time, could be the fact that the RF combiner used was not isolated and allowed such differences.

With this drawback, it was taken the opportunity to use a different setup test. Figure 4.32 shows the schematic setup used, where only one signal generator is used, instead of two as in the IM3 LNA test. This setup test allows achieve a greater accuracy with respect to the fundamental signals, since the two fundamental signals are generated from the same signal generator, so the non-linearities of the signal generator affect the two fundamental signals in the same way.

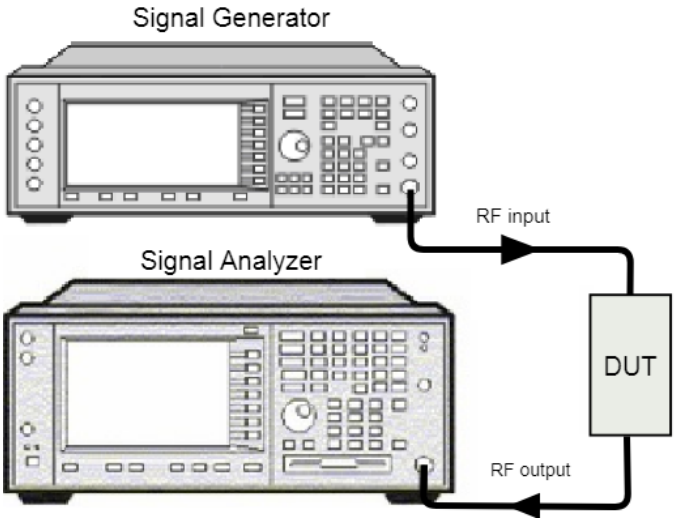

Figure 4.30: IM3 Schematic Test PA

Figure 4.31 shows the setup used to measure IM3 as well as the efficiency of the PA. Where, after performing the IM3 tests, the necessary components were added to carry out the efficiency measurements.

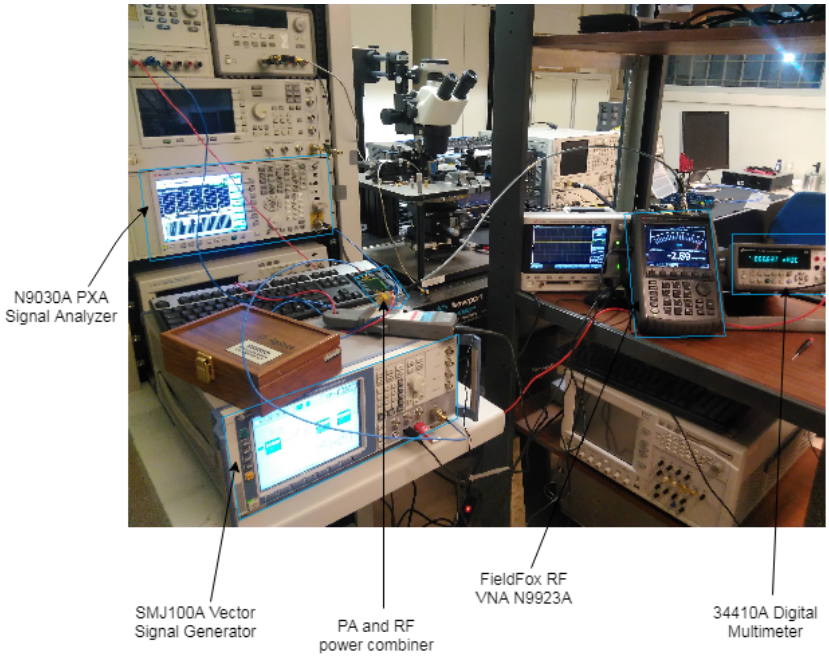

Figure 4.31: IM3 and Power Efficiency Setup

Signal generator is unable to produce two signals with distinct frequencies, so it was necessary generate two baseband signals in Matlab, separated by 2 MHz, and upload to the signal generator. The two baseband signals were internally mixed by the signal generator with the carrier at 865 MHz, which allowed to produce a two-tone signal at 864 MHz and 865 MHz.

With the two-tone signal supplied to the PA input, the respective amplified output signal can be seen in Figure 4.32. The spectrum signal analized, with 10 MHz, allow to inspect not only the 3-order products but 5-order products at 860 MHz and 870 MHz. The five signals plotted with a 4 dB step, between -11.64 dB and 4.36 dB allow to understand that the IM3 products increse with a higher ratio than the fundamental signals.

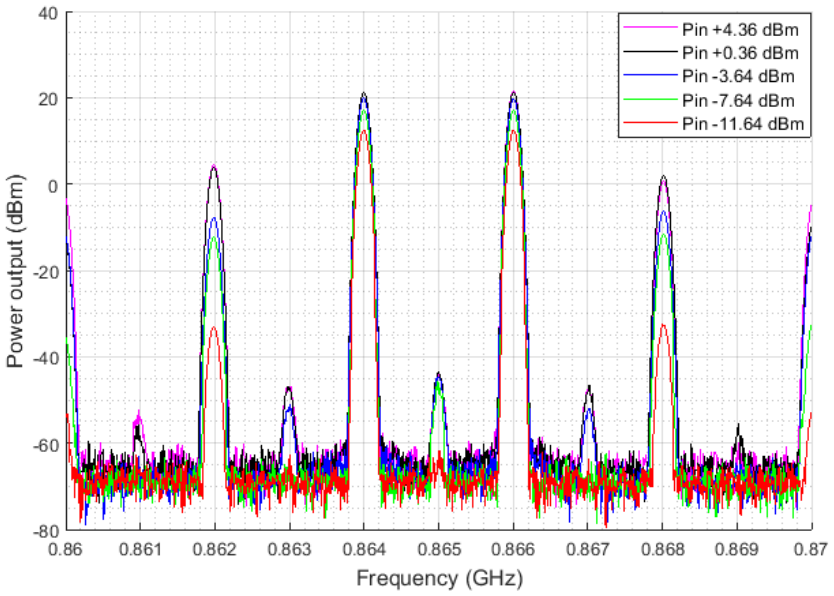

Figure 4.32: IM3 spectrum PA

The intemodulation products were thoroughly studied and analyzed in the previous sections, in particular during the analysis of the IM3 LNA, however the different setup used with all the advantages, introduced a carrier leakage, at 865 MHz, due to the mixing of the carrier with the baseband signal. When the two-tone signal with the carrier leakage is supplied at the PA input, this produce spurious components at $865 \pm m * 2$ $(m > 1)$ MHz, where the most notorious occur at 863 MHz and at 867 MHz.

Despite these spurious produced by the signal generator due to their mixing inaccuracies, they occurred outside the frequencies of the two-tone signals and the IM3 signals, which did not affect the accuracy of the test.

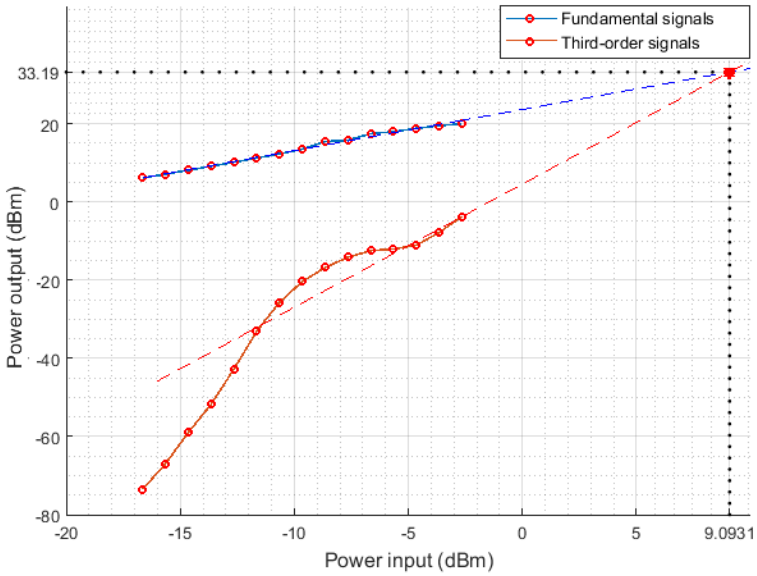

Figure 4.33: IM3 PA

Through the several power signals supplied at the PA input, it was possible plot the IM3 curve and the line representing the two-tone signals. Figure 4.33 shows the IM3 and the two-tone signal, as well as the expected lines, which represent the expected linear performance of the fundamental signals and the third-order products. Due to the lack of a linear growth of the third-order signals, the expected line was extrapolated from the points of the curve having the highest power since they have a 3: 1 relation to the expected line representing the fundamental signals.

With the expected lines, it was possible extract the IP3, when the input power signal is 9.0931 dBm and the output power signal is 33.19 dBm

The IP3 never will be reached, as mention previously during the LNA analysis, since the P1dB is reached before.

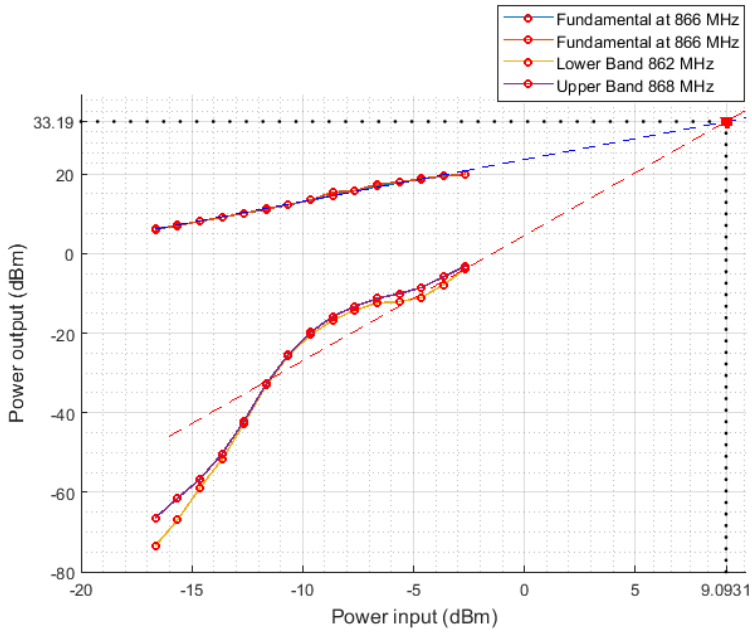

Figure 4.34: IM3 with all tones

Due to the deviations found, that motivate a different setup to measure the IM3, and to the non-linear curve representing IM3, it becomes imperative to analyze each of the tones separately.

Figure 4.34 shows the two IM3 tones superimposed on the expected line and the two fundamental signals superimposed with the expected line. Regarding the two-tone signals, the deviation is approximately zero, however IM3 tones show a small deviation below -15 dBm power input and another deviation approximately at -5 dbm power input.

4.5.2 PA Efficiency

As mentioned earlier, the two setups, IM3 and Efficiency tests were combined. Figure 4.35 shows the schematic setup developed to measure the PA efficiency.

To perform the efficiency test it was necessary to disconnect the PA from the signal analyser and introduce an directional coupler (RF power combiner), which allowed to measure the output power signal, through the FieldFox RF VNA N9923A, with power metering capabilities.

Also was necessary connect the 34410A digital multimeter to the supply power, in order to measure the current consumption.

Although signal analyzer was not entirely necessary during this test, it helped to inspect whether signal output was the expected.

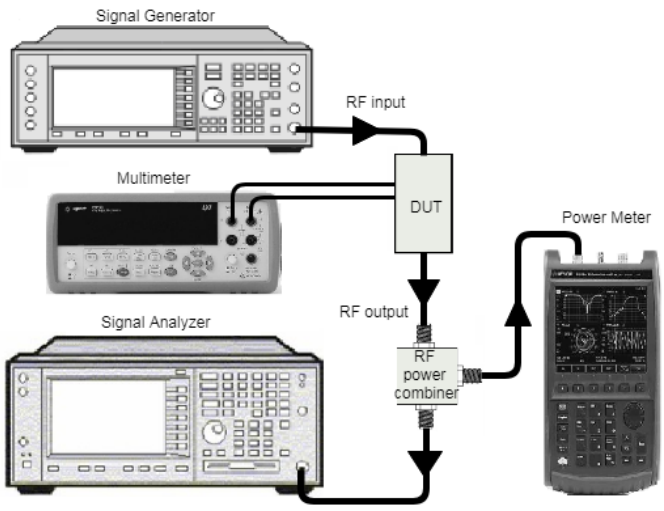

Figure 4.35: Schematic Power effeciency

4.5.2.1 P1dB

To perform the P1dB test, the PA input was supplied with one tone signal through the SMJ100A signal generator at 865 MHz. The PA output power signal was measured on the FieldFox RF VNA N9923A and inspected in N9030A PXA, both can measure the output power, although the first can achieve greater accuracy.

From figure 4.36 it can be seen the curve that represent the actual output power response over the various power signals supplied to the PA.

Through the data points extracted, which represent the actual response, it was computed the line, red dashed line, that represent the expected response of the PA.

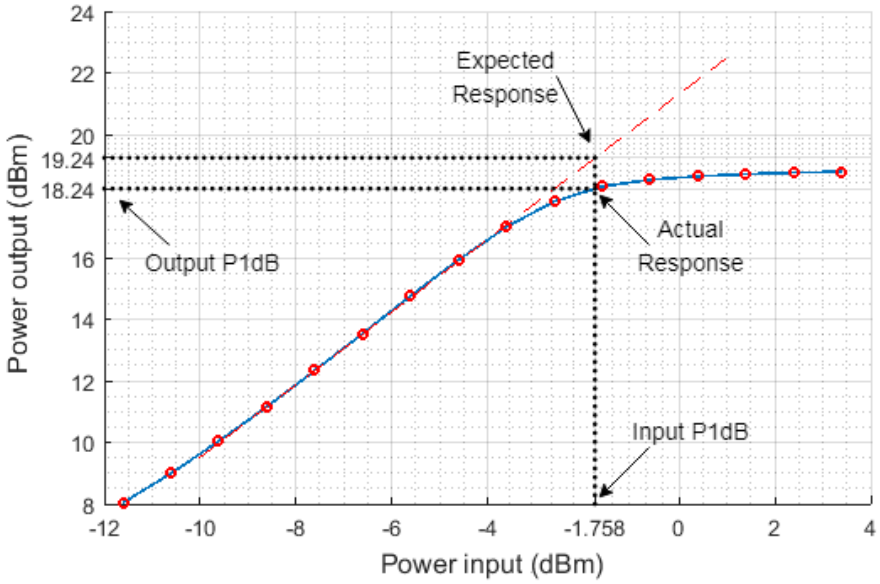

Figure 4.36: P1dB PA

Overlapping both, the expected response with the actual response, it was possible to find the P1dB at -1.758 dBm power input with the actual response, at 18.24 dBm output power.

4.5.2.2 Efficiency and Gain

The Power Added Efficiency (PAE) and drain efficiency are shown in figure 4.37. Both are superimposed until they reach at -1.758 dBm input power, where they begin to deflect smoothly.

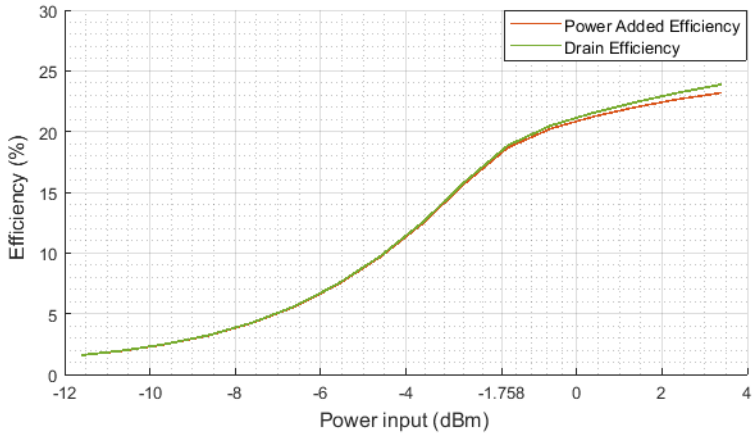

Figure 4.37: Power efficiency and gain

The maximum PAE of 23.87% and the maximum drain efficiency of 23.19% are reached at 3.39 dBm input power. However, at this point, P1dB as already been crossed, what means the PA is saturated.

During the S-parameter analyzes, it was analysed the parameter S21, which represents the gain versus frequency. With the several power levels supplied to the PA, it was possible analyse the gain versus input power.

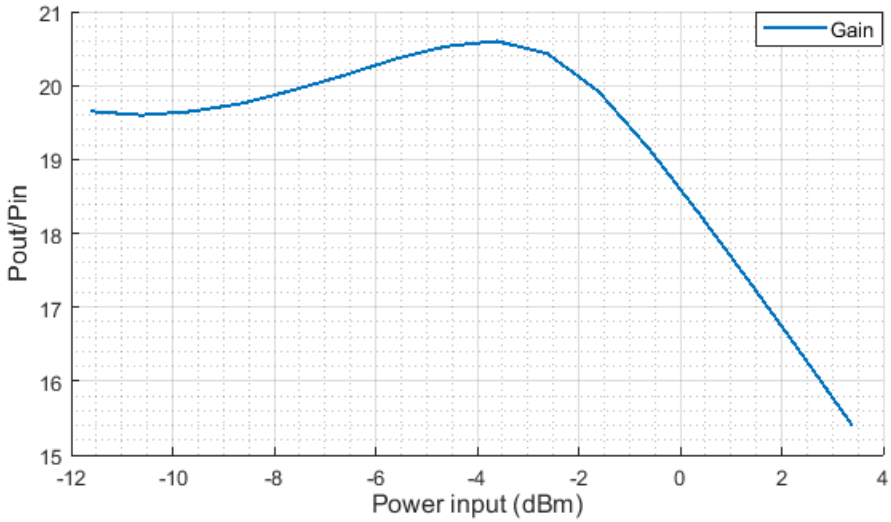

Figure 4.38: GainVsP$_{in}$

Figure 4.38 shows a maximum gain of 20.6 dBm at -3.61 dBm power input and a minimum gain of 15.4 dBm at 3.39 dBm.

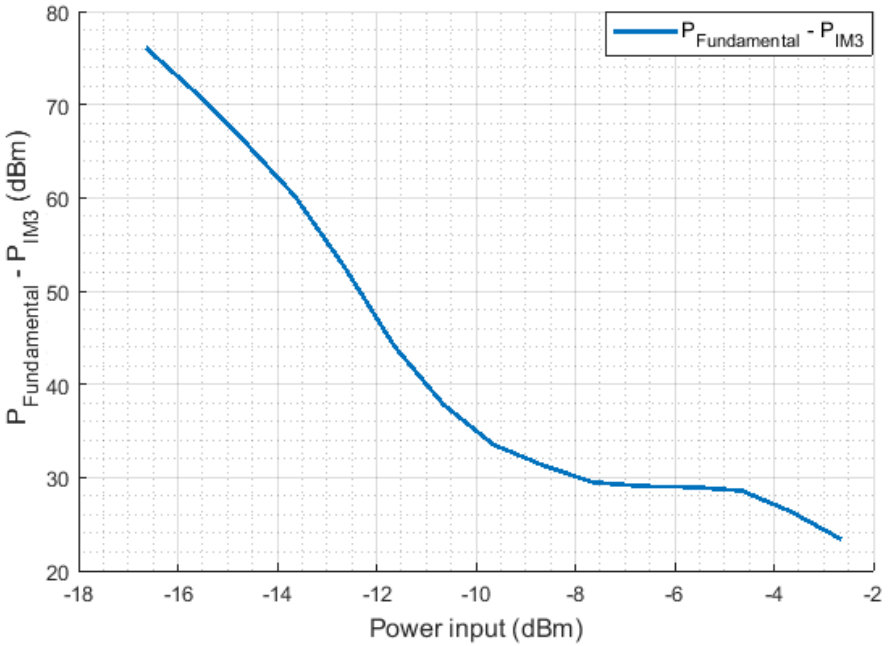

Figure 4.39: P$_{Fundamental} - P_{IM3} VsP_{in}$

Figure 4.39 shows the difference between the two-tone signal and IM3 versus input power, where the minimum difference of 23.47 dBm is reached at -2.647 dBm input power.

As done with other devices in the previous sections, it was applied an 16 QAM signal with 6 M symbols, which represents a bandwidth of 6 MHz.

Figure 4.40 shows the output signal centered at 865 MHz, with three different input powers. The out-of-band distortions are clear at the two highest input powers, where the rate of growth is greater than the in-band signal.

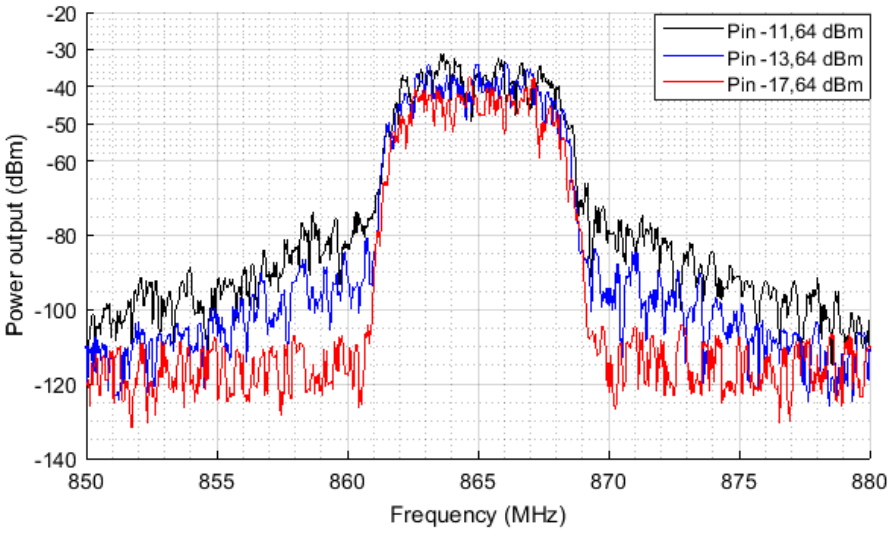

Figure 4.40: IM3 PA

4.5.3 Error Vector Magnitude (EVM)

When a digitally modulated signal is generated it is no perfect and it has some differences regarding the reference signal that should be generated. These measures are generally quantified by calculating the difference of the amplified signal to the reference signal, quantified as the EVM. The transmission and reception chain will add their non-linear distortions to this signal, which will further increase the EVM.

One of the main contributors to the EVM degradation is the non-linear PA in the transmitter.

Figure 4.41 shows the setup used to measure the EVM, where the signal generator is connected to the PA input and the signal analyzer is connected to the PA output. It was also necessary to connect the signal analyzer with the signal generator in order to share the same clock reference, 10 MHz. Which allowed both to follow the same internal clock.

Through a ethernet cable connected between a computer and the signal analyser, it was possible extract the data measured.

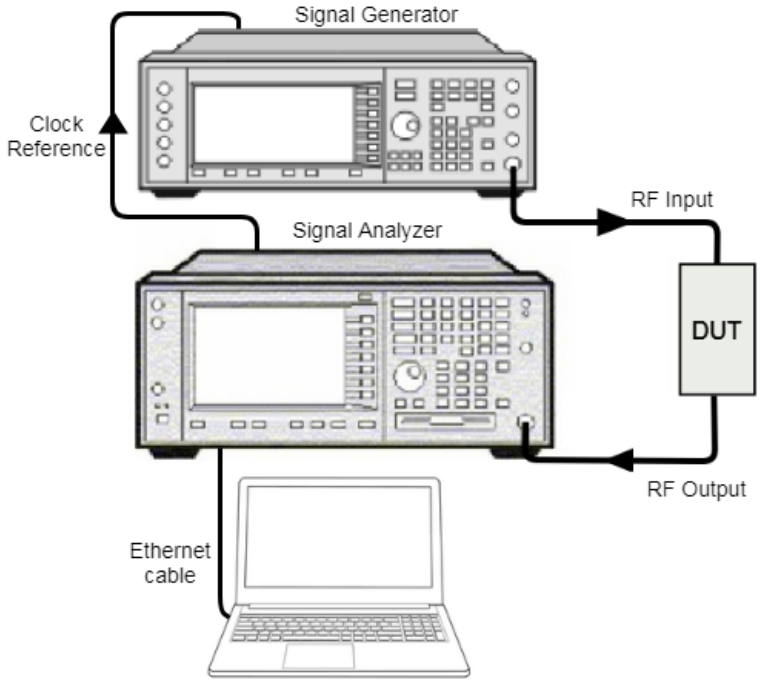

Figure 4.41: Schematic EVM PA

On the computer was running the 89600 VSA software, with a comprehensive set of tools for demodulation and vector signal analysis. These tools enable to explore virtually every facet of a signal and perform all the required calculations regarding with the EVM.

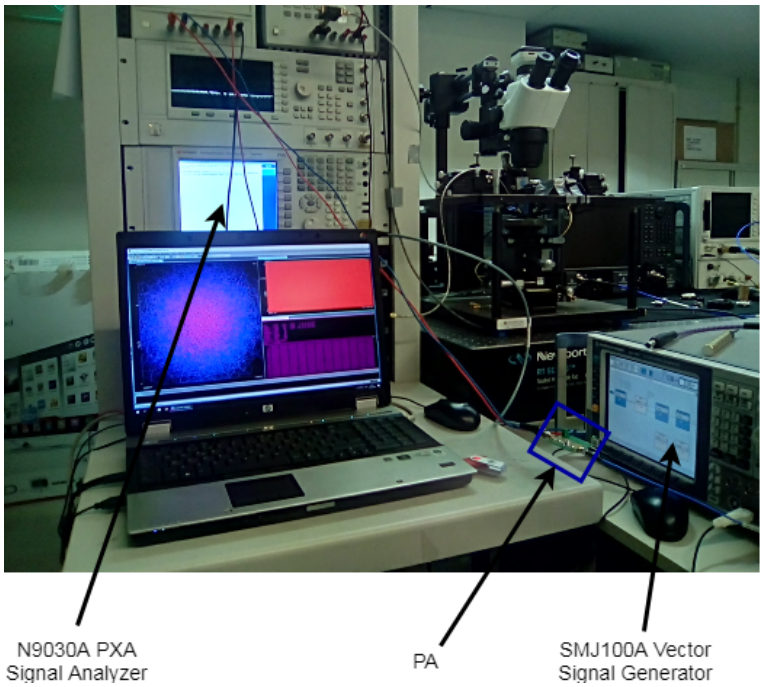

Figure 4.42: Laboratory setup EVM

Figure 4.42 shows the laboratory setup, where before perform any test, was measured the EVM

floor of the setup with the SMJ100A Vector Signal Generator connected directly to the N9030A PXA Signal Analyzer, without the PA.

All EVM results presented in this section were calculated using the 89600 VSA software, where it was used a normalization RMS. Both, the reference signal and the measured signal passed through a Root Raised Cosine filter with a roll-off α =0.35.

During measurement of the EVM setup, it was used a symbol rate of 10 M symbols which resulted in a noise floor of 0.7%. This test showed an EVM of 0.54% and an EVM peak of 1.55%, which means that a lower EVM can not be reached with respect to the EVM PA measurements.

	$P_{in} = -6dBm$
EVM RMS	0,54%
EVM Peak	1,55%

Table 4.2: EVM setup

The first EVM measurement was performed with a 16QAM signal, a symbol rate of 10 M symbols, a power input of -6 dBm with a a PAPR of 5,38 . This showed an EVM of 3.8% and an EVM peak of 12% .

	$P_{in} = -6dBm$	$P_{in} = -2dBm$	$P_{in} = 6dBm$
EVM RMS	3.8 %	3.18 %	9.3%
EVM Peak	12 %	9 %	26%

Table 4.3: EVM results with PA

In this second measurement, the same input signal was used, but with a power input equal to 6 dBm. The EVM increased up to 9.3% and EVM peak to 26%, which is according with the expected, since the increase of the input power make the EVM increase too.

During the third and last EVM measurement, it was used a 16QAM signal, with a symbol rate of 2 M symbols, a power input of -2 dBm and a PAPR of 3.4 dB. The EVM measured is 3.18 % and the EVM peak is 9% , as expected, since lower symbol rates and lower power inputs lead to lower EVM values in relation to higher power inputs and higher symbol rates.

The EVM measurement performed with a input power of 6 dBm means that P1dB has already been crossed at -1.758 dBm. The PA is in a non-liear zone which explains such EVM degradation regarding with the remaining results.

4.6 Wired Test

With all components tested and performing the expected behaviour, it was performed wired tests, where all the components of the communication system were connected by cable.

Figure 4.43 shows the setup test developed to perform this test, where the only equipment that had never been used previously was the DSOX2022A Oscilloscope with a range between 0 MHz and 200 MHz.

To avoid exceeding the maximum power input limits, it was introduced an attenuator of 10 dB between the PA and LNA, and another 20 dB attenuator between the LNA and the demodulator.

To perform this test, it was generated in the Signal Generator a 16QAM baseband signal with 6 M symbols. As a carrier frequency, the local oscilator of the modulator and demodulator has been programmed to operate at 865 MHz.

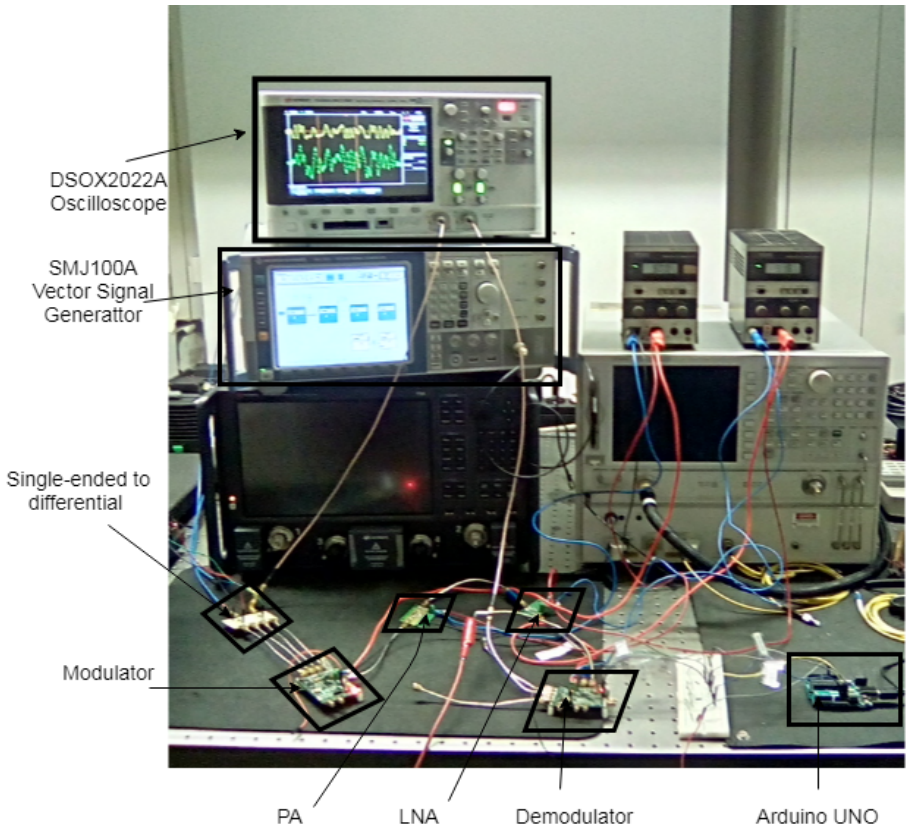

Figure 4.43: Wired loopback test setup

During this test several power levels were tested through the power control provided by the modulator and demodulator. The first test was performed with a 40 dB amplification of the modulator and a 40 dB amplification of the demodulator. Figure 4.44 shows the quadrature baseband signal generated by the SMJ100A VSG and the same signal after passing through all the communication chain.

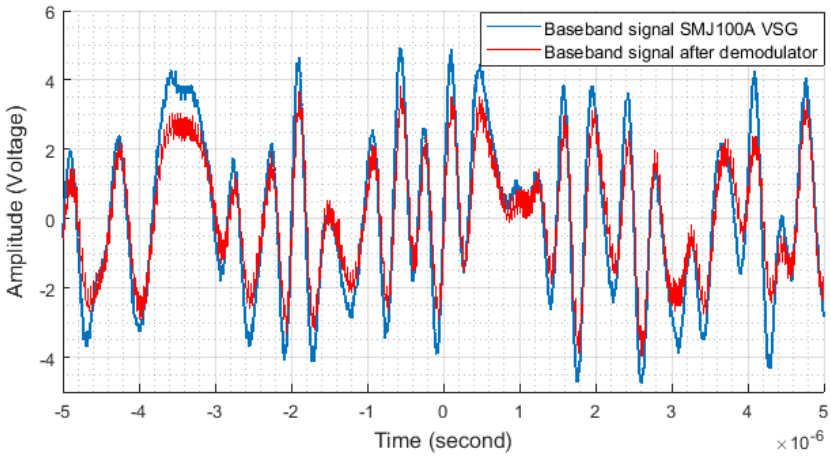

Figure 4.44: Wired loopback test without amplification

Both signals are very similar where the reference signal has a higher amplitude than the demodulated signal, which has passed through an amplification chain. The attenuators and cables present between the components cancelled the amplification imposed by the communication system.

Figure 4.45 shows the same signals used in the previous test, both with a maximum of 47 dB provided by the modulator and 60 dB provided by the demodulator. Despite the attenuation induced by the attenuators, the communication system has already crossed P1dB, where the baseband is saturated due to amplification in a non-linear zone.

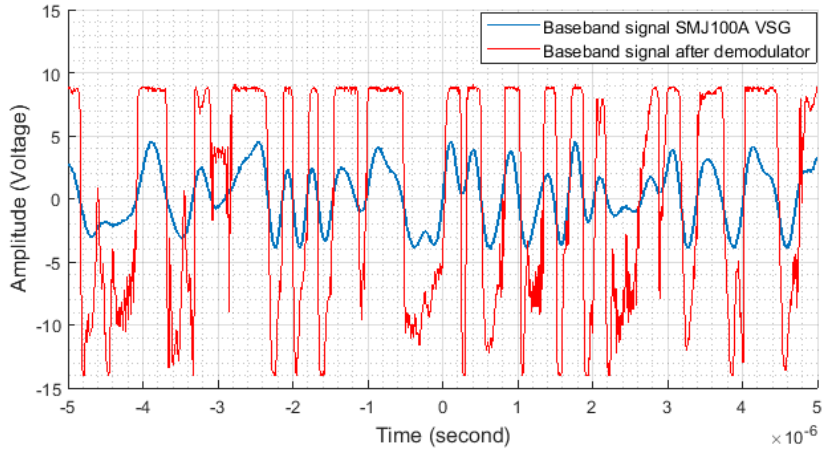

Figure 4.45: Wired loopback test saturated

During the last test it was used an 7 dB amplification by the modulator and an 60 dB amplification by the demodulator. Figure 4.46 shows both banseband signals, where due the attenuation induced by the attenuators, the amplitude of the demodulated signal is bellow the reference baseband signal.

Despite the low amplification imposed by the modulator, which increases the difficulty of detecting the correct signal, it can be seen that the demodulated is the same as the baseband signal.

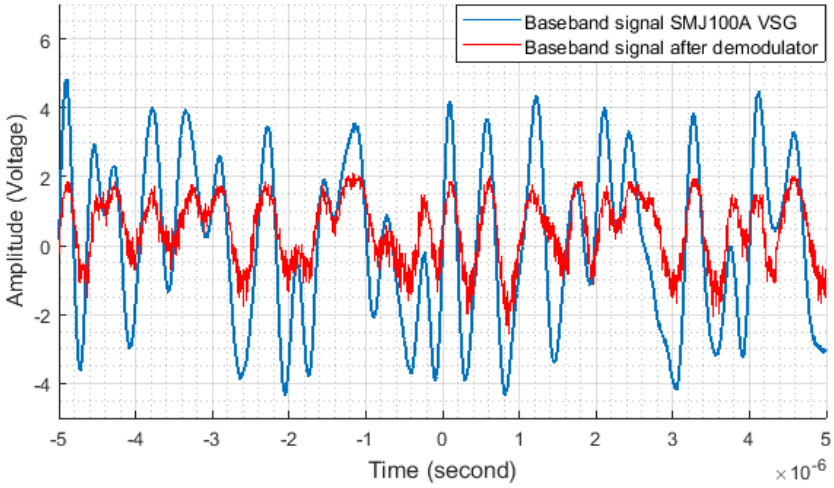

Figure 4.46: Wired loopback test attenuated

During this test some EVM calculations could have been made to understand how much the communication system degrades the communication, however as can be seen in figure 4.43, the oscilloscope has only two channels, which limited the acquisition of the baseband signals in-phase and quadrature at the same time.

Chapter 5

Conclusion and future work

5.1 Concluions

The purpose of this dissertation was to develop an RF transmitter and receiver capable of supporting an OFDM based navigation system. One of the biggest challenges was finding and developing solutions capable of operating in all frequency bands below 1 GHz.

The solutions developed and tested in the previous chapters allowed to conclude that the purposed solution in this dissertation was accomplished, where the RF transmitter and receiver can operate in all the frequency bands between 0.2 GHz and 1 GHz, if not taken into account the limited bandwidth of Antennas.

The frequency operation of each component was one of the main reasons that made them preferable to the rest in the electronics market. Other reasons were low energy consumption and low cost, which could be an obstacle in future integration.

Some stages of the baseband communication system have not yet been developed, such as the acquisition board that will connect the baseband communication with the RF transmitter and receiver. This limitation made the complexity of the tests of this solution increase severely, although, through the advanced laboratory equipment, it was possible to perform a complete test of each component that was developed in this dissertation.

When the baseband communication is completed, it will be possible to extract information on how much the communication system increase the BER through de-embedding techniques. Metrics as BER, commonly used, will allow to understand if it meets the need of the final project.

Despite the tests with the board that will provide the baseband communication was not performed, all components of the transmitter and receiver were fully tested with special focus on LNA and PA. Through the IM3 and EVM tests was possible to understand how much communication can be degraded when these devices are in non-linear zone.

Looking at the results of the solution developed, if not operated in non-linear zone, this solution is a candidate to provide the RF communication.

5.2 Future work

All the components that compose the transmitter and the receiver must be integrated into a single PCB. Through this new version, some errors made during the design of the modulator and demodulator can be corrected.

Antennas must be developed as they are the main obstacle to achieve a wide band communication.

Tests with the baseband board must be conducted to be able to inspect the performance of the entire communication system. Such tests will allow to compute the BER and EVM of the transmitter and receiver. To make the tests more realistic, it should be done in Douro vineyards, where it would be possible to inspect the actual frequency bands available to establish the communication.

Appendix A

Modulator

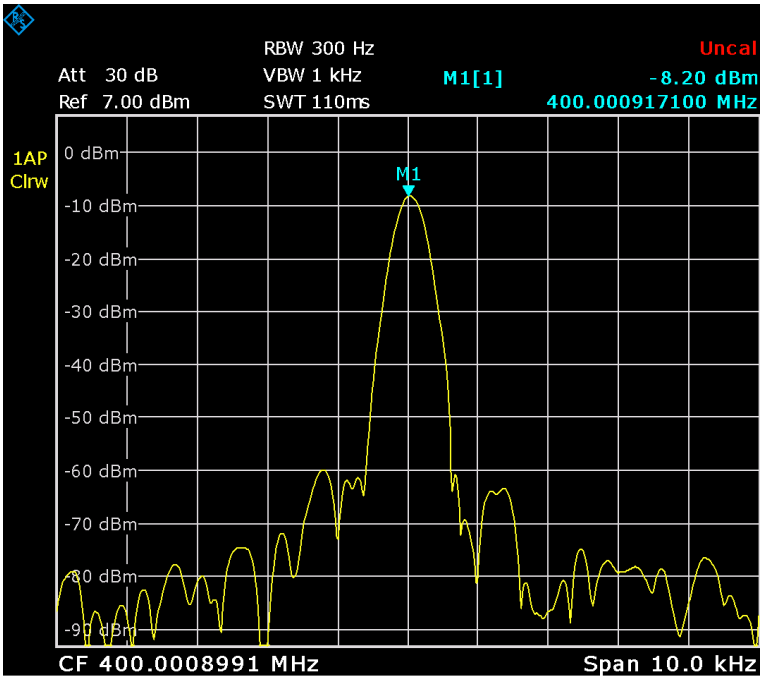

Figure A.1: Local oscillator at 400 MHz with 0.9171 kHz offset

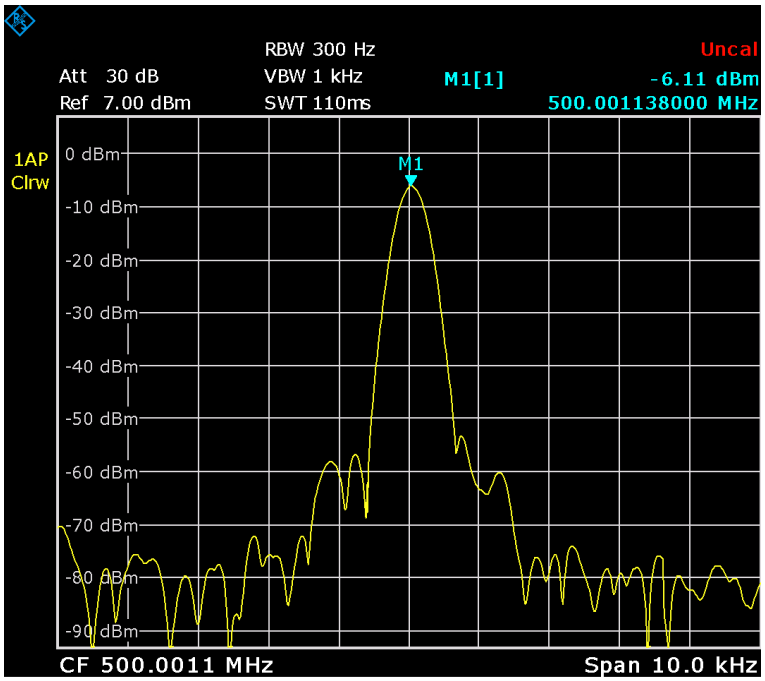

Figure A.2: Local oscillator at 500 MHz with 1.1138 kHz offset

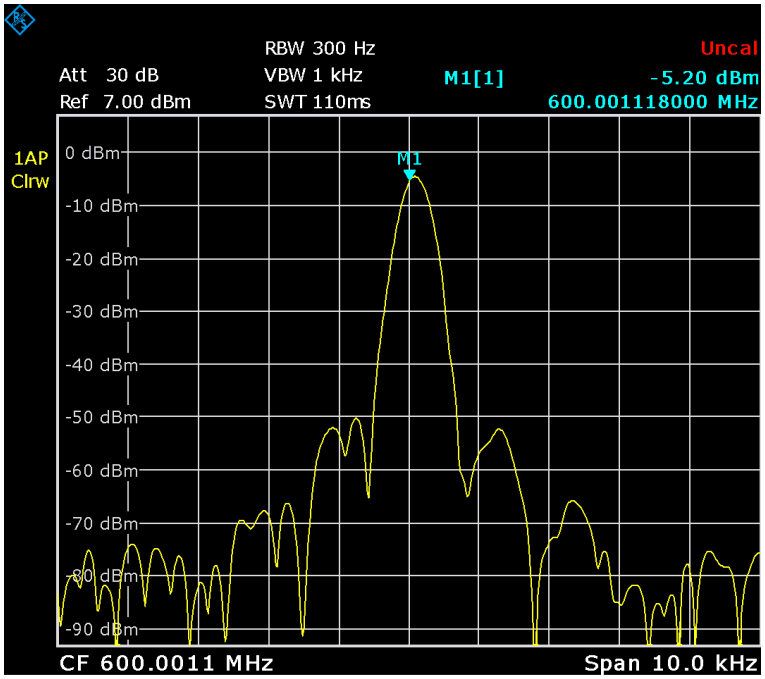

Figure A.3: Local oscillator at 500 MHz with 1.118 kHz offset

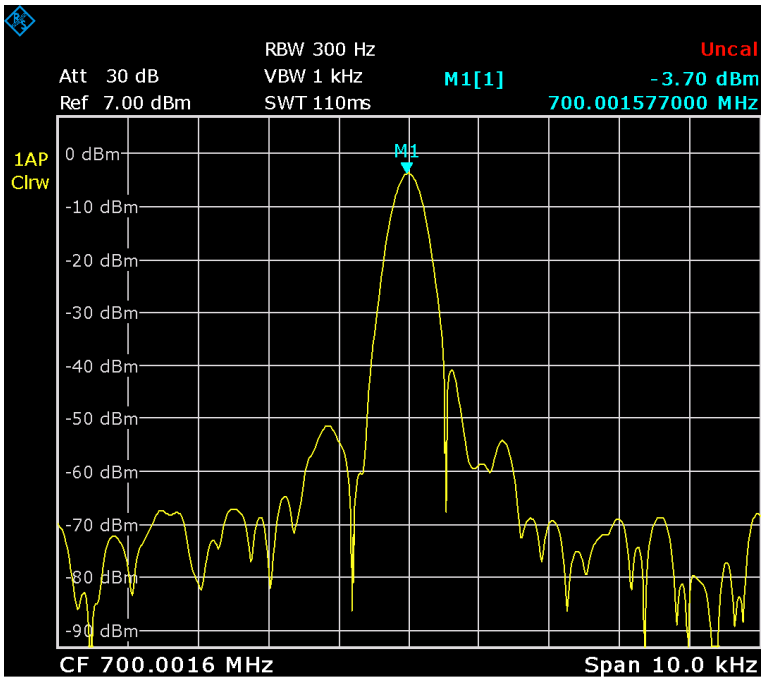

Figure A.4: Local oscillator at 700 MHz with 1.577 kHz offset

Appendix B

Demodulator

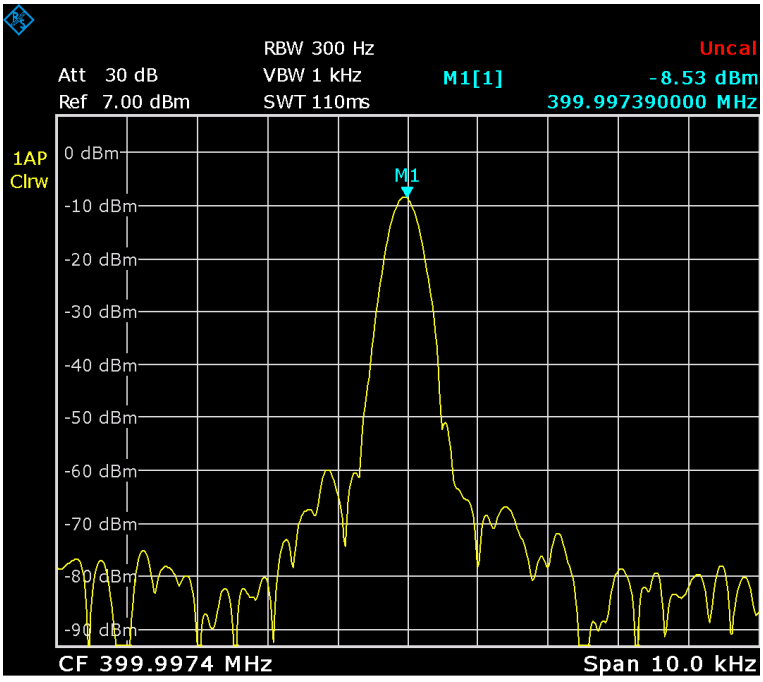

Figure B.1: Local oscillator at 400 MHz with 2.61 kHz offset

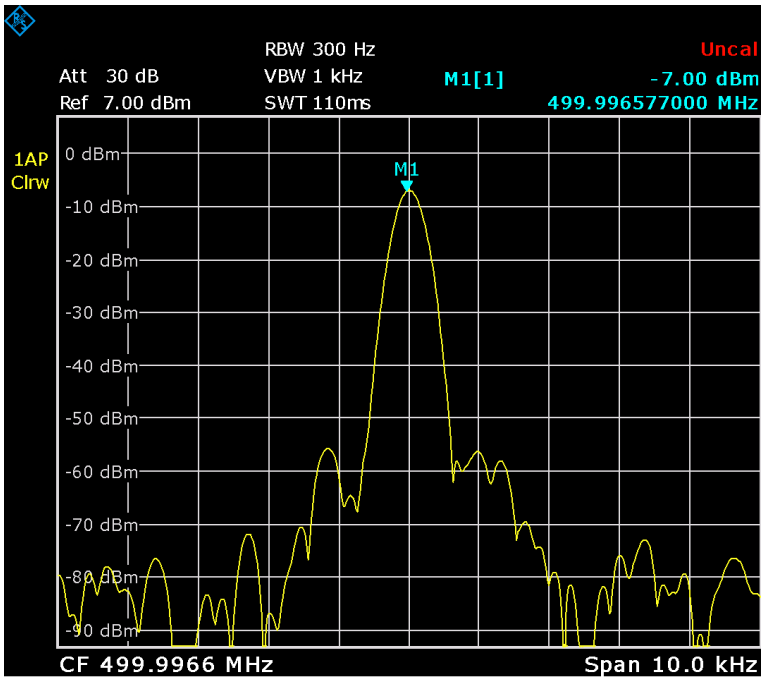

Figure B.2: Local oscillator at 500 MHz with 3.423 kHz offset

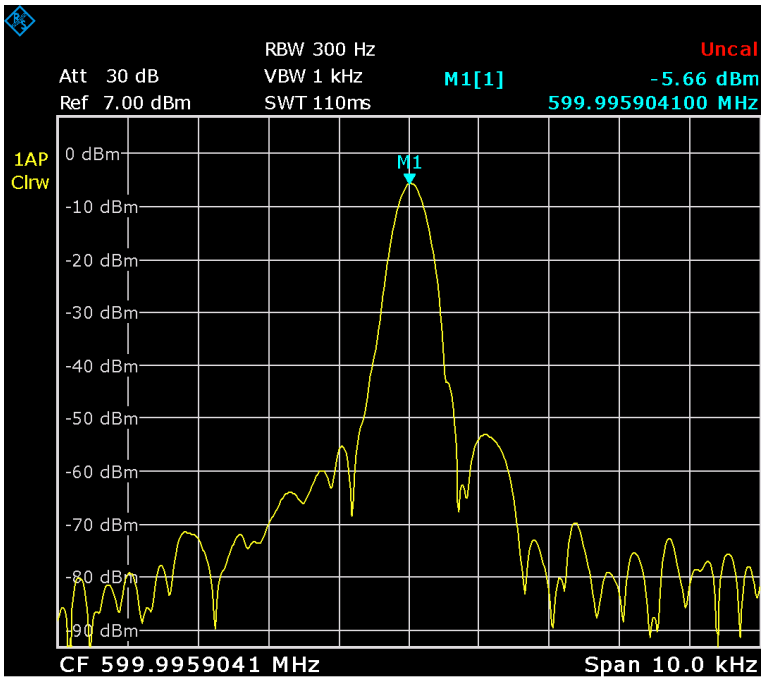

Figure B.3: Local oscillator at 600 MHz with 4.0959 kHz offset

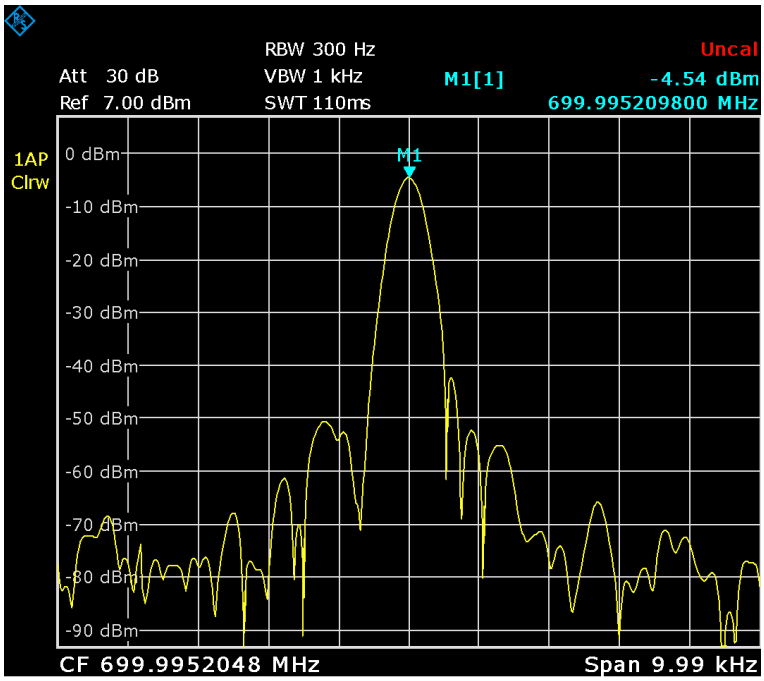

Figure B.4: Local oscillator at 700 MHz with 4.7952 kHz offset

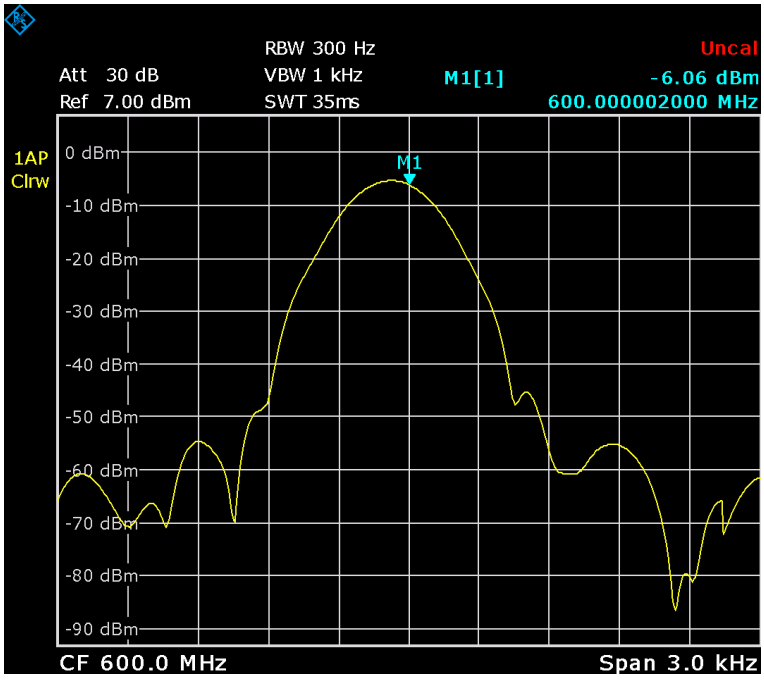

Figure B.5: Local oscillator at 600 MHz with balanced offset by 25-bit fractional number

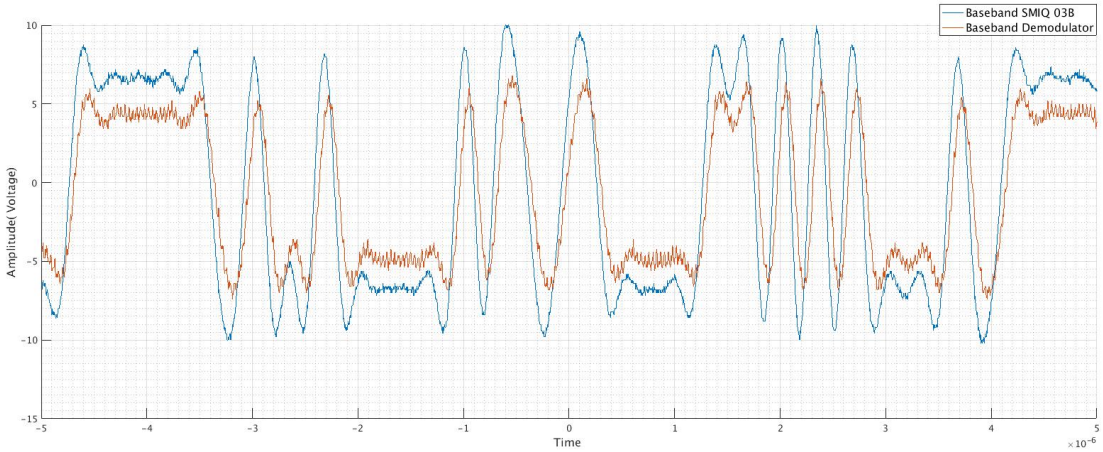

Figure B.6: Baseband signal channel in-phase BPSK

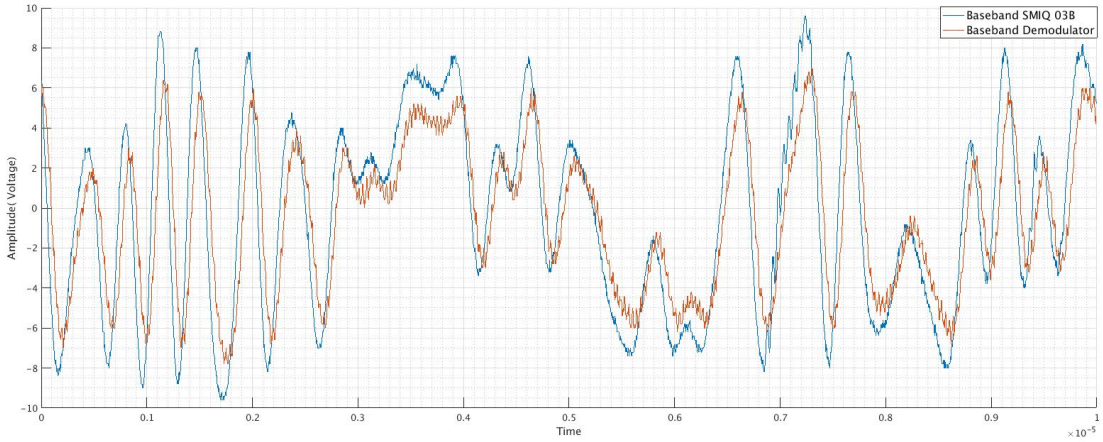

Figure B.7: Baseband signal channel in-phase 16 QAM

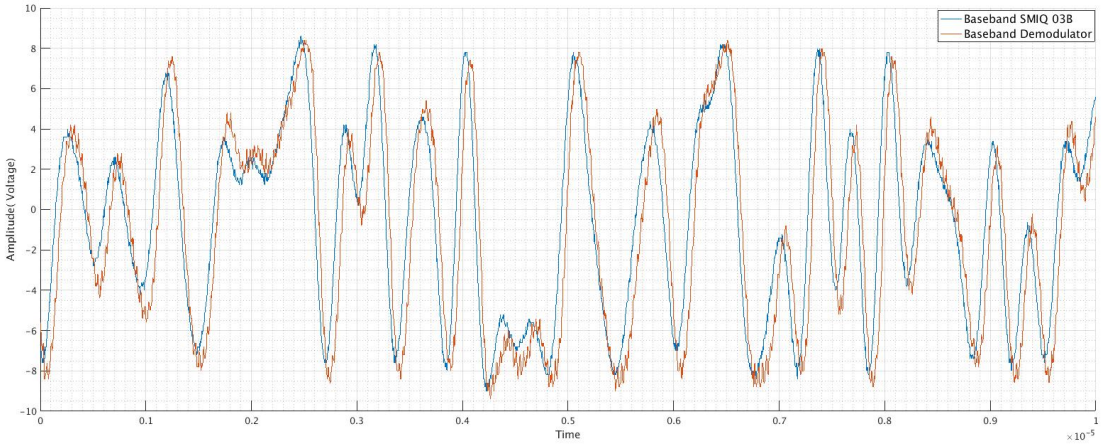

Figure B.8: Baseband signal channel quadrature 16 QAM

Appendix C

Loopback test

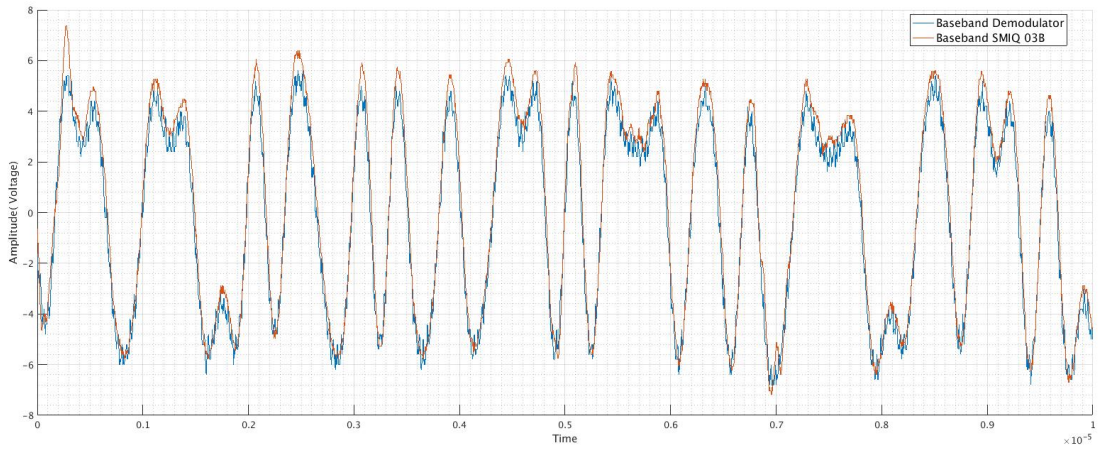

Figure C.1: Baseband signal channel in-phase BPSK

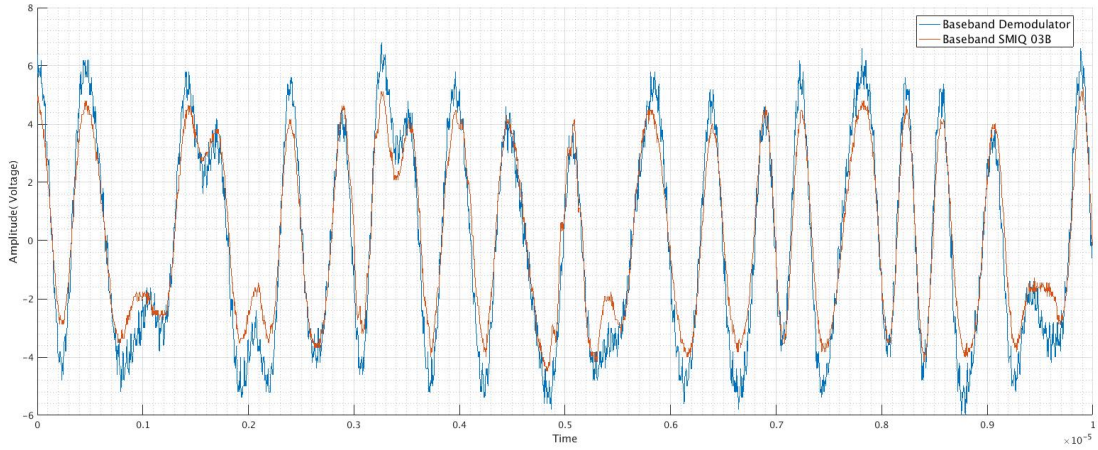

Figure C.2: Baseband signal channel in-phase QPSK

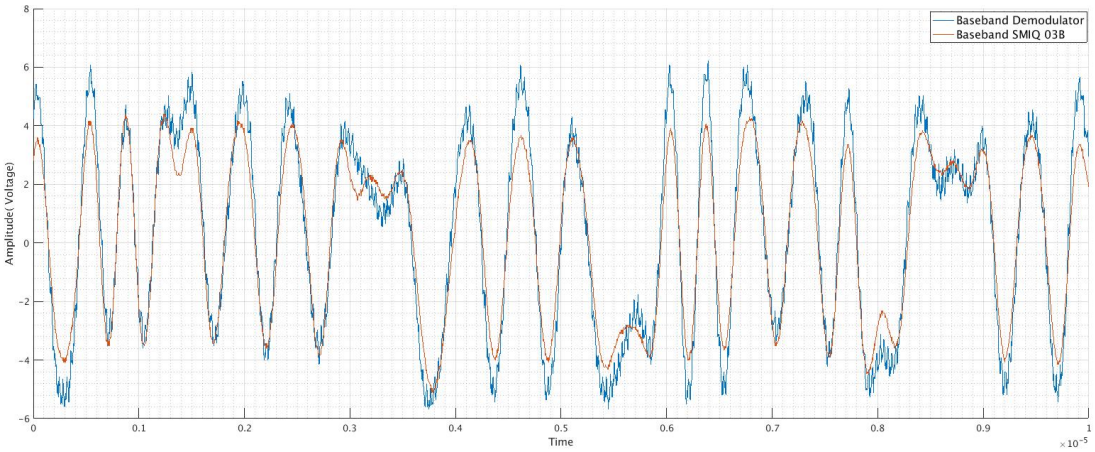

Figure C.3: Baseband signal channel quadrature QPSK

Appendix D

LNA test

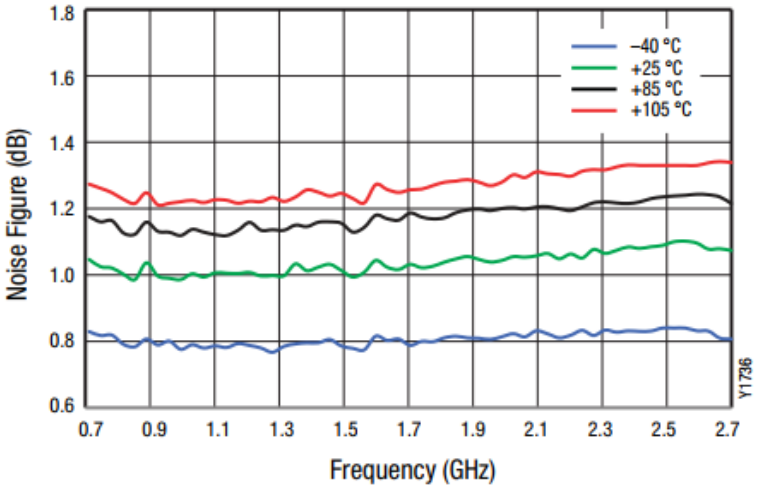

Figure D.1: Noise figure datasheet manufacturer

References

[1] R. Chang. “"Synthesis of band-limited orthogonal signals for multichannel data transmission"”. *Bell Systems Tech*, Jornal,vol. 45:pp.1775–1796, March Dec. 1966.

[2] E. M. D. Conde. “"Técnicas de detecção para o sistema lte no sentido ascendente"”. *Thesis*, Universidade de Aveiro.

[3] A. A. Coskun, S. Member, and A. Atalar. Noise Figure Degradation in Balanced Amplifiers. 27(9):848–850, 2017.

[4] J. Creech. S-Parameters Allow High-Frequency Verification of RF Switch Models. 2011.

[5] L. Frenzel. "What,s the difference between the third-order intercept and the 1-db compression points?". *Electronic Design*, 2013.

[6] R. Hassun, M. Flaherty, R. Matreci, and M. Taylor. Efffective Evaluation. pages 89–94, 1997.

[7] N. Instruments. "RF Simulation Demo: Third Order Intercept (TOI) and Intermodulation Distortion (IM3)". 2013.

[8] D. M. Poznar. Microwave and RF Design of Wireless Systems. *John Wiley & Sons, Inc*, pages 98–105.

[9] B. Razavi. RF Microelectronics. *Theodore S. Rappaport, Series Editor*, pages 11–24, 1998.

[10] H. Rohling. A simple extended-cavity diode laser. *Concepts for Future Communication Systems*, Springer Science Business Media:1236–1239, 2011.

[11] R. A. Shafik, S. Rahman, A. H. M. R. Islam, and N. S. Ashraf. On The Error Vector Magnitude As A Performance Metric And Comparative Analysis. (November):13–14, 2006.

[12] A. Technology. Stability Analysis and Demonstration of an X-band GaN Power Amplifier MMIC. pages 221–224, 2016.

[13] S. B. Weinstein and P. M. Ebert. "”Data transmission by frequency division multiplexing using the discrete Fourier transform"". *IEEE Trans. Communications*, vol. 19, issue:5:pp. 628–634, Oct. 1971.